Studies on Origami-Inspired Metamaterials with Tunable Stiffness

by

Zirui Zhai

A Dissertation Presented in Partial Fulfillment
of the Requirements for the Degree
Doctor of Philosophy

Approved October 2021 by the
Graduate Supervisory Committee:

Qiong Nian, Chair
Houlong Zhuang
Huei-Ping Huang
Wenlong Zhang
Yongming Liu

ARIZONA STATE UNIVERSITY

December 2021

ABSTRACT

Stiffness and flexibility are essential in many fields, including robotics, aerospace, bioengineering, etc. In recent years, origami-based mechanical metamaterials were designed for better mechanical properties including tunable stiffness and tunable collapsibility. However, in existing studies, the tunable stiffness is only with limited range and limited controllability. To overcome these challenges, two objectives were proposed and achieved in this dissertation: first, to design mechanical metamaterials with metamaterials with selective stiffness and collapsibility; second, to design mechanical metamaterials with in-situ tunable stiffness among positive, zero, and negative.

In the first part, triangulated cylinder origami was employed to build deployable mechanical metamaterials through folding and unfolding along the crease lines. These deployable structures are flexible in the deploy direction so that it can be easily collapsed along the same way as it was deployed. An origami-inspired mechanical metamaterial was designed for on-demand deployability and selective collapsibility: autonomous deployability from the collapsed state and selective collapsibility along two different paths, with low stiffness for one path and substantially high stiffness for another path. The created mechanical metamaterial yields unprecedented load bearing capability in the deploy direction while possessing great deployability and collapsibility. The principle in this prospectus can be utilized to design and create versatile origami-inspired mechanical metamaterials that can find many applications.

In the second part, curved origami patterns were designed to accomplish in situ stiffness manipulation covering positive, zero, and negative stiffness by activating

predefined creases on one curved origami pattern. This elegant design enables in situ stiffness switching in lightweight and space-saving applications, as demonstrated through three robotic-related components. Under a uniform load, the curved origami can provide universal gripping, controlled force transmissibility, and multistage stiffness response. This work illustrates an unexplored and unprecedented capability of curved origami, which opens new applications in robotics for this particular family of origami patterns.

ACKNOWLEDGMENTS

I would like to thank my supervisors Dr. Hanqing Jiang and Dr. Qiong Nian for their supports and guidance. Dr. Jiang had supervised me since I was an undergraduate student, and taught me everything about academic research. He could always give me inspiration when I got stuck in my research. Dr. Nian took me into new research topics in my last year of PhD study and gave me valuable guidance on my dissertation. Without their supports, I could not have today's accomplishments.

I would also like to thank Dr. Houlong Zhuang, Dr. Huei-Ping Huang, Dr. Wenlong Zhang, and Dr. Yongming Liu for their help and advice when serving on my committee.

I would like to thank my colleagues and collaborators, Dr. Xu Wang, Dr. Haokai Yang, Dr. Lingling Wu, Rui Dai, Zihang Yang, and Dr. Yong Wang, Dr. Yingzhu Wu, Dong Wu, Jiaqi Song, for their helpful discussions on my research.

I also want to thank my parents, grandparents, and other family members for their accompany and encouragement over the years. At last, I want to thank my wife, Saisai, for sharing joys and sorrows with me in this long journey.

.

TABLE OF CONTENTS

Page

LIST OF TABLES

LIST OF FIGURES

Figure Page

Figure Page

Figure Page

Figure Page

CHAPTER 1

INTRODUCTION

1.1 Background

Mechanical metamaterials are artificially engineered materials with unusual mechanical properties.[1, 2] In recent years, the ancient paper arts of origami (paper folding; in Japanese, "ori" means "fold" and "gami" means "paper") and kirigami (paper cutting; in Japanese, "kiri" means "cut") have become popular for building mechanical metamaterials and now provide valuable design guidelines.[3, 4] By means of folding and cutting, simple two-dimensional thin-film materials can be transformed into complex three-dimensional structures with unique and programmable mechanical properties, such as shape morphing,[5] flexibility,[3] tunable Poisson's ratio,[4] tunable stiffness,[6] and multi-stability.[7] Recently, origami and kirigami structures have been created from not only paper but also metals,[8-10] polymers,[11] hydrogels,[12, 13] and graphene,[14] with sizes ranging from macroscale to microscale[15] to nanoscale.[10] Origami- and kirigami-based Mechanical metamaterials have be applied in many fields, including flexible electronics,[16-19] medical devices,[20] and robotics.[6, 21-25]

Regarding mechanical properties, origami and kirigami are similar because both folding and cutting are mechanical means of dividing thin materials into flexible areas (i.e., creases in origami, and linkages in kirigami) and stiff areas (i.e., thin panels in both origami and kirigami). Therefore, the mechanical behavior of origami or kirigami structures is determined to a considerable degree by the balance between flexibility and rigidity conferred by the origami or kirigami pattern. However, origami and kirigami offer different

and unique behaviors. An origami structure is folded from the initial planar state into a compacted volume,[4-9, 12, 15, 16, 18, 20-24, 26-115] whereas a kirigami structure is stretched from the initial state into an expanded configuration.[10, 11, 14, 17, 19, 25, 116-136] Also, hybrid origami–kirigami designs are emerging that combine the two concepts to take advantage of both.[21, 22, 81, 92, 98, 120, 137-165]

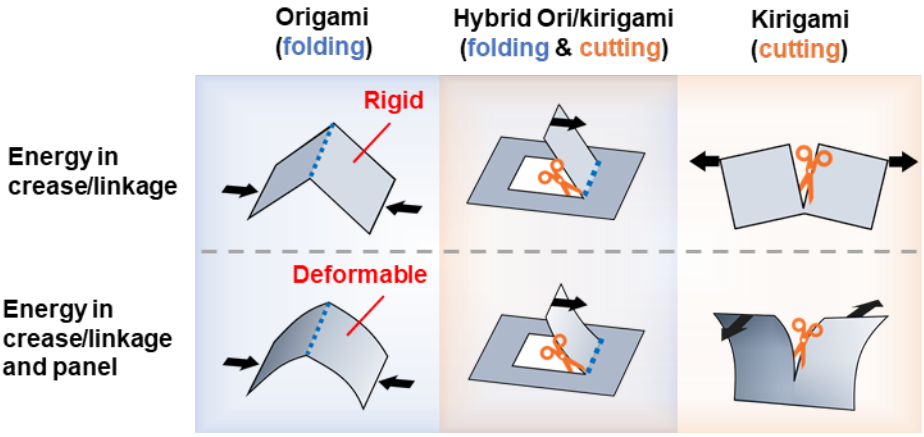

Figure 1. Venn graph with schematics showing the category of origami- and kirigami-based mechanical metamaterials.

1.2 Catogary of Origami and Kirigami-Based Mechanical Metamaterials

When designing mechanical metamaterials, one of the most important concepts is the mechanical energy landscape, which describes how the strain energy varies with different geometrical and/or deformation variables in the deformed configuration space of metamaterials . The mechanical energy landscape affects almost all the properties of an mechanical metamaterial, such as its deployability, stability, and stiffness.[2] For example, bistability is due inherently to the double local minima of elastic energy,[7] and self-deployment occurs as the mechanical energy decreases along the deployment path.[7, 24] Origami and kirigami both provide elegant ways to design the energy landscape through the folding and cutting patterns. As shown in Fig. 1, for some origami and kirigami patterns

under specific conditions, the panels remain rigid during deformation and energy is stored only in the crease or linkage areas; known as rigid origami or kirigami, this type confers more-predictable kinetics and mechanical behavior and is ideal for applications such as shape morphing.[5, 26, 116-118] Otherwise, the panels deform as well, and elastic energy is stored in both the crease or linkage areas and the panel areas; known as deformable origami or kirigami, the complex energy landscape of this type offers more programmability regarding forces, stiffness, and stability.[6, 7, 12, 24, 95]

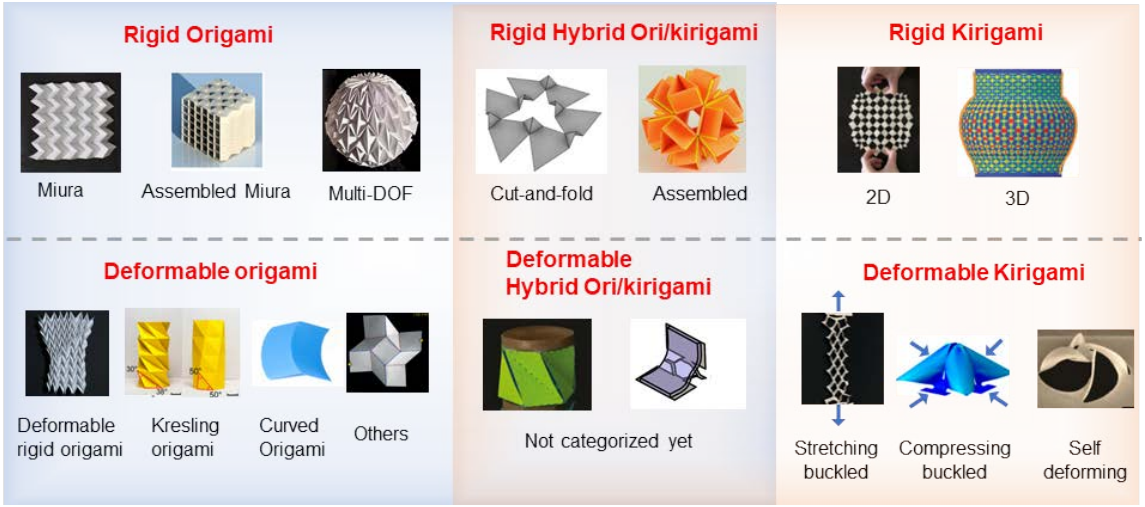

Figure 2. Subcategories of each group of origami- and kirigami-based mechanical metamaterials.

1.3. Mechanical Metamaterials Based on Rigid Origami

Rigid origami (also known as rigid foldable origami) involves folding and unfolding without deforming the origami panels. There are three requirements for origami to be rigid: (i) the pattern must be mathematically foldable[166]; (ii) the panels must be much stiffer than the creases; (iii) the material should be under uniform loading along the folding/unfolding directions instead of under concentrated, bending, or twisting loads. In

rigid origami, elastic energy (or strain) is stored only in the folding creases, so the energy can be expressed in terms of only the changes of the dihedral angles of the creases.

Depending on the transformation mode, rigid origami can be divided into one-DOF (i.e., degree of freedom) and multi-DOF types. The DOF of rigid origami depends on the number of creases at each vertex,[166] e.g., rigid origami with four creases per vertex has only one DOF. The best-known one-DOF rigid origami is the Miura pattern, which has an elegant geometry and unique mechanical properties.[4, 49, 72] Assembled Miura-based mechanical metamaterials can be formed by assembling multiple layers of Miura origami and have more-complex geometries and performances.[40, 43, 54, 64, 72] Multi-DOF origamis have more than four creases per vertex, e.g., Ron Resch and waterbomb origamis.[4, 22, 39, 50, 52] Multi-DOF rigid origami is more flexible than one-DOF origami.

Miura origami (one-DOF)

As a periodic parallelogram pattern, the Miura pattern was designed by Koryo Miura in the 1970s.[74] The geometry of Miura origami can be determined by the lengths a and b and the plane angle β, and the folding state of Miura origami can be determined by the folding angle ϕ.[4, 49, 72] All the other geometric variables during folding (e.g., the dihedral angles) can be expressed in terms of these four parameters.[4, 72]

The Miura pattern has many unique yet intrinsic mechanical properties during folding and unfolding, such as tunable Poisson's ratio, panel directions, and stiffness.[4, 72] These behaviors of the Miura pattern have been harnessed to make flexible lithium-ion batteries,[16] artificial muscles,[22] heat-dissipation enhancement,[122] and solar cells.[167] Depending on the geometry, the Poisson's ratio can be either negative, positive, or in

transition between negative and positive during folding. More interestingly, Miura origami exhibits bistability when the geometrical and mechanical parameters are in a specific range, thereby conferring efficient deployment.[37] By changing the folding direction of Miura origami between upward and downward, different chirality can be tuned for electromagnetic behaviors.[35] Similar functions of Miura origami are used to control electromagnetic waves,[31, 70] deflect light,[58] and reduce radar cross section.[71] Miura origami also has interesting dynamic properties. By analyzing and designing the transformation dynamics of Miura origami, a branching Miura origami structure can have 17 distinct configurations activated by different dynamic inputs of a single actuator.[168]

The mechanical properties of Miura origami can be programmed by modifying the creases. By changing the material distribution at the creases and panels, a metamaterial based on Miura origami can have a tunable coefficient of thermal expansion (CTE), from negative to zero to positive, with potential applications in aerospace and optics.[65] Stretchable materials are also used at the creases of Miura origami to realize dual stiffness, which has been applied in robotics for rapid and robust gripping.[21] Moreover, photoactive materials and four-dimensional printing methods are applied to control the deformation of creases and realize self-folding Miura origami.[169] Thin creases design are realized via three-dimensional (3D) printing, thereby enabling Miura origami to confer either loadbearing or flexibility properties.[46] Meanwhile, for enhanced panel rigidity for better application in engineering structures, origami with thick panels has been designed and the related theories have been developed.[27, 75]

By modifying the geometry of Miura origami facets from periodic parallelograms to aperiodic general quadrilaterals, complex surfaces with designed curvature can be created.[5, 36] The modified Miura origami tessellations can be folded into complex curvatures, such as cylinders or spheres.[63] Optimization algorithms have also been developed for designing the 3D shapes of folded Miura origami.[26, 170] Modified Miura origami strings are used in robot hands for programmed motions.[171]

Assembled Miura origami (one-DOF)

Although Miura origami has many interesting mechanical properties, the original single-layer Miura origami can only be folded as a plane or a shell, which somehow limits its applications. To develop metamaterials that can deploy in 3D, the original Miura origamis are assembled in different ways to form 3D metamaterials, while keeping their original mechanical properties, e.g., negative Poisson's ratio. The most straightforward assembly method is to connect identical Miura origami sheets layer by layer and form cellular materials.[42] Layer-stacked Miura origami-based mechanical metamaterials are flexible in the in-plane directions but stiff along the stacking direction. These simply assembled Miura origamis can be used as sandwich cores for anti-blast structures and as frequency-selective surfaces.[68, 172]

Miura origami sheets with different geometries and layers can be assembled and have more interesting and nonlinear mechanical properties. Assembled Miura-origami-based metamaterials with "ABAB" stacking mode have been designed that enable self-locking behavior due to their mathematical nonflat-foldability.[72] A more general case is shown in Fig. 2(d), where the unit cell of the Miura pattern is modified into a collinear

pattern consisting of four different parallelograms.[54] The assembled metamaterials have even more programmability with multi-stage nonlinear force responses. The stacking of Miura origami has been widely used for graded stiffness.[56, 67, 121] The assembled origami has nested-in and bulged-out design with bistability[34] and can be used as a mechanical dianode,[57] as well as metamaterials with tunable bandgaps.[69] The bistability can also be realized by coupling the elasticity of origami with magnetics.[41] Inspired by the fluid mechanism of plants, Miura origami tubes can be assembled with pressurized air pouches inside for tunable stability,[173] tunable stiffness,[64, 174] and vibration isolation.[175, 176]

Using nonidentical parallelogram patterns instead of the original Miura pattern, tubular origami structures can be designed with reconfigurable polygonal cross sections.[30, 55] Using polygonal cross-sectioned origami tubes as building blocks, cellular origami metamaterials with either foldable or self-locking properties can be achieved.[33, 177] Another family of Miura-derived polygonal tubes is based on the Tachi–Miura polyhedron (TMP), fabricated by connecting two identical papers with different patterns.[76] The TMP structures have negative Poisson's ratio and bistability between concave and convex configurations.[43] Metamaterials assembled by TMPs provide a platform for forming rarefaction waves because of their controllable strain-softening behavior.[44, 66] Moreover, TMP structures can be tuned between a collapsible state and a load-bearing state.[77]

Other than changing the Miura origami pattern in each layer, the manners of assembly play an even more important role in tuning the stiffness of Miura origami. By assembling two stripes of Miura origami together, a Miura tube can be made.[9, 60] A "zipper" Miura origami tube made of two perpendicular tubes has much higher bending stiffness

than that of the original Miura origami.[40] This "zipper" tube design provides Miura origami tubes and tessellations with much higher stiffness and so is excellent for load bearing and rapid deployment. Zipper-coupled Miura origami tubes are also fabricated using 3D direct laser writing fabrication, thereby achieving tunable stiffness and deployability at the microscale.[15]

Multi-degree-of-freedom rigid origami

More DOFs are desired in some applications, e.g., multi-state shape morphing. When there are more than four creases at one vertex, rigid origami has multiple DOFs. A well-known multi-DOF origami is Ron Resch origami, which can be folded in different modes. The fully folded state of Ron Resch origami is a flat plate that has remarkable load-bearing capacity because of its six-fold structure.[4] When forming a tubular structure, Ron Resch origami still has good load-bearing ability for axial loads because of its negative Poisson's ratio and self-locking phenomenon. Based on these properties, Ron Resch-inspired structures have been designed for impact protection.[47, 178]

Another well-known multi-DOF origami is waterbomb origami (also known as magic-ball origami). The unit cell of the waterbomb pattern has six creases on each vertex. The unit cell of waterbomb origami has bistability and can represent binary states 0 and 1 by upward and downward folding, respectively.[51, 52, 62] Therefore, the tessellation of waterbomb origami can be designed for mechanical logistic calculation,[52] in which humid sensitive materials are used for the creases to enable humidity-responsive computation. Waterbomb origami has also been used for tunable robotic wheels to adapt to different environments[38]; wheels made using waterbomb origami can change radius because of the

rich DOFs of the latter. Integrated with a pneumatic system, waterbomb origami has also been designed into a soft gripper that can grip different objects by shape transformation.[22] The radius-changing property of waterbomb origami has also been harnessed to design crawling robots.[34] Under symmetric folding, the number of DOFs of waterbomb origami reduces to one, and it can be used in deployable structures with predictable kinetics.[73] Waterbomb origami has been used as a building block to design metamaterials with programmable stiffness and deformation,[39, 45, 48, 50] and topology optimization has been performed on waterbomb-like origami to design actuators with specific movement.[29] By adding a single quadrilateral face to the unit cell, multi-DOF origami can become one-DOF origami and is easier to control.[78]

1.4 Deformable Origami-Based Mechanical Metamaterials

Deformable origami involves storing energy in both creases and panels during folding, and so it confers a complex energy landscape and mechanical performances. Patterns of deformable origami include rigid-foldable patterns, Kresling/Yoshimura patterns, and curved patterns, among others. In rigid-foldable origami, although the panels remain rigid during folding in theory, they may still deform in reality. Therefore, these patterns are still categorized as deformable origami and specifically deformable rigid origami. For the other patterns that are not mathematically foldable, panels must undergo deformation to be folded.

Deformable Rigid Origami-Based Mechanical Metamaterials

In practice, during folding and unfolding, theoretically rigid origami will introduce deformation in the panels, especially when they are flexible. Consequently, these

deformable rigid origami patterns have more DOFs and unusual behaviors. For example, Miura origami made of paper can be easily bent or twisted, although these deformations are not theoretically allowed by rigid-body kinetics.[49, 83] Consequently, the deformation energy of the panels is as important as the energy stored in the creases when analyzing the mechanical responses of deformable rigid origami structures. To analyze the stiffness of Miura tubes under bending, eigenvalue analysis is performed by considering the deformation of both creases and panels. Zipper-coupled Miura tubes have much higher eigenvalues of bending and so are stiffer under bending.[40, 106] A bar-and-hinge model can efficiently capture the elastic energy of both creases and panels to simulate the mechanics of deformable Miura patterns.[84, 90, 106]

Deformable rigid origami patterns enable many applications. Considering the energy absorption of both crease folding and panel bending, deformable rigid origami has been used for impact energy absorption.[8, 23, 32, 104] Deformable Miura origami also allows flexible and nonuniform deformation that is effective for protecting robots from rotary collisions.[23] The elastic behavior of panels also enables rigid origami tessellations to work as acoustic metamaterials.[103] The non-rigid deformation of Miura origami has been harnessed for complex shape morphing by using distributed actuators.[105, 110] With some panels being floppy while others are rigid, the designed metamaterials can have a certain number of DOFs and so can be used to store information.[28]

Imperfection can be introduced artificially and locally into Miura origami panels to reprogram their mechanical properties. Pop-up defects have been introduced at the vertices of Miura origami to change the latter into defected stable states.[95] Defects on vertices can

improve the in-plane stiffness of Miura-origami-based metamaterials. By tuning the number and locations of the defects, the stiffness response of the metamaterial can be reprogrammed in situ. It has been discovered that small imperfections and modifications in rigid origami can influence the mechanical properties considerably.[87, 89] Topological principles have also been used to understand and design deformable-origami-based mechanical metamaterials.[85]

Kresling Origami-Based Mechanical Metamaterials

Kresling origami is folded to a cylindrical shape with triangulated unit cells. The folding pattern is shown in Fig 3(c), where the parameters n, α, and β determine the geometry as well as the mechanical performance of the Kresling origami. To satisfy the flat-foldable condition, the smallest angle of the triangular unit cell is π/n, where n is the number of edges per circle.[179] By modifying the unit-cell geometry (α and β), Kresling origami can become either stiff or flexible. Flexible Kresling origami (left) can be fully collapsed from its deployed state and exhibits bistability, whereas diamond origami (or Yoshimura origami, which can be modified from the Kresling pattern) is stiff and not foldable.[7] The differences between Kresling and diamond origamis can be analyzed using a truss-based model.[7, 91, 96] From the perspective of energy, Kresling origami has double-well energy and an in-plane strain of less than 2% (as shown in Fig 3(c)). The vanishing strain energy at initial and deployed states means that Kresling origami has zero strain at both states. For the other configuration of Kresling origami ($\alpha = \beta = 50^\circ$), the elastic energy under compression increases monotonically and the in-plane strain is much higher. Compared with diamond origami, Kresling origami has more unusual mechanical

properties, including bistability, tunable stiffness, and coupled compressing-twisting deformation.

One of the most interesting properties of Kresling origami is tunable stiffness. By combining the flexible Kresling pattern and the rigid diamond pattern, truss-based mechanical metamaterials have been designed for on-demand deployability and tunable stiffness.[7] In the designed origami-inspired metamaterials, two paths can be triggered selectively by direct compressing or twisting-compression, corresponding to a collapsible state with low stiffness or a non-collapsible state with high stiffness. The two different collapsing paths can be visualized by an energy landscape varying with deploying state and rotating state. The metamaterial deploys along the energy valley, where the normalized energy has local minimum around 0.1. There are two possible paths for collapsing. Without twisting, the metamaterial experiences a load-bearing path where the normalized energy is around 1,000. If twist is applied before compressing, the metamaterial enters an easy-collapsing state, which is the same as the deploying path, and the energy is around 0.1. Four orders of magnitude differences of the strain energy during deploying and collapsing explain the mechanical responses of the metamaterial. In the load-bearing state, the prototyped metamaterials can hold 1,600 times their own weight. A series of Kresling-origami-inspired structures has been assembled with decreasing stiffness under compression loading. When an impact load is imposed on the left side, the strain field exhibits a rarefaction wave (i.e., tensile wave) travelling from left to right. This unique behavior of the designed Kresling structures can be used in reusable impact-mitigating systems. By tuning the compressive stiffness, Kresling origami can also be used for the

transmission of rarefaction solitary waves,[80] tunable frequency bands,[86] tunable dynamic behaviors,[88] and vibration isolation.[99]

The bistability and compression-twist coupling of Kresling origami have been explored for other applications, such as mechanical memory operation,[81, 96] binary switches,[79] haptic feedback mechanisms,[108] and crawling robots.[101, 114] Kresling origami has been coupled with magnetism to change the mechanical information remotely.[81] The coupling between rotation and compression in Kresling origami allows the magnetic field to control the origami structure remotely. A Kresling origami unit cell can be triggered into binary states 0 and 1 by rotating the magnetic field. By connecting multiple magnetic Kresling origamis in series, the designed metamaterial can store binary information and perform digital computation via its multi-stable states.

Curved Origami-Based Mechanical Metamaterials

Curved origami is origami with curved creases and/or panels. Curved origami has a more elegant geometry compared to the corresponding straight-crease origami. Curved-crease origami has one crease and two panels, compared with similar Miura origami with four creases and four panels.[6] Moreover, a simple circular strip with a curved crease can be folded into unusual buckled and symmetric shapes.[109] Because of its elegant geometry, curved origami has been used for face shields and generating curved surfaces.[20, 111]

Unlike in the aforementioned deformable origami patterns, the bending energy in the curved panels makes an important contribution to the mechanical properties of curved origami. Recently, curved origami has been designed for the in-situ manipulation of mechanical stiffness. By changing the curvature of the curved creases, the stiffness of

curved origami can be tuned from negative to zero to positive.[6] The crease folding in the designed curved origami provides negative stiffness, while the panel bending provides positive stiffness. Therefore, via the competing folding and bending deformations, the stiffness of curved origami can be elegantly tuned. The energy and force variation of the curved origami with negative stiffness is shown on the right side of Fig 4(a). The energy of crease folding and panel bending (and stretching) both contributes to the mechanical response of the curved origami. However, the strain energy of crease folding contributes to the negative stiffness, and the strain energy of panel bending leads to the positive stiffness. At small deformation, crease folding and panel bending have similar contribution to the total energy, while at larger deformation the panel bending contributes more than 90% to the total energy. The balance between crease folding and panel bending results in the different stiffness of the curved origami, which can be realized by tuning the normalized curvature and folding modulus of the curved creases. Because the deformation of panel bending is totally elastic, it also resolves the issue of plastic hysteresis on origami creases.[6] The designed curved origami can be applied to robotics and many other fields. In deployable and reconfigurable structures, the coupling relationship between crease folding and panel bending has been harnessed to design self-folding curved origami, where the bending of panels also folds the curved creases.[102] A pre-cut curved crease pattern on a tube can be used to control the buckling mode and so thus improve the load-bearing capacity.[112] The bending stiffness of curved origami can be strengthened by corrugation,[113, 115] with application for reinforcing lightweight structures.[94]

Curved-panel origami is origami with curved panels but straight creases. Curved-panel origami has been designed based on inspiration from the ladybird beetle for fast actuation.[24] The undeformed configuration of the curved-panel is shown on the left side, where the origami consists of a curved compliant facet and a folding crease. At a small folding angle, the curved-panel origami has high positive bending stiffness and high bending moment, leading to the self-locking property; when the folding angle is larger than the critical angle (around 10°), it has negative stiffness and low bending moment, leading to the flexible and snap-through collapsing behavior. The prototyped curve-panel origami has a self-locking moment of about 0.02 N • m, which is about 20 times higher than its folding moment. When released in a folded state, the stored bending energy can quickly become dynamic energy, resulting in rapid deployment and locking functions. Curved-panel origami has also been used in designs such as those for solar deployment systems, where smooth panels are preferred rather than discrete creases.[107]

Other Origami-Based Mechanical Metamaterials

Other deformable origami patterns include square-twist origami and hypar bistable origami. The folding crease pattern of the square-twist origami has zero DOFs when considered as rigid origami, but it has a twisting DOF when panel bending is allowed.[12] Square-twist origami exhibits bistable and bifurcated behaviors and can be used to build mechanical metamaterials with multi-stability. With $\alpha = 45^\circ$, the negative stiffness of square-twist origami leads to a snap-though phenomenon, while with $\alpha = 10^\circ$, the square-twist origami has only positive stiffness and no snap-through is observed. The bending of panel provides negative stiffness while the folding of creases provides positive stiffness.

By changing the angle α, the energy landscape of both the crease bending and panel folding alters. Larger angle α will result in higher bending energy but lower folding energy. At α = 45°, the square-twist origami has the most pronounced bistability and negative stiffness. By using thermally reactive materials, metamaterials based on square-twist origami have been designed with five stable states and self-deploying properties.[100] Another deformable origami is hypar origami with a pattern of concentrically pleated squares. Hypar origami is folded between two saddle-shaped stable states.[82, 93] During deformation, the crease folding energy, panel bending energy, and panel stretching energy vary. Among the three energies, the panel stretching energy has the least contribution to the total strain energy (i.e., less than 5%). At the two stable states, crease folding and panel bending have a similar contribution to the strain energy. When the hypar origami is closing to the planar state, folding has larger contribution; when the hypar origami is more bent, panel bending has more contribution. The bistability and negative stiffness of hypar origami is mainly resulted from the crease folding deformation, since the crease folding provides a double-well energy landscape while the panel bending provides much lower energy gaps. Based on those distinct mechanical behaviors, the hypar origami can be used to from multi-stable meta-surfaces with non-Euclidean geometries.

CHAPTER 2

ORIGAMI WITH TUNABLE DEPLOYABLILITY

2.1 Introduction

A deployable structure is a structure that can reconfigure and change shape/size mainly from folding and unfolding, and has many applications from daily essentials (e.g., umbrella), vascular stents[180], to solar panels[181] for spacecraft. Origami, the art of paper folding, thus naturally provides inspirations for deployable structures. In addition to deployable structures, origami recently has gained lots of attention as it has offered an appealing strategy on the development of 3D architectures across different length scales[182-184] and metamaterials with tunable properties[65, 185-190]. Many origami-inspired deployable structures are based on rigid origami patterns, in which the kinematic deformation is solely limited to the folding lines while the panels remain undeformed. Well-known representatives of deployable rigid origami patterns are the Miura folding[181] and its derivates[185, 191]. In addition to rigid origami, another type of origami is deformable origami where the panels and the folding lines all bear deformation, such as the twisted square pattern[192]. Due to the simplicity of the kinematics of rigid origami, much attention has been focused on this type of origami.

Despite of recent active research in origami and related deployable structures, one critical aspect seems being overlooked: if the deployed structure can remain at the deployed state under loading, such as vibration experienced by a deployed structure used in spacecraft. From the perspective of mathematics of origami, deployability means the kinematics of the pattern geometry allows deploy and collapse. Since this is a pure

mathematic point of view, there is no energy associated with deploy and collapse. Therefore, a deployable structure at the same time also allows it to collapse through which it deploys. Thus, easy deploy, one of the many attractive attributes of some origami patterns (e.g., Miura pattern and its derivates), simply also indicates easy collapse. In addition to utilize mechanical mechanisms to lock the deployed state, the discovery of deployable and yet stiff origami patterns, such as zipper-coupled tubes[185], has gained attentions. However, the stiffness along the deploying direction is not enhanced in order to ensure readily retracting to the collapsed state in the same way it deploys. To fully harness the exemplar properties of origami in terms of its deployability and tunable properties, it is essential to create a deployable structure with on-demand deployability and collapsibility, i.e., while keeping the easy deploy, the collapse can be selective, either hard or easy, depending on the collapse path.

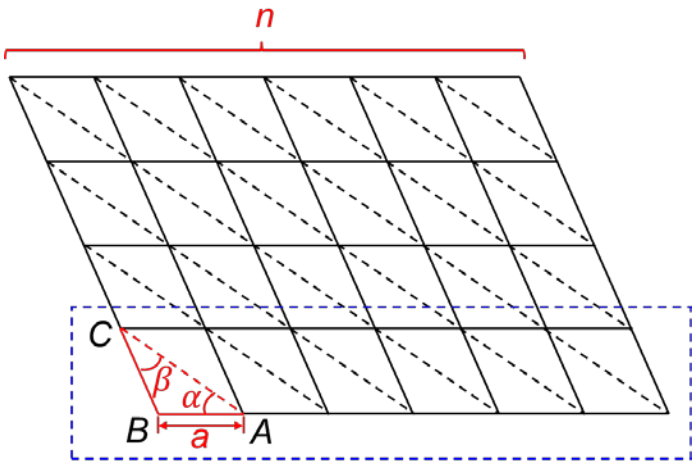

Figure 3. Crease pattern of a triangulated cylinder origami.

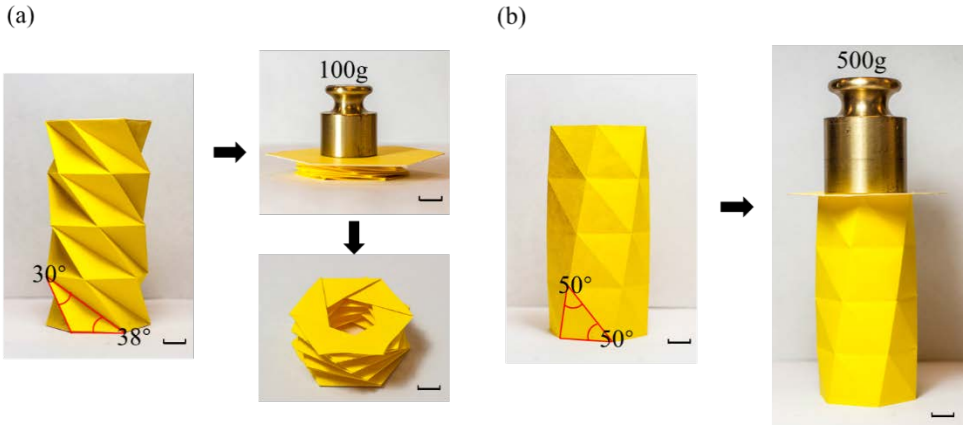

Figure 4. The load-bearing performance of different triangulated cylinder origami.

Here in this paper, an origami – inspired mechanical metamaterial was created with on-demand deployability, collapsibility, and tunable stiffness, where the deploy and collapse can follow two paths. Thus, easy deploy and hard collapse, seemly contradictory attributes, are achieved simultaneously. The metamaterial is inspired by a triangulated cylinder pattern[193, 194] that has been studied as one type of deformable origami patterns. Its crease pattern is shown in Fig. 3. By altering the angles α and β, two distinct cylinders can be folded (Fig. 4). For $\alpha = 38^{o}$ and $\beta = 30^{o}$ (left panel of Fig. 4), a construction paper-folded triangulated cylinder can be deployed in the axial direction but at the same time a small compressive load (e.g., a 100-g weight) will collapse it along the same way. This suggests an "easy deploy and easy collapse" structure. For $\alpha = 50^{o}$ and $\beta = 50^{o}$ (right panel of Fig. 4), the construction paper-folded cylinder is not deployable (or collapsible) and can bear much larger compressive load (e.g., a 500-g weight). This pattern is "hard deploy and hard collapse". This paper combined these two patterns and created an on-demand "easy deploy and selective collapse" origami-inspired truss structure, as illustrated by the middle panel of Fig. 4. To create such a metamaterial, I first analyzed the deformation energy of

triangulated cylinder patterns and elucidated the deployability and collapsibility from the energy and strain perspectives. This provides an inspiration to develop this metamaterial by employing a member with an asymmetric tensile and compressive behavior and leads to distinct deploy and collapse paths. A representative model was then built and its on-demand deployability and collapsibility along with tunable stiffness were characterized. This work provides an unprecedented and unappreciated perspective to achieve truly deployable and stiff origami-inspired mechanical metamaterial with great on-demand tunability, which can find tremendous applications in many fields.

2.2 Results

Deformation energy analysis of triangulated cylinder patterns

The triangulated cylinder has many identical triangles and its unit cell is highlighted in Fig. 3 and can be characterized by three parameters, namely one side *a*, two angles, α and β. The lengths of three folding lines at the planar state are given by $L_{AB} = a$, $L_{BC} = a\dfrac{\sin\alpha}{\sin\beta}$, and $L_{AC} = a\dfrac{\sin(\alpha+\beta)}{\sin\beta}$. *n* is the number of triangles to sew the right and left boundaries for a closed cylinder, i.e., *n* = 6 for Fig. 3. At the folded cylindrical state (Fig. 5), the positions of the representative unit cell ΔABC are characterized by the height *h* and twist angle ϕ between two neighboring lines in the vertical direction, as well as the radius *r* of the triangulated cylinder. Thus, the lengths of the three folding lines at the folded state are given by $l_{AB} = 2r\sin\left(\dfrac{\pi}{n}\right)$, $l_{BC} = \sqrt{h^2 - 2r^2\cos\phi + 2r^2}$, and $l_{AC} = \sqrt{h^2 - 2r^2\cos\left(\dfrac{2\pi}{n}+\phi\right) + 2r^2}$. As illustrated by Fig. 5, there are many folded

cylindrical states characterized by different height h, twist angle ϕ, and radius r, which apparently cannot be determined by three constants a, α, and β. Strains ε_{AB}, ε_{BC}, and ε_{AC} are thus introduced as variables to link these three variables (h, ϕ, and r) to three constants (a, α, and β), e.g., $\varepsilon_{AB} = \frac{l_{AB} - L_{AB}}{L_{AB}}$. For the sake of simplicity, the deformation of the panel (i.e., ΔABC) is solely concentrated at the three folding lines, AB, BC, and AC. In other words, the unit cell is represented by a three-member truss structure. Thus, the deformation energy stored in one strip as marked in Fig. 3 is given by $U = \frac{nEA}{2}\left(L_{AB}\varepsilon_{AB}^2 + L_{BC}\varepsilon_{BC}^2 + L_{AC}\varepsilon_{AC}^2\right)$, where EA is the tensile rigidity of the truss. At a given height h, i.e., a prescribed deploy/collapse height, minimization of the deformation energy U with respect to twist angle ϕ and radius r gives the folded states.

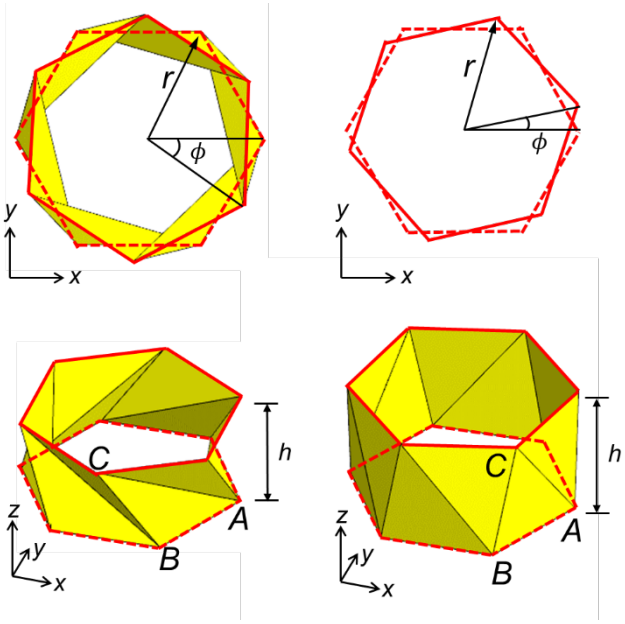

Figure 5. Geometrical parameters to define the folded states of triangulated cylinder origami.

Figure 6 shows the variation of normalized deformation energy $\frac{U}{EAL_{total}}$ and strains in *AB*, *BC*, and *AC* members during the deploy and collapse processes for the triangulated cylinder in the left panel of Fig. 4 ($\alpha = 38^{\circ}$ and $\beta = 30^{\circ}$), characterized by normalized height $\frac{h}{L_{AB}}$ with $\frac{h}{L_{AB}} = 0$ for a completely collapsed state. Here $L_{total} = n(L_{AB} + L_{BC} + L_{AC})$ is the total length of the truss members. The 3D illustrations were generated using the calculated results. The deformation energy suggests an apparent bistable states, where both the completed collapsed state and deployed state have the minimum energy. An energy barrier exists between these two equilibrium states, which indicates that this energy barrier needs to be overcome during deploy and collapse. It is observed that the strains are vanishing at the two equilibrium states and the maximum strain during the processes of deploy and collapse is approximately 1%, which is within the fracture strain of construction papers[195, 196]. The triangulated cylinder is thus clearly a deformable origami. The same deploy and collapse paths indicate this pattern does not possess on-demand or selective deployability and collapsibility.

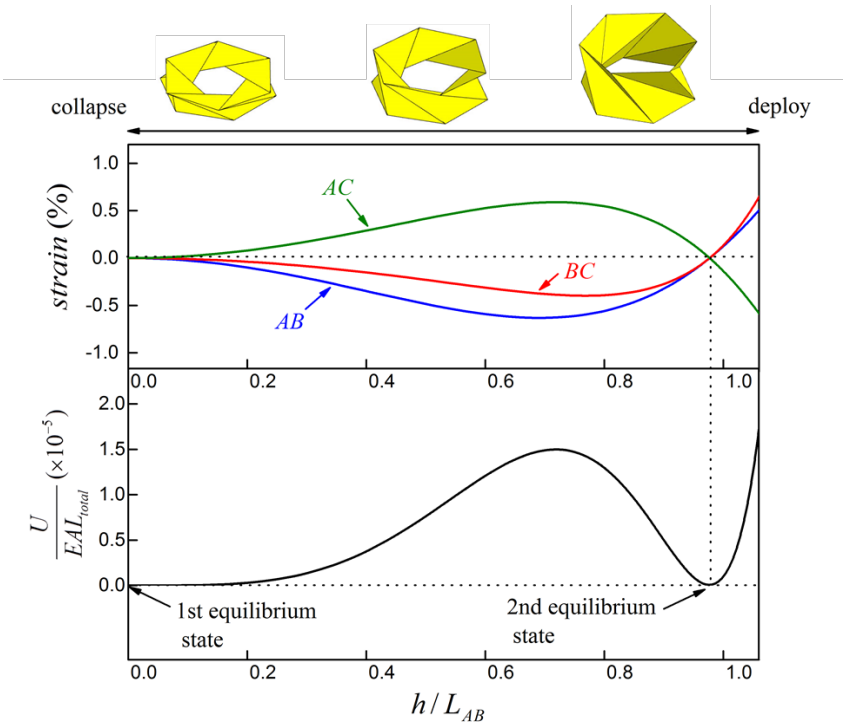

Figure 6. Energy landscapes and strain variations during the deploy and collapse processes for a collapsible pattern.

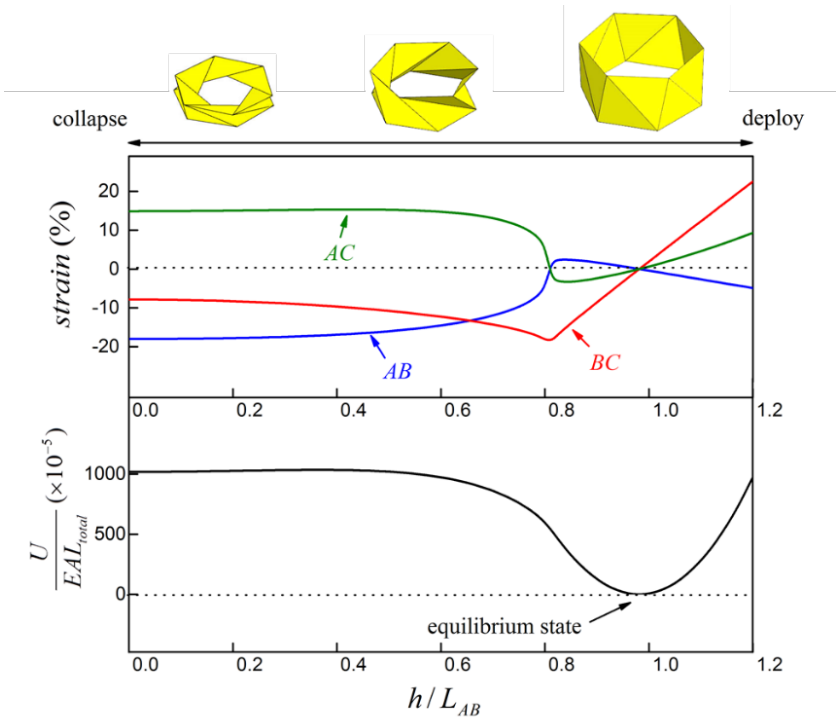

Figure 7. Energy landscapes and strain variations during the deploy and collapse processes for a load-bearable pattern.

For another triangulated cylinder shown in the right panel of Fig. 4 (with $\alpha = 50^{\circ}$ and $\beta = 50^{\circ}$), as shown in Fig. 7, qualitatively distinct deformation energy and strains present. Instead of a bistable state as in Fig. 6, the completed collapsed state is no longer an equilibrium state but rests at an elevated energy state, and only the deployed state remains at the equilibrium configuration. This energy landscape indicates that the deploy process can be autonomous since there is no energy barrier, and during collapse, there is an energy barrier to overcome. Moreover, this energy barrier is about 600 times higher than that in Fig. 6. However, this origami pattern cannot be claimed as an "easy deploy but hard collapse" pattern because of the large strain. The maximum strain exceeds 10%, which in fact explains the reason construction paper-folded pattern cannot be collapsed (right panel of Fig. 4) because a construction paper cannot bear this large strain. This pattern has been considered as non-foldable origami. However, the energy landscape indicates that this origami pattern is in fact foldable, but the required strain cannot be achieved using paper as the folding materials. Another distinct feature of this pattern is that the strain for the members varies between tension and compression. For example, *AC* truss is in tension during most of the deploy process and turns compressive right before reaching the deployed state. For collapse, *AC* member needs to be compressed and then stretched.

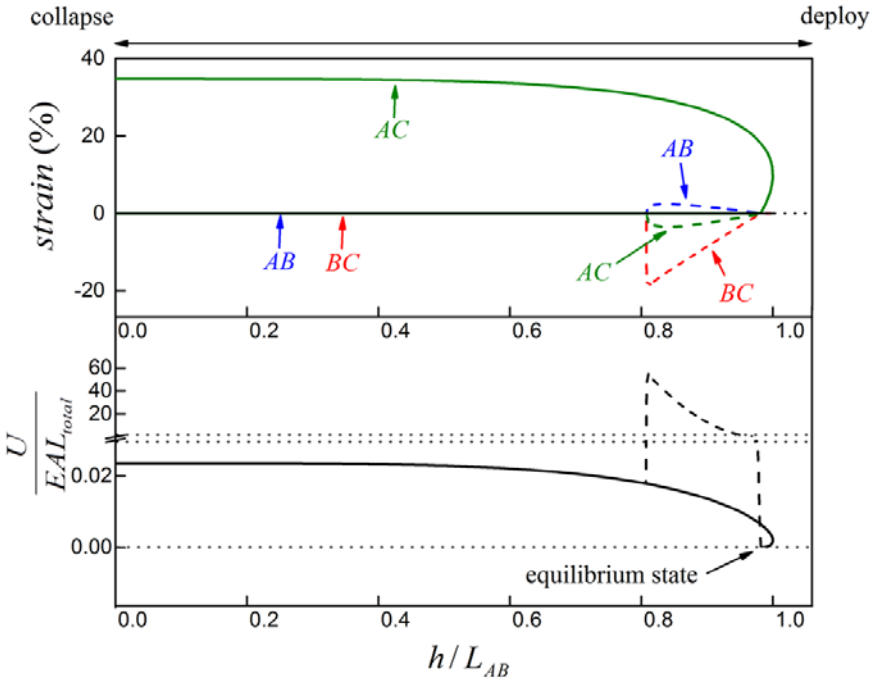

Figure 8. Energy landscapes and strain variations during the deploy and collapse processes for a mechanical metamaterial inspired by a triangulated cylinder origami.

The distinct strain variations between Fig. 6 (for $\alpha = 38^{\circ}$ and $\beta = 30^{\circ}$) and Fig. 7 (for $\alpha = 50^{\circ}$ and $\beta = 50^{\circ}$) are attributed to the measure of another angle $\angle ABC$ in the unit triangle (Fig. 3). When $\angle ABC > 90^{\circ}$, the strain in each member remains tension or compression throughout the deploy and collapse processes (e.g., in Fig. 6). When $\angle ABC < 90^{\circ}$, the strain may vary between tension and compression (e.g., in Fig. 7). The threshold is $\angle ABC = \alpha + \beta = 90^{\circ}$, which is a catastrophic point that governs the strain variations in *AC* and *AB* trusses[197]. Non-energy barrier, and particularly strain variation between tension and compression, together suggest an origami-inspired mechanical metamaterial to achieve "on-demand deploy and selective collapse".

Rationale of origami-inspired mechanical metamaterials with on-demand deploy and collapse

An on-demand deploy and collapse needs “easy deploy” and “selective collapse”. In other words, distinct and selective deploy and collapse paths are necessary. The strain paths of *AC* and *AB* trusses that vary between tension and compression suggest such a possibility: if *AC* truss is easy to be stretched and hard to be compressed, or *AB* truss is easy to be compressed and hard to be stretched, the desired distinct and selective deploy and collapse paths should become possible. For the same triangulated cylinder pattern with $\alpha = 50^{\circ}$ and $\beta = 50^{\circ}$, I have studied three combinations with asymmetric tension/compression behavior for just *AC*, just *AB*, and both *AC* and *AB*. The details of *AC* truss are provided here because it offers the most desired energy landscape and is experimentally achievable. *AC* truss is assigned an asymmetric tension/compression behavior. Its tensile rigidity is four orders of magnitude smaller than its compressive rigidity that is as the same as that for *AB* and *BC* trusses. Now the deformation energy and strain variation are shown in Fig. 8. In addition to the similar energy landscape that the collapsed state has an elevated energy and the deployed state is at equilibrium, an apparently distinct feature for the deformation energy is that during collapse, a different path appears (① -> ② -> ③ -> ④) with a much higher energy barrier for collapse. Thus, during deploy, the energy decreases and the collapsed state autonomously deploys; *AC* truss experiences large strain while other members barely deform because of the low tensile rigidity of the *AC* truss. While during collapse through path ① -> ② -> ③ -> ④, in which the strain variations are marked as the dashed lines, the energy barrier can be very high because of the high compressive rigidity. It is noted that the strain in *BC* member during

collapse (dashed line) is too high to be practically achievable and thus the high energy barrier just represents an ideal limit.

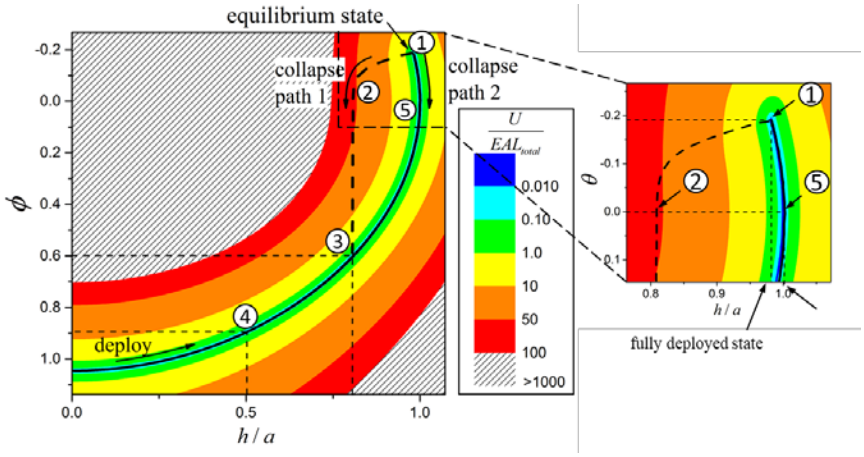

Figure 9. Energy contour showing two collapse paths.

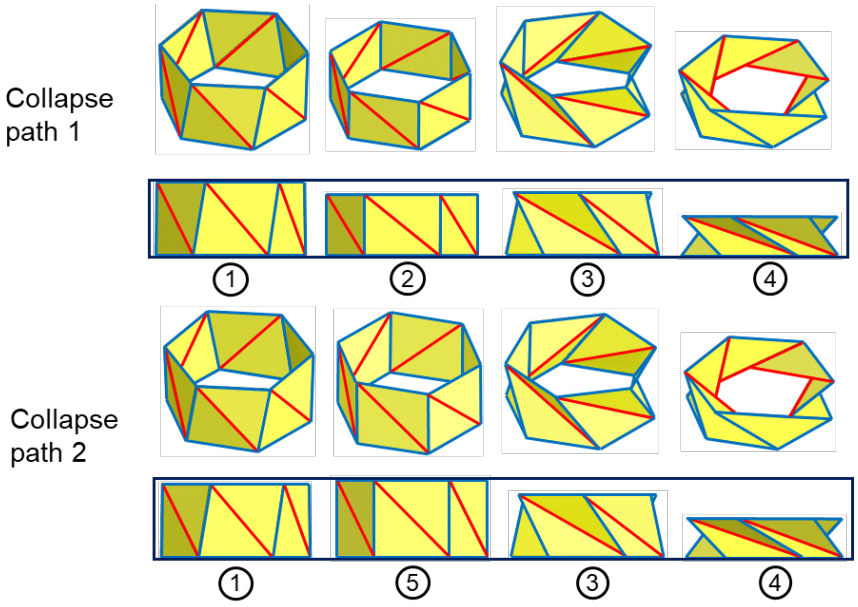

Figure 10. The configurations of the mechanical metamaterials along two collapse paths.

At the completely deployed state, a subtle feature that the height *h* is not at its extrema in fact defines two selective collapse paths. The first collapse path is distinct from the deploy path (i.e., ① -> ② -> ③ -> ④). It starts by directly compressing the structure, i.e., decreasing height *h*, and leads to a much higher energy barrier. The second collapse

path (i.e., ① -> ⑤ -> ③ -> ④) is by firstly increasing the height h (① -> ⑤) followed by a compression (⑤ -> ③ -> ④), which leads to the same path as deploy. Consequently, an on-demand deploy and collapse origami-inspired mechanical metamaterial is just created that can always be autonomously deployed and selectively collapsed, hard or easy, depending on two different paths.

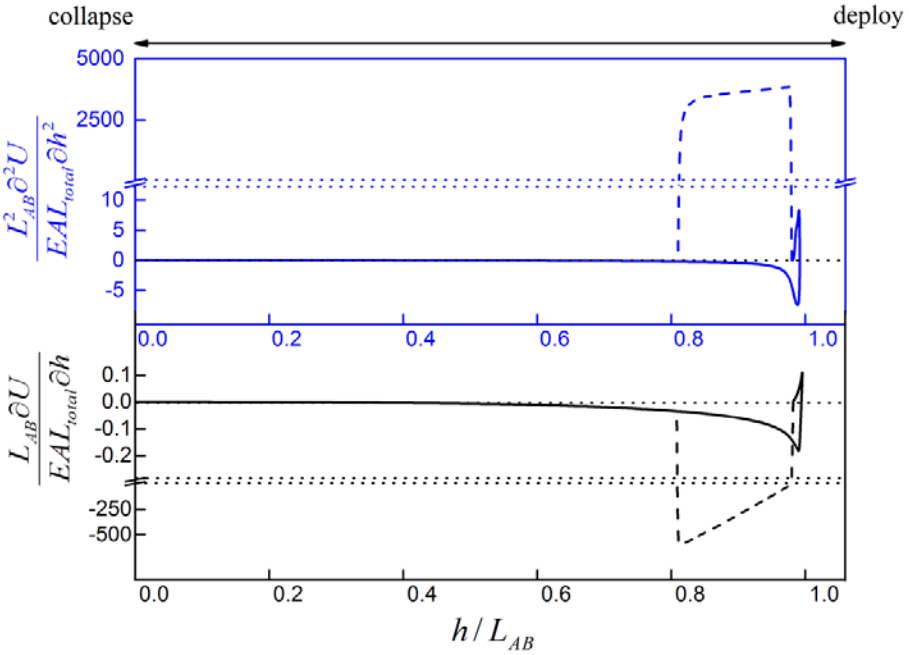

Figure 11. Tunable reaction force and stiffness of the origami-inspired mechanical metamaterial during deploy and collapse.

This new deploy and collapse property can be further shown in the contour plot of the deformation energy as a function of height h and twisting angle ϕ (Fig. 9). The deploy path is along the minimum energy "valley" from the collapsed state to the deployed state (i.e., an equilibrium state). The zoom-in near the deployed state (marked as ① in Fig. 10) shows that the deployed state does not have an extreme height h. The first collapse path (① -> ② -> ③ -> ④) involves directly decreasing the height h and thus experiences a very

high energy barrier, i.e., hard collapse. The second collapse path (① -> ⑤ -> ③ -> ④) needs to increase the height *h* to pass the extrema (⑤) and then decreasing, which leads to the same path as deploy. To pass the extrema from the deployed state, i.e., ① -> ⑤, a tensile load in the axial direction (i.e., along the deploy direction) or a torque to change the twisting angle ϕ needs to be applied. The 3D configurations (i.e., ① to ⑤) are based on the calculated results.

This structure also has tunable axial reaction force and stiffness. The normalized axial reaction force $\frac{L_{AB}}{EAL_{total}}\frac{\partial U}{\partial h}$ and stiffness $\frac{L_{AB}^2}{EAL_{total}}\frac{\partial^2 U}{\partial h^2}$ are provided in Figs. 11. At the collapsed state, both the reaction force and the stiffness are infinitesimal, which suggests just a vanishing force is needed to hold the collapsed structure. At the deployed state, for the easy collapse path (① -> ⑤ -> ③ -> ④), a very small axial force, in tension and then in compression is needed to collapse the structure. The corresponding stiffness is also low. It is apparently different from that for the hard collapse path (① -> ② -> ③ -> ④), a compressive axial force with magnitude $\left|\frac{L_{AB}}{EAL_{total}}\frac{\partial U}{\partial h}\right| \approx 12,000$ (2,000 time higher than that for the easy deploy path) needs to be applied in order to collapse the structure. The corresponding stiffness is also 3 orders of magnitude higher than that for the easy deploy path.

As can be imagined, the variation of deformation energy strongly depends on the geometry of the crease patterns, specifically, the number of triangles in the circumferential direction *n*, angles α, and β. Another pattern was also studied, with $n = 4$, $\alpha = 50^\circ$, and

$\beta = 50^\circ$. The pattern has a collapsed state with elevated energy and an equilibrium state for a deployed configuration. Also, distinct deploy and collapse paths also present when the asymmetric tension/compression behavior is prescribed. It also confirms that the condition $\alpha + \beta \geq 90^\circ$ leads to this behavior and *n* does not play an important role. Thus, these two structures all suggest an on-demand deployability and collapsibility: autonomous deployability and selective collapsibility.

Deformation energy analysis of triangulated cylinder with *n* = 4, $\alpha = 50^\circ$, and $\beta = 50^\circ$

However, there is still an energy barrier to overcome from the collapsed to deployed states, which is similar to that shown in Fig. 6. This energy barrier is about 300 times higher than that in Fig. 2a. For strain variations, the maximum strain exceeds 10%, such that a construction paper-folded pattern cannot be collapsed because a construction paper cannot bear this large strain. Also, similar to the strains in Fig. 2b, strains vary between tension and compression. For example, AC truss is in tension during the most of the deploy process and turns compressive right before reaching the deployed state.

The energy landscape and strain distribution for the triangulated cylinder with *n* = 4, $\alpha = 50^\circ$ and $\beta = 50^\circ$ are shown in Fig. 12. It can be seen that this pattern shows very similar feature as that for *n* = 4, $\alpha = 50^\circ$ and $\beta = 50^\circ$. Specifically, the completed collapsed state is at a higher energy state and the deployed state remains at an equilibrium configuration. However, there is still an energy barrier to overcome from the collapsed to deployed states, which is similar to that shown in Fig. 6. This energy barrier is about 300 times higher than that in Fig. 6. For strain variations, the maximum strain exceeds 10%, such that a construction paper-folded pattern cannot be collapsed because a construction paper cannot

bear this large strain. Also, similar to the strains in Fig. 7, strains vary between tension and compression. For example, AC truss is in tension during the most of the deploy process and turns compressive right before reaching the deployed state.

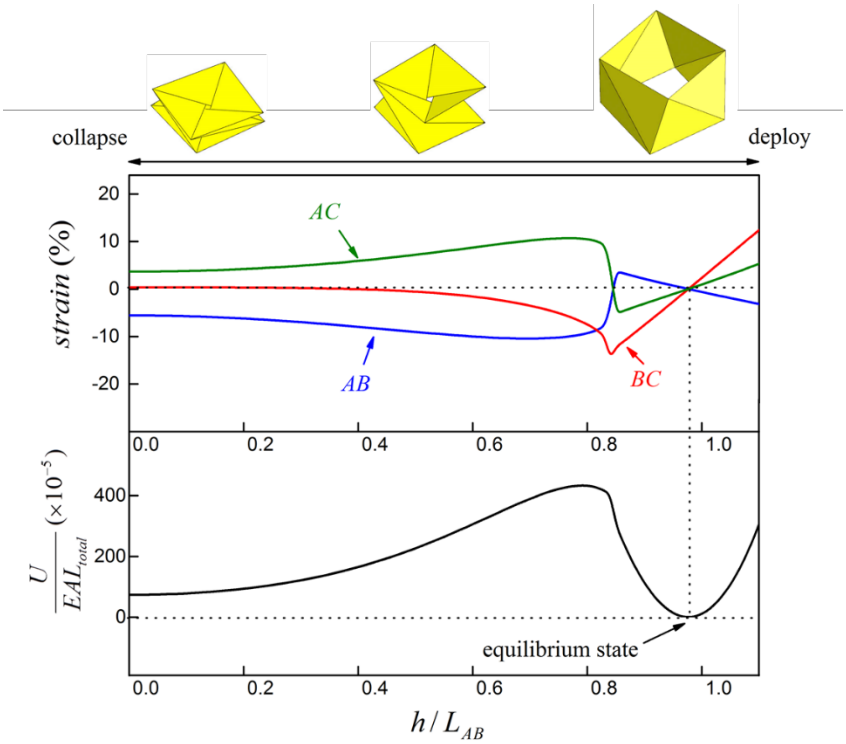

Figure 12. Energy landscapes and strain variations during the deploy and collapse processes for origami with n = 4.

Similar to Fig. 8, AC member is assigned asymmetrical tension and compression behavior. Figures 13 and 14 show the energy landscape, strain variations, and stiffness. This pattern again shows autonomous deploy and selective collapse as there are two collapse paths, with one for easy collapse and one for hard collapse.

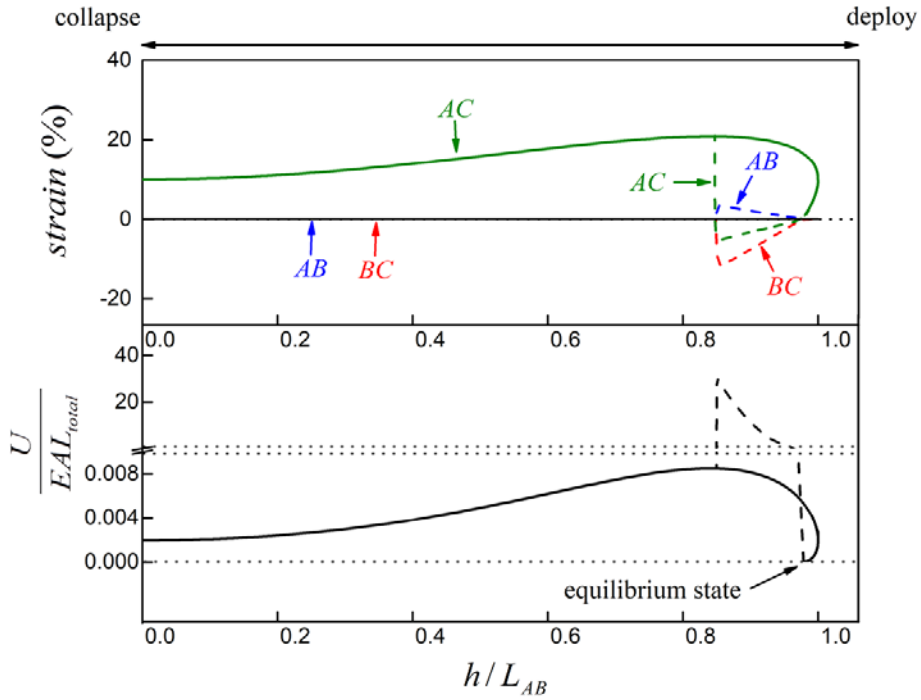

Figure 13. Energy landscapes and strain variations during the deploy and collapse processes for a mechanical metamaterial with n = 4.

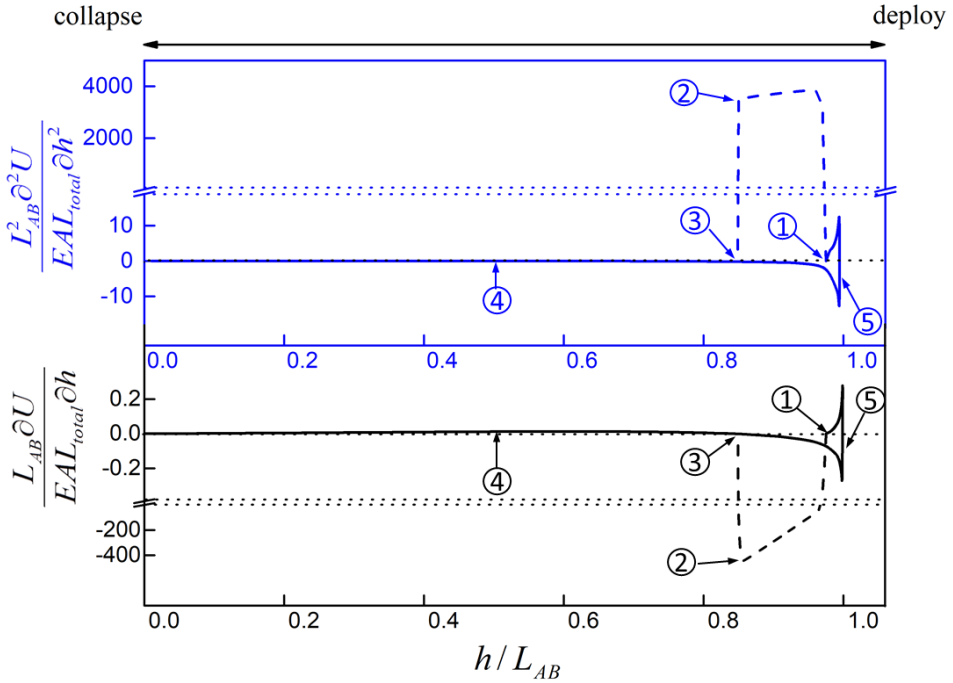

Figure 14. Tunable reaction force and stiffness of the origami-inspired mechanical metamaterial with n = 4.

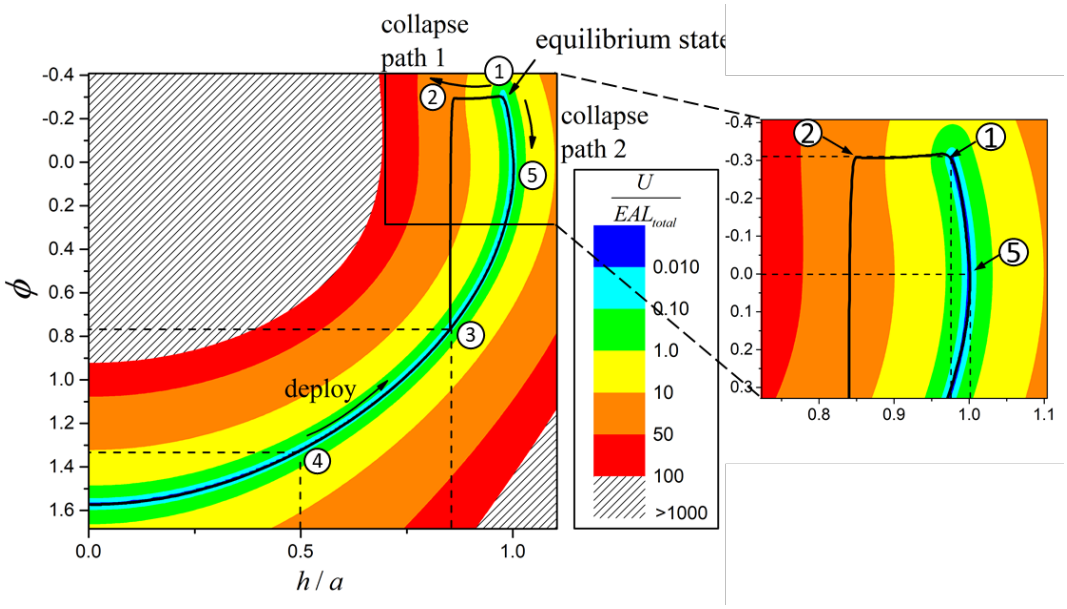

Figure 15. Energy contour showing two collapse paths of metamaterials with n = 4.

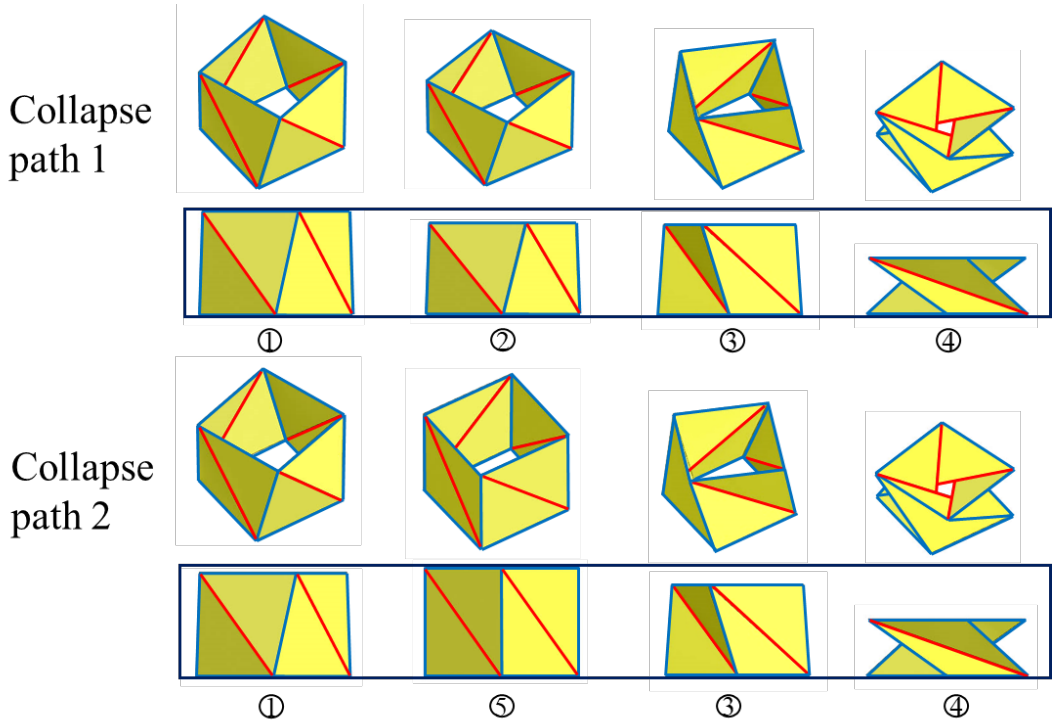

Figure 16. Two collapse paths of metamaterials with n = 4.

Experimental realization of on-demand deployable and collapsible origami-inspired mechanical metamaterials

To realize the merit of on-demand deployability and collapsibility, models were built using standard components, such as bolts, rod end bearing, springs, tubes, and acrylic plates. Figure 20 shows the deployed and collapsed states. The list and details of the components are provided in Table 1**.** The key component to achieve the tension/compression asymmetrical behavior is *AC*, consisting of a spring inside a tube, where the spring bears tension while the tube resists compression. Rod end bearing enables smooth rotation at the joints. The design has deployability and selective collapsibility yet strong load bearing capability of the mechanical metamaterial. I characterized the load bearing capability of this origami-inspired mechanical metamaterial by directly placing the deployed structure between two plates of a uniaxial compression machine, and the load/displacement curve is shown in Fig. 21, provided with a few representative snapshots of the metamaterial during compression. For the 1st compression, the maximum load approached 2,700 N, more than 1,600 times of the weight of this metamaterial (~160 g). Beyond the peak compressive load, a few *BC* members fractured and the load dropped. The fractured members after compression is consistent with the strain variation in Fig. 8 where *BC* member bears larger strain while being collapsed along the path 2, i.e., hard collapse path. After the 1st compression, the structure can still be deployed and collapsed, though with a few *BC* members fractured. Then the deployed structure with a few fractured *BC* members after the 1st compression was subjected to the 2nd compression. The peak load can achieve ~ 1,500 N, which is still 900 times its weight. This defected structure is still deployable and collapsible, though the collapsed configuration is not perfect. A 3rd compression was run and again this very damaged structure can still carry significant load

~ 1,500 N. With more *BC* members fractured after the 3rd compression, the on-demand deployability and collapsibility still present. These observations confirm this origami-inspired metamaterial possesses on-demand and defect insensitive deployability and collapsibility. The unprecedented load bearing capability leads to more practical applications.

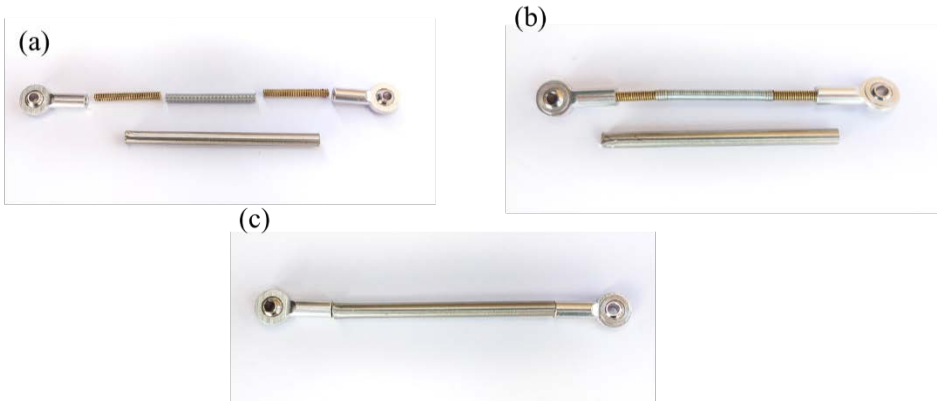

Figure 17. A spring inside a tube to achieve tension/compression asymmetry.

Figure 18. Rod end bearing which enables smooth rotation.

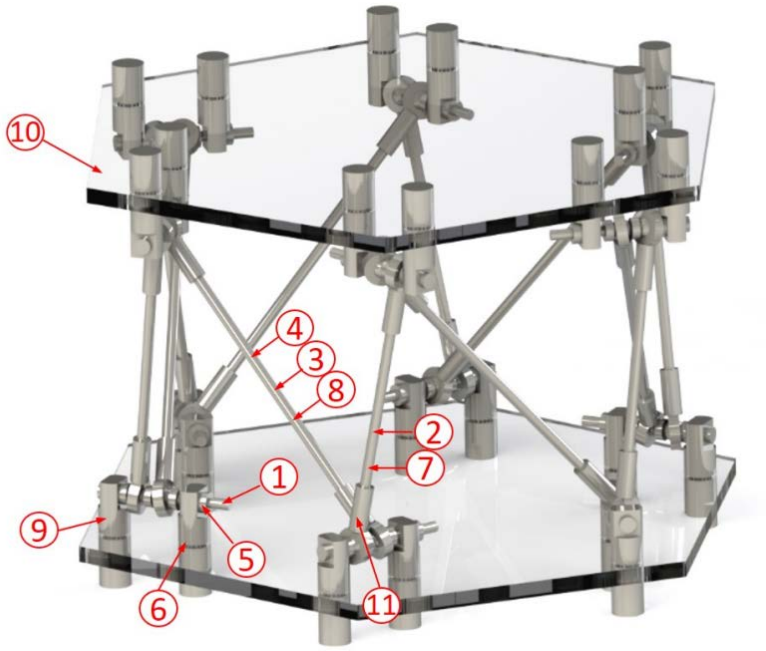

Figure 19. SolidWorks model for the truss-based mechanical metamaterial.

Table 1. List of components to build the truss-based mechanical metamaterial

No.	Description	Quatity
1	M2 × 10mm screw	12
2	M2 × 25mm screw	12
3	M2 × 40mm screw	6
4	Spring	6
5	M2 hex nut	48
6	M4 hex nut	48
7	Tube 2mm × 27mm	6
8	Tube 2mm × 43mm	6
9	Customized M4 × 20mm screw	24
10	Customized PMMA	2
11	Rod end bearing	24

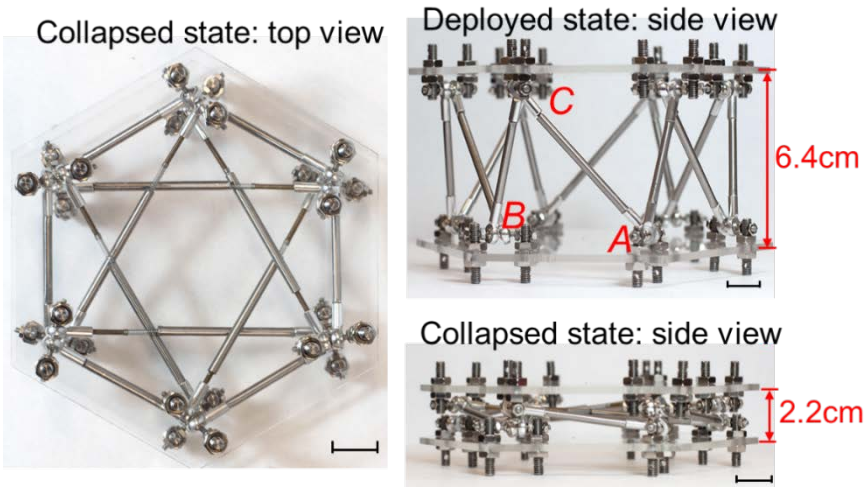

Figure 20. Photos of the structure at the deployed and collapsed states.

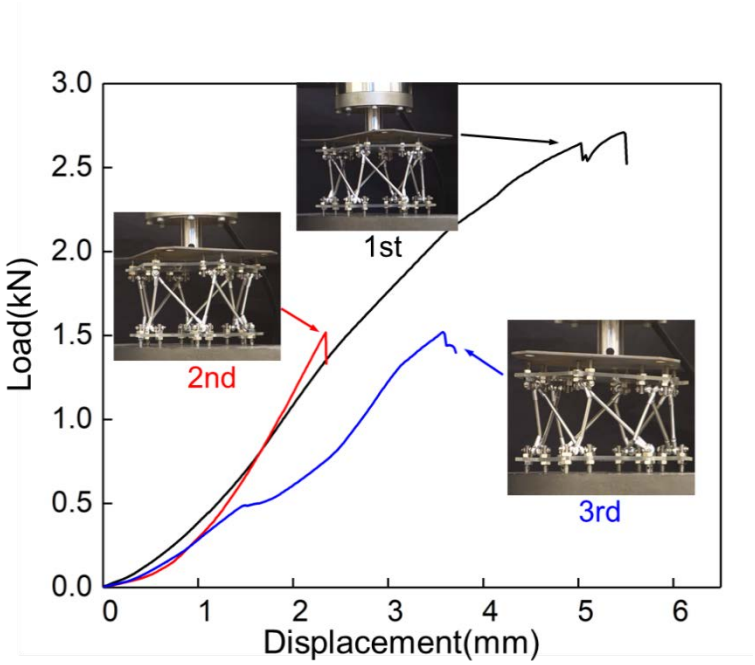

Figure 21. Load versus displacement curve for the metamaterial under compression.

As shown in Fig. 22, simpler version of this origami-inspired mechanical metamaterial can be built by just using construction papers and rubber bands. A rubber band inside of a tube made of construction paper functions as the asymmetric tension/compression member. The similar load bearing and on-demand deployability and selective collapsibility have been achieved.

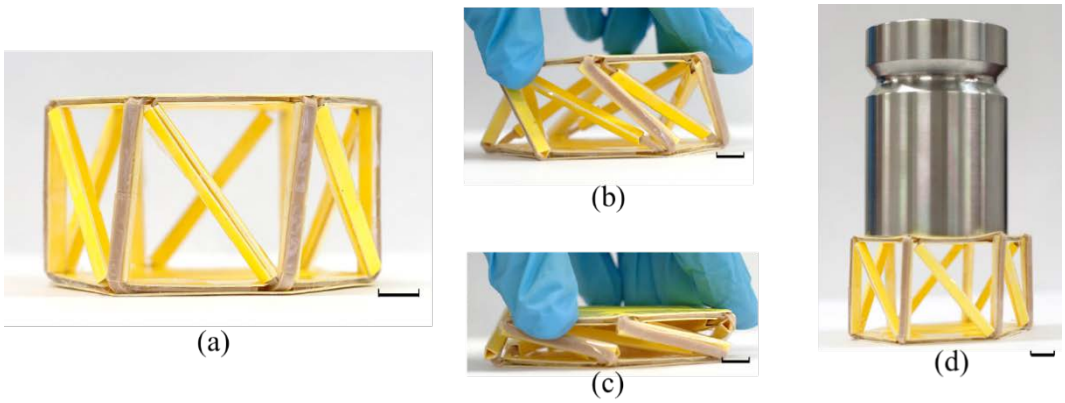

Figure 22. Rubber band design of the origami inspired metamaterial.

2.3 Discussion

We have introduced an on-demand deployable and selectively collapsible origami-inspired mechanical metamaterial whose configurations and stiffness are greatly tunable, depending on different states and loading paths, which leads to many unprecedented applications as reconfigurable and stiff mechanical metamaterials. The principle discovered in this work can be readily applied to other metamaterials. Still taking triangulated cylinder as an example, one can simply increase number of triangles (i.e., *n*) to create a deployable cylinder or tube with great axial stiffness. By altering the angles α and β with $\alpha+\beta \geq 90^{\circ}$, the strains can be designed eventually across *AB*, *BC*, and *AC* members during the hard collapse path and all strains do not exceed the fracture threshold of the constitutive materials; thus, one can create on-demand deployable and very stiff mechanical metamaterials. The lesson to create such a metamaterial can be greatly extended to other structures by achieving non-monotonic strain path, or in other words, deformable origami with interesting strain path. Though deformable origami was not extensively studied or discovered, one can create deformable origami patterns using rigid origami as the building block. For example, two Miura unit cells can be brought together

to form composite, deformable origami patterns. The similar approach has been utilized to create a Miura tube[185], though this tube is a rigid origami because it satisfies a certain constraints. Without these constraints, the formed composited origami patterns are in general deformable. It is expected that this work can be employed to create more versatile mechanical metamaterials with tunable deployability and stiffness.

CHAPTER 3

ORIGAMI WITH TUNABLE STIFFNESS

3.1 Introduction

The stiffness of a material or a structure is of key importance in most, if not all, applications, with positive stiffness as a common property for bearing loads and transferring motion [198], zero (or quasi-zero) stiffness for vibration isolation and protection [199], and negative stiffness for fast switching between states [200], high-speed actuation [201-203], and programmed deformation [204]. Many species possess ingenious mechanisms to switch among different stiffnesses to maintain motion, save energy, or deliver high power [205, 206]. Scientists and engineers have also deliberately created various means to manipulate stiffness for various applications, including in automotive [207], robotics [208], and aerospace components [209]. However, these mechanisms are rather complicated (e.g., spring structures) and often require considerable energy inputs (e.g., electromagnetic and piezoelectric mechanisms [203, 210]), which unfortunately cannot be employed in size-limited applications (e.g., small robots [211], soft robots without rigid parts [212] or passive systems without power input [213]), even though these applications may represent the true need for in situ stiffness manipulation. To somewhat circumvent the complex structures and expensive energy input, mechanical metamaterials have been designed to achieve stiffness manipulation using simple mechanisms [40, 95, 214, 215]; however, for a given metamaterial, the range of manipulation is limited and cannot switch all the way from positive to negative. Mechanical metamaterials with elegant mechanisms for manipulating the stiffness of the structure in situ covering positive, zero, and negative ranges are highly desired.

Origami provides an elegant means to design metamaterials with tunable properties, such as diverse spatial configurations [40, 216-218], on-demand deployability [7], controllable multistability [219], and tunable thermal expansion [65] and stiffness [7, 40, 54, 64, 95, 220]. However, these strategies for tunable stiffness cannot achieve in situ stiffness manipulation, i.e., the stiffness cannot be altered on demand once the pattern is determined. In addition to the incapability for in situ stiffness manipulation, note that the current origami-based metamaterials are solely based on straight-creased patterns, particularly the so-called rigid origami patterns, in which the deformation energy is theoretically only stored at the creases, not in the origami panels. For example, the well-known Miura pattern and its derivatives have been extensively utilized [4, 40, 95, 220]. Though simple, rigid origami patterns have an inherent limitation when used for tunable stiffness, a single energy input from the folding of creases leads to a simple energy landscape and thus a limited range of stiffness tunability. To create a complex energy landscape, another energy input should be considered: energy in the origami panels. Deformable origami falls in this category, although the candidate patterns are very limited [7]. In addition to in-plane energy in the panel, bending energy in the panel can also be introduced. By combining folding energy at the creases and bending energy in the panel, curved origami can be created [109]. In contrast to straight creases, there can be multiple curved creases between two points rather than just one straight crease [221]. The competition between bending energy in the panel and the folding energy at the creases, along with multiple curved creases between two points, would lead to in situ stiffness manipulation covering positive, zero, and negative ranges, which forms the key aspects of this paper.

In this dissertation, I designed a family of curved origami-based metamaterials for in situ stiffness manipulation. A specific unit cell of curved origami-based metamaterials was studied, which can be manipulated in situ to exhibit positive, zero, or negative stiffness and functions as a fundamental building block to design curved origami-based metamaterials with different stiffnesses. Then, three applications were presented to demonstrate the unique functions of the metamaterials: a curved origami-based gripper with a negative-stiffness rapid mode or a positive-stiffness precise mode, curved origami cubes for in situ switching between a zero-stiffness vibration isolation mode and a positive-stiffness responsive mode, and a two-dimensional modular metamaterial for programmable, multistage stiffness responses upon homogenous loading. This work provides an unprecedented principle for curved origami-based mechanical metamaterials for in situ manipulation of stiffness in full ranges, which can be applied in many fields.

3.2 Results

Rationale of curved origami-based in situ stiffness manipulation

We started by studying two fundamental deformation modes of origami, namely, crease folding and panel bending, with the former for the deformation between creases and the latter for that in the panel. Figure 23 shows the simplest folding (hereinafter referred to as “folding I”) where a horizontal valley crease (marked by a dashed line) is subjected to a compressive load F in the vertical direction. As rigid origami, the only resistance during compression is from the bending at the creases, which provides positive stiffness during the 1st loading cycle. Upon unloading, the plastic deformation leads to a permanent shape and defines the folded state. The 2nd loading cycle follows the unloading path of the 1st

cycle, and the subsequent loading/unloading cycles follow the same route. Another folding mode (hereinafter referred to as “folding II”) is when the folding direction is close to the loading direction (Fig. 23), where a common cell for quadrilateral rigid origami (e.g., Miura pattern)—a single-vertex, four-crease pattern with an angle $\beta = 80^\circ$ between a mountain crease (marked by solid line) and valley creases (marked by dashed lines)—is subjected to a compressive force F in the vertical direction. Upon compression, this rigid origami exhibits a higher positive stiffness than that shown in Fig. 23. In fact, as shown in the analytical analysis in the Appendix B, for an ideal rigid origami, the initial positive stiffness should be infinite. Then, this positive stiffness quickly transitions to a negative stiffness due to the snap-through at the two vertical valley creases. Theoretical analyses and experimental tests have shown that a positive to negative stiffness transition appears for larger β angles. Upon unloading, this pattern has plastic deformation, which is also observed in other “folding II” deformations with different β angles. The 2nd loading cycle follows the unloading path of the 1st cycle and does not exhibit negative stiffness, because the permanent folded state after the 1st load has exceeded the critical point for the snap-through of the vertical creases. These two types of crease folding describe the key features of rigid origami: positive stiffness from the creases perpendicular to the loading direction and negative stiffness from the creases close to the loading direction due to snap-through, though the negative stiffness may not reappear after the 1st loading cycle. The third deformation mode is simply a bending mode, which provides positive stiffness and elastic deformation (Fig. 23). When the vertical straight creases are replaced with a curved crease and the horizontal creases are replaced by the bending mode, curved origami appears.

Depending on the curvature of the curved crease, negative stiffness may occur during compression due to the snap-through when the curvature is small (corresponding to a larger β angle for straight creases), whereas the bending mode provides positive stiffness. Connecting two points, there can be multiple curved creases with different curvatures (κ_1, κ_2, κ_3) and possibly different stiffnesses (H_1, H_2, H_3) via means such as creases with different thicknesses (Fig. 24), which would provide a means to switch in situ between different modes for various stiffnesses. This is the rationale to use curved origami for stiffness manipulation.

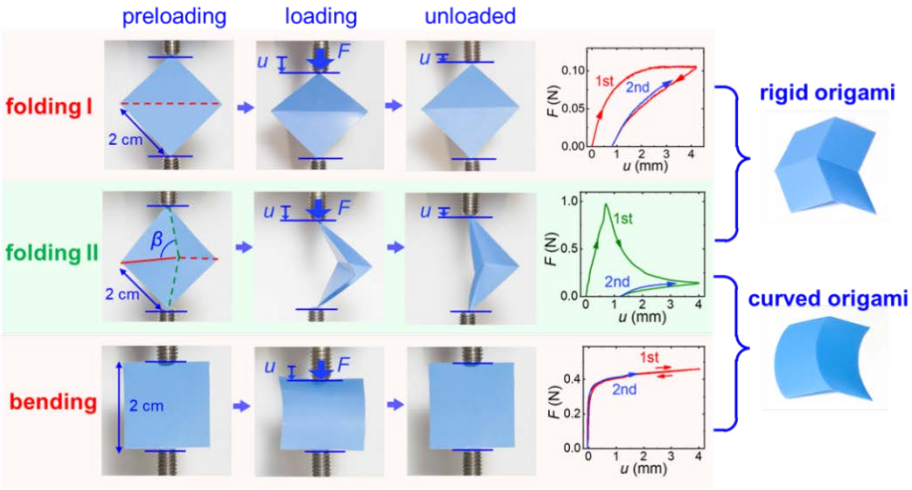

Figure 23. Mechanical behaviour of a unit cell of the Miura origami

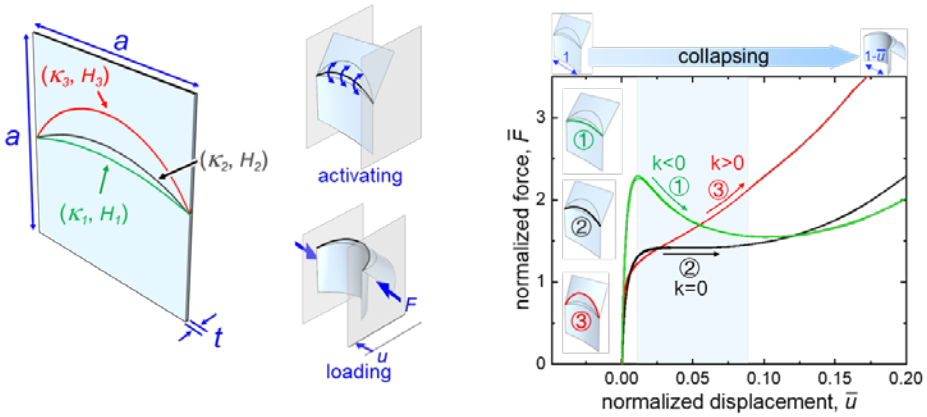

Figure 24. Mechanical behaviour of a unit cell of the curved origami

Finite element simulations were conducted in ABAQUS to study the stiffness of the square-shaped panel (length *a*, thickness *t*, and elastic modulus *E*) with the coexistence of three arc-shaped creases (curvatures κ_1, κ_2, and κ_3) in the middle (Fig. 24). Details of the finite element simulation can be found in APPENDIX B. The crease modulus *H* is defined as the applied bending moment per folding angle per crease length and is normalized as $\bar{H} = \frac{Ha}{Et^3}$. The arc-shaped crease can be activated by applying a bending deformation α = 70° (Fig. 24), and then a compressive load is applied (Fig. 24). For a specific crease modulus $\bar{H}_1 = 0.07, \bar{H}_2 = 0.03, \text{and } \bar{H}_3 = 0.01$, the deformed configurations and the relationship between the normalized force $\bar{F}$ ($= \frac{Fa}{Et^3}$) and the compressive displacement $\bar{u}$ ($= \frac{u}{a}$) are shown in Fig. 24. Clearly, the same square with different creases has different stiffness values, which can be positive, zero, or negative, as highlighted in the blue shadowed area. Specifically, crease ① (shown in green) with a smaller curvature κ_1 exhibits negative stiffness due to the snap-through similar to the folding II mode in Fig. 23, crease ② (shown in black) with a median curvature κ_2 exhibits zero stiffness, and crease ③ (shown in red) with a larger curvature κ_3 exhibits positive stiffness. Hence, hereinafter, I use red, black, and green to represent positive, zero, and negative stiffness, respectively. Thus, the correlation between the curvature and the origami stiffness provides an elegant way to manipulate stiffness.

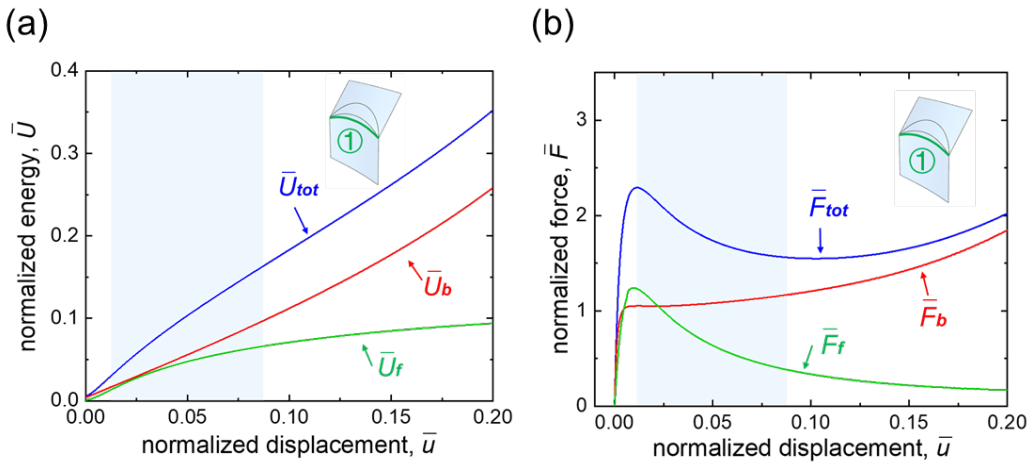

Figure 25. Normalized total energy, bending energy, and folding energy of the curved origami with crease 1 activated as a function of normalized displacement.

Figure 25 presents the essential mechanism for using curved origami to provide in situ stiffness manipulation. During the collapse of curved origami, there are two parts of deformation energy: panel bending energy and crease folding energy. For curved origami with only crease ① activated (Fig. 24), the normalized bending energy in the panel $\bar{U}_b$ ($=\frac{U_b}{Et^3}$), the folding energy at the curved crease $\bar{U}_f$ ($=\frac{U_f}{Et^3}$), and the total energy $\bar{U}_{tot}$ ($=\frac{U_{tot}}{Et^3}$) are plotted for various displacements $\bar{u}$ ($=\frac{u}{a}$) in Fig. 25 (a). The total normalized reaction force $\bar{F}_{tot}$ ($=\frac{Fa}{Et^3}=\frac{\partial \bar{U}_{tot}}{\partial \bar{u}}$), which is the derivative of the energy with respect to the displacement, can also be divided into two parts: $\bar{F}_b$ ($=\frac{\partial \bar{U}_b}{\partial \bar{u}}$) due to panel bending and $\bar{F}_f$ ($=\frac{\partial \bar{U}_f}{\partial \bar{u}}$) due to folding at the crease, which are plotted in Fig. 25 (b) for crease ①. It is found in all cases that the forces due to panel bending $\bar{F}_b$ and crease folding $\bar{F}_f$ are increasing and decreasing during compression, respectively. Now, it is clear that the

bending deformation of the panel provides positive stiffness, whereas the folding at the curved crease provides negative stiffness. By adjusting the contributions of the panel and crease, positive, zero, and negative stiffness can be achieved.

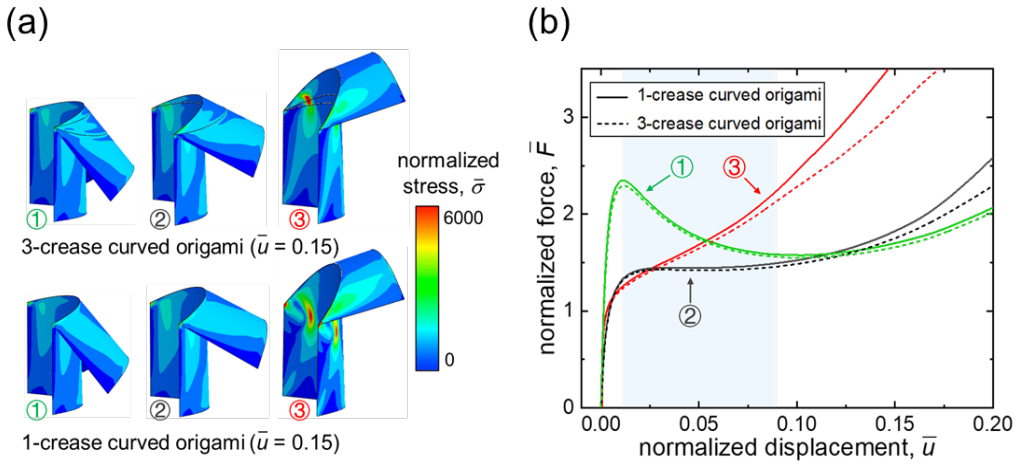

Figure 26. Comparison of the deformation, stress contour, and force-displacement relationship for curved origami with three coexisting creases but only one activated crease and its counterpart with only one curved crease.

Individual activation of one of multiple coexisting curved creases without (or with negligible) interference is a required characteristic for in situ stiffness manipulation using curved origami. To verify this characteristic, Fig. 26 (a) compares the deformation and stress contour for curved origami with three creases but only one activated crease (Fig. 24) and its counterpart with only one curved crease at a given normalized displacement $\bar{u} = 0.15$. It is clear that these two scenarios are undifferentiable at a given displacement. The relationship between the reaction force $\bar{F}$ and displacement $\bar{u}$ for curved origami with three creases but only one activated crease and its counterpart with just one crease is shown in Fig. 26 (b), where negligible differences are observed for a given displacement range $0.025 < \bar{u} < 0.075$ for all three curvatures. Moreover, finite element simulations show that only one crease can be activated at a given time, thus ensure the precise control of

creases. The negligible interference among the curved creases suggests that the design principle for a single curved crease can be applied to design curved origami with multiple curved creases, providing astounding merit to build a universal phase diagram of a single curved crease through two control parameters: normalized curvature $\bar{\kappa}$ $(=\kappa a)$ and crease modulus $\bar{H}$ $(=\frac{Ha}{Et^3})$. Figure 27 (a) provides such a phase diagram for a single crease with a normalized curvature $0.4<\bar{\kappa}<1.8$ and a crease modulus $0.01<\bar{H}<0.09$. More than 400 cases were simulated through finite element analysis to calculated the stiffness $\bar{k}$ $(=\frac{ka^2}{Et^3})$, and an interpolation was conducted to smooth the plotting. It is observed that by changing the two control parameters $\bar{\kappa}$ and $\bar{H}$, one can readily design curved origami that exhibits a wide spectrum of stiffness $\bar{k}$ $(=\frac{ka^2}{Et^3})$, including positive, zero, and negative values. Given that it is not operationally trivial to change the crease modulus $\bar{H}$ and that it is relatively easy to alter the curvature $\bar{\kappa}$, I presented a relationship between the reaction force $\bar{F}$ and the displacement $\bar{u}$ for a given crease modulus $\bar{H}=0.05$ and varying crease curvatures $\bar{\kappa}=0.4, 0.8, 0.9, 1.4, \text{and}\, 1.7$ in Fig. 27 (b), where the dots in dark red to dark green are also shown in Fig. 27 (a). This figure again shows that in practice, one can achieve positive, zero, and negative stiffness by simply changing the curvature of a crease. Given the negligible interference among different creases, Fig. 27 (a) essentially provides a design map to create origami with multiple curved creases with any range of stiffness manipulation in two steps: (1) choosing a desired value of stiffness $\bar{k}$ from the stiffness phase diagram and (2) then locating the corresponding crease curvature and crease modulus.

I will demonstrate the in-situ stiffness manipulation of curved origami using the following three applications.

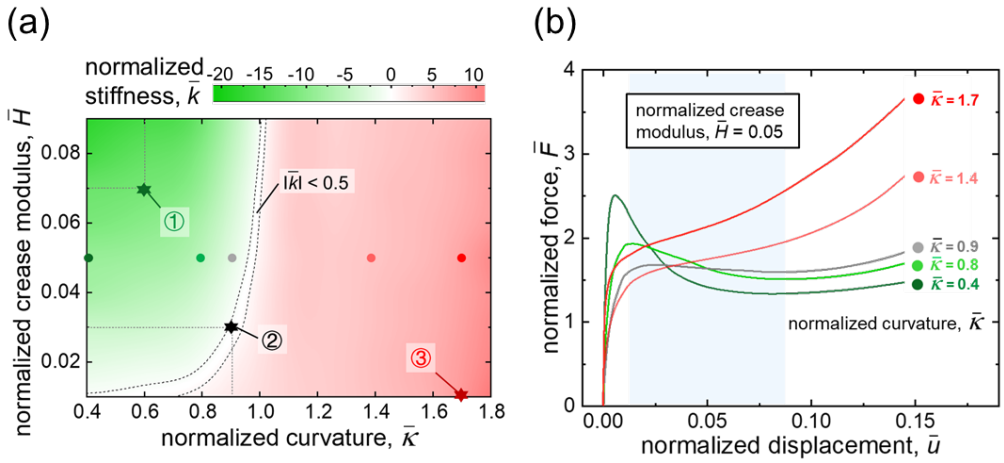

Figure 27. Phase diagram of normalized stiffness for single-crease curved origami with different normalized curvature and crease modulus

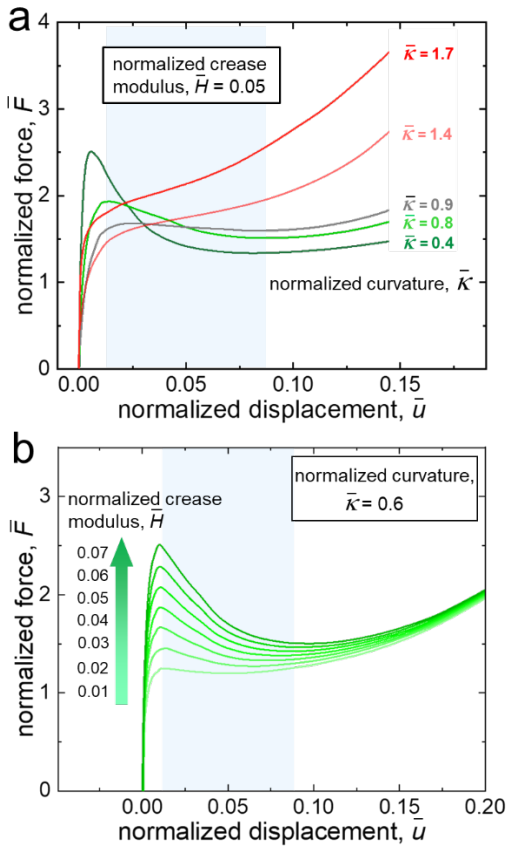

Figure 28. Force-displacement relationship of single crease curved origami.

Demonstration I: A lightweight, universal gripper

The first demonstration is a lightweight, universal gripper with two modes: a negative stiffness mode for fast gripping and a positive stiffness mode for precise gripping. The gripper consists of two plastic films: one handler with an ON/OFF switch for fast and precise gripping and one clipper for gripping objects (Fig. 29). The ON/OFF switch is realized by activating two curved creases (dashed green lines, $\bar{\kappa}$ = 0.46, and $\bar{H}$ = 0.072) with negative stiffness ($k = \frac{\Delta F}{\Delta u} = -0.489$ N/mm at 0.3 mm < u < 2 mm; k = -0.016 N/mm at 3 mm < u < 12 mm) for ON and deactivating the creases for OFF (k = 0.001 N/mm at 0.3 mm < u < 12 mm). The clipper has two curved creases (solid red lines, $\bar{\kappa}$ = 1.68, and H = 0.072) and has a positive stiffness (k = 0.109 N/mm at 0.3 mm < u < 12 mm) for actual gripping. The two pieces are connected by tape, as shown in Fig. 29 (a). The overall stiffness of the gripper can be switched between ON and OFF modes by (de)activating the green curved creases. Top and side views of the gripper in the ON and OFF modes are shown in Fig. 29 (b). Rubbery pieces were added to increase friction for gripping. To trigger the gripper to switch between ON and OFF modes, one can easily apply bending on the green curved creases to lock the gripper in a desired mode. Figure 29 (c) shows the force vs. displacement relationship for the ON/OFF modes. Under the same precompression with displacement u_0 at point A, the ON mode needs a larger preload than the OFF mode, i.e., $F_{ON} > F_{OFF}$. Under displacement-controlled loading, the ON mode has a smaller force increment ΔF_{ON} to reach the peak force, and then a snap-through occurs, causing an instantaneous jump to the final state at point B with displacement u_1, whereas

for the OFF mode, the force gradually increases to the peak with a larger force increment ΔF_{OFF}. It is clear that because of the negative stiffness for the ON mode, high power can be achieved through instantaneously large deformation from $u_0 = 0.5\,\text{mm}$ at the initial state to the final state $u_1 = 11.6\,\text{mm}$, whereas for the OFF mode, monotonically increased gripping force can achieve precise handling.

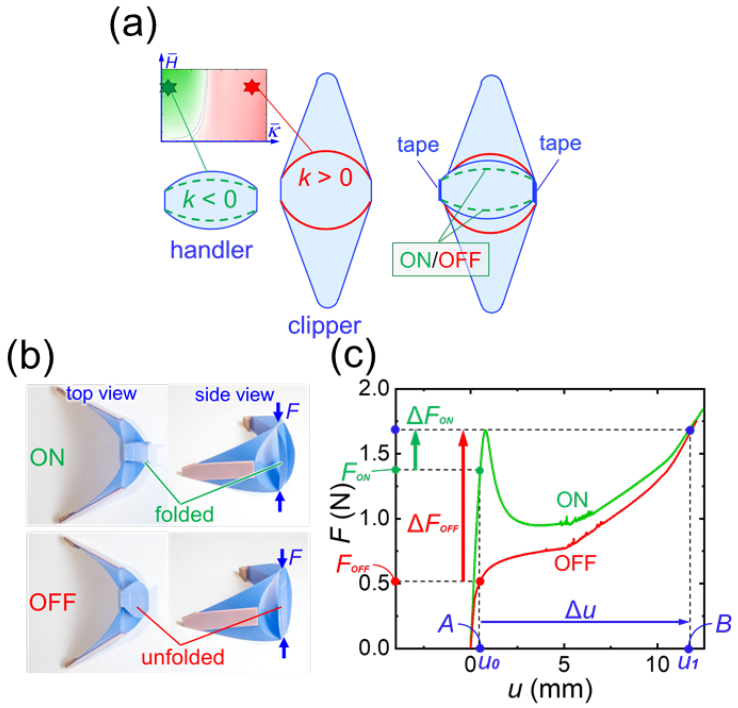

Figure 29. Design and testing of a curved origami-based lightweight, universal gripper.

We conducted experiments to grip different objects with both modes in Fig. 30 to demonstrate the importance of switching between ON and OFF modes. For easy-to-grip objects, which are of medium size and regular shape and have a frictional surface, the ON mode will save much time with rapid actuation. In Fig. 30 (a), when the ON mode is activated, the gripper spent 0.033 s (0.029 s before snap-through and 0.004 s after snap-through) with a speed of 10 m/s (40 mm in 0.004 s), whereas 0.504 s elapsed in the OFF

mode. The speed of gripping is higher than the speed of a frog's tongue when capturing prey (1.67 m/s; 50 mm in 0.030 s [222]). Compared with the OFF mode, the ON mode for gripping objects such as a Lego block saves up to 0.471 s (i.e., 93.5% of the time), providing a means for high-efficiency gripping. However, there are also some hard-to-grip objects. Though the ON mode saves time, it may not be successful or even do harm to the objects. An example is a grain of rice (Fig. 31 (b)), which is small, lightweight, and irregularly shaped. Using the ON mode to grip results in the rice slipping and being kicked away. Using the OFF mode can accurately grip rice without slipping. Another example is soft objects that are likely to be damaged for fast gripping. In Fig. 31 (c), soft tofu (modulus = 8.005 kPa, strength = 3.298 kPa, and toughness = 875 J/m^2) is damaged when gripping with the ON mode, whereas it is safely and effectively gripped with the OFF mode for precise gripping. These demonstrations suggest that one can use the same principle to design grippers with more than two modes to realize more selectable modes of different speeds, gripping forces, and actuation responses.

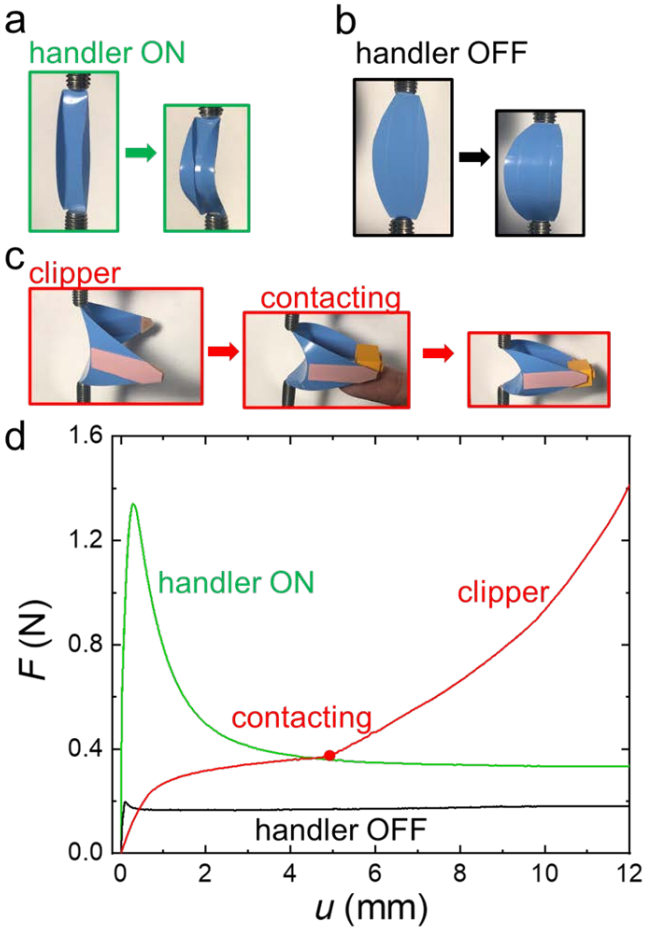

Figure 30. Mechanical characterization of the gripper.

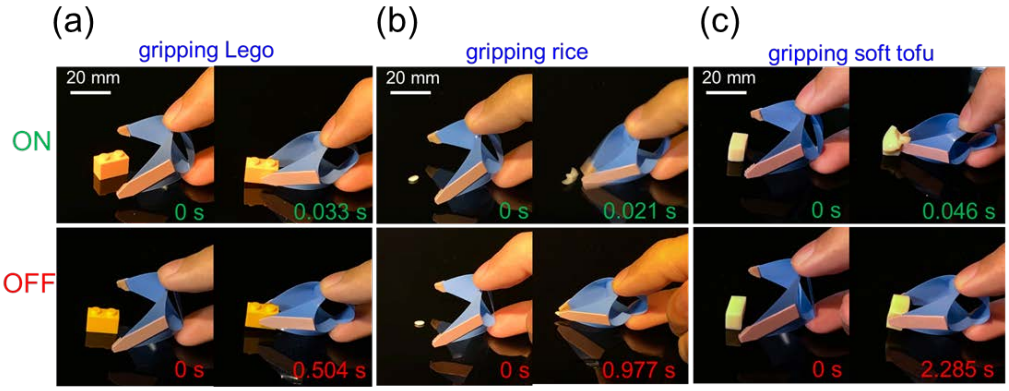

Figure 31. Process of gripping a Lego block, a grain of white rice, and a piece of soft tofu.

Demonstration II: a cube with tunable stiffness for controllable force transmissibility

Another demonstration is to use the in situ stiffness manipulation from the curved origami to control force transmissibility. The in situ tunability of force transmissibility is necessary in many situations. For example, people in many areas of the world habitually carry heavy loads on their head instead of by hand or on their shoulders to save energy [223, 224] because the lower stiffness of the neck results in a lower force transmissibility and thus a reduced energy cost from the vibrations of loads. Another example is the suspension system in an automobile, which can be switched to a higher stiffness for responsive driving (i.e., sport mode) and a lower stiffness for smooth driving (i.e., comfort mode). Unfortunately, this system is too bulky and complicated to be applied in areas such as robotics. Here, I designed curved origami-based cubes that can switch between an isolating mode and a responsive mode for low frequency ranges (e.g., lower than 20 Hz). The planar folding pattern is shown in Fig. 32 (a), in which white, 0.6-mm-thick, plastic panels are used for the top and bottom plates, whereas blue, 0.125-mm-thick, plastic panels are used for the side plates. Tape was used to connect the panels and is represented by thick bars in the folding pattern. The folding creases for modes *A* ($\bar{\kappa}=1$, $\bar{H}=0.084$) and *B* ($\bar{\kappa}=1.8$, $\bar{H}=0.084$) are represented by black and red lines, respectively, with mode *A* for zero stiffness and mode *B* for positive stiffness, and their locations on the stiffness phase diagram are explicitly shown in the inset of Fig. 32 (a). The finished cubes at modes *A* and *B* are shown in Fig. 32 (b). Figure 32 (c) provides the reaction force-displacement relationship during compression for both modes, which clearly shows that mode *A* exhibits a quasi-zero stiffness and mode *B* exhibits a positive stiffness. Specifically, at a load of 2.35 N, mode *A* exhibits approximately zero stiffness. Hence, 2.35 N is the matching force

to achieve quasi-zero stiffness. Near the critical load of 2.35 N, mode *B* exhibits a positive stiffness of k = 0.584 N/mm.

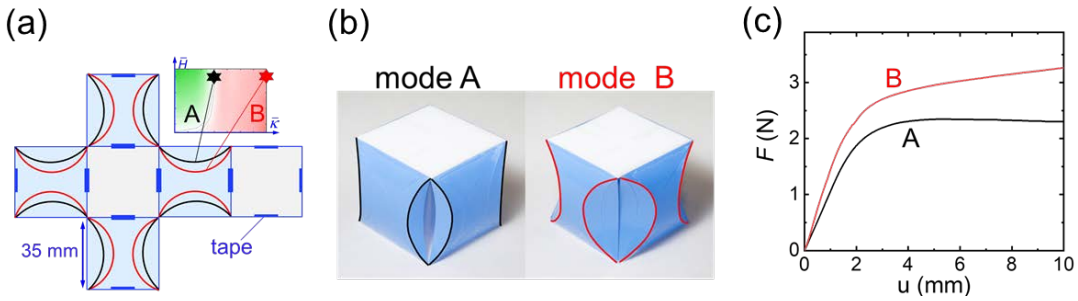

Figure 32. Design of the curved origami cube with predefined curved creases A and B.

We used four curved origami cubes as an array for vibration isolation experiments. Figure 33 (a) shows that the four curved origami cubes of mode *A* can stay balanced at any position when the matching mass of 960 g (= 4 × 2.35 N) is applied. A frequency sweep vibration with a power spectrum spreading was used to test the performance of the curved origami isolators. Figure 33 (b) shows the setup of the experiments. An electromechanical shaker (S 51120 from TIRA Vibration Test Systems Inc.) was used to generate vertical vibrations at varied frequencies, and two identical acceleration sensors (352C33 from PCB Piezotronics Inc.) were attached on the bottom and top surfaces to record the input and output accelerations a_{in} and a_{out}, respectively. Comparisons of the output and input accelerations of modes *A* and *B* for a frequency sweep vibration are shown in Fig. 34 (a). The transmissibility of the curved origami isolators in dB is defined by $20\log_{10}\left|\frac{a_{out}}{a_{in}}\right|$. Fig. 34 (b) shows the transmissibility at frequencies from 1 Hz to 30 Hz for modes *A* and *B*. The isolators at mode *A* can isolate vibrations (i.e., transmissibility less than 0) when the frequency is higher than 5 Hz. The transmissibility of mode *B* is approximately 20-30 dB

higher than that of mode *A*, which means that mode *B* can transfer vibration. Larger output vibrations can be observed at mode *B* for all ranges, suggesting a responsive mode. For mechanical vibrations, the isolation range exists when the vibration frequency is higher than the critical frequency ($f_c = \frac{1}{2\pi}\sqrt{\frac{k}{m}}$ [225]). For mode A, the theoretical critical frequency is 0 because the stiffness *k* is zero, which enables ultralow frequency vibration isolation. However, because of the plasticity of the creases, the viscoelastic damping of the panels, and the existence of the tape, the isolation is only effective for frequencies higher than 5 Hz. For mode *B*, the theoretical critical frequency is $f_c = \frac{1}{2\pi}\sqrt{\frac{4\times 584\ \text{N/m}}{4\times 240\ \text{g}}} = 7.85\ \text{Hz}$, which results in the isolation range (frequency higher than 12.5 Hz) of mode *B*. It is believed that this lightweight curved origami-based isolator can be used in many applications in soft and small robotics.

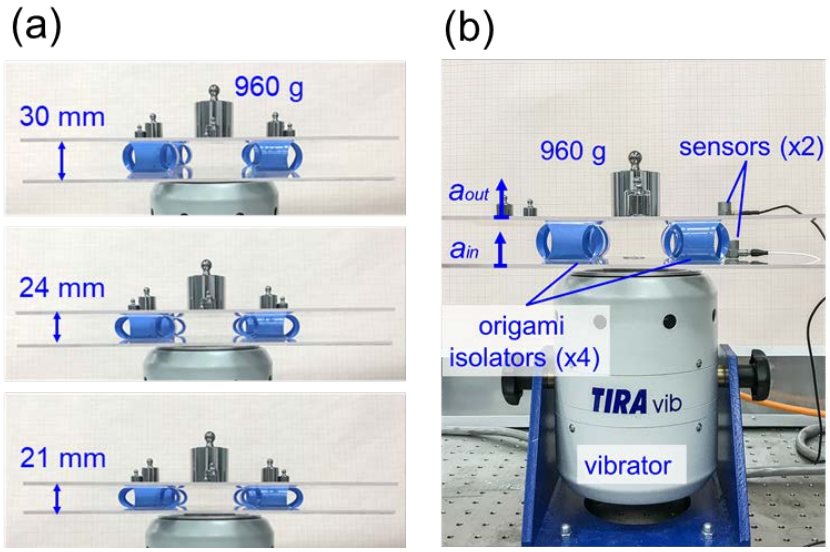

Figure 33. Experimental setup used to measure the acceleration transmissibility of the curved origami cubes.

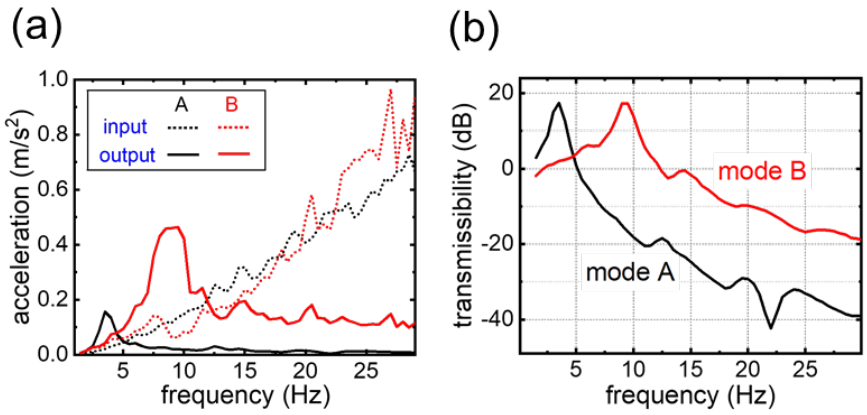

Figure 34. Acceleration transmissibility of curved origami cubes in modes A and B under various vibration frequencies.

Demonstration III: curved Miura pattern for in situ multistage stiffness response

Here, I design two-dimensional (2D) modular metamaterials using curved origami as building blocks, taking a similar approach as the Miura pattern, and demonstrate their unprecedented capability of in situ multistage stiffness response under a uniform load. Figure 35 (a) shows a 3 × 3 Miura pattern, a 3 × 3 curved Miura pattern, and their corresponding unit cells. The curved Miura pattern replaces the mountain creases in the Miura pattern (shown in green) with a curved crease and the two other creases (shown in red) with curved plates. When the top and bottom boundaries are constrained, the curved Miura pattern exhibits different behaviours from the Miura pattern during compression. Different deformation modes of curved Miura are observed under different loading conditions (i.e., concentrated loading on the concave side or convex side and uniform loading), and it is found that the deformation can only transfer from the concave side to the convex side. Moreover, when the concave segment is confined, the curved Miura becomes very stiff. Figure 35 (b) shows the deformation of a curved Miura with identical unit cells characterized by the curvature $\bar{\kappa}$ (= 0.56) of the crease subjected to a compressive load

along the *A*-*A* direction. The concave segment snaps and moves to the right. This snap is ubiquitous, for another crease with curvature $\bar{\kappa}$ = 1.10 that has negative stiffness. For curved Miura patterns that have positive stiffness, snap does not occur, and the applied force monotonically increases with respect to the displacement for curved origami with curvature $\bar{\kappa}$ = 1.62. Figure 35 (c) compares these three curved Miura patterns with $\bar{\kappa}$ = 0.56 for ①, $\bar{\kappa}$ = 0.95 for ②, and $\bar{\kappa}$ = 1.62 for ③. When 0.125-mm-thick plastic film is used, the normalized crease modulus is $\bar{H} = 0.063$. Based on the stiffness diagram, these three curved origami patterns have normalized stiffness $\bar{k} = -10.9, -1.6$, and 6.1, which leads to snap-through behaviours for ① and ② and gradual deformation without snap-though for ③. Upon compressive loading along the *A*-*A* path at progressive displacement *u* = 0 mm, 5 mm, and 10 mm, these three patterns exhibit different responses. Pattern ① has the highest negative stiffness $\bar{k} = -10.9$ and the highest transverse displacement of 25 mm, whereas pattern ③ has positive stiffness $\bar{k} = 6.1$ and the lowest transverse displacement of 9 mm. For the curved Miura with homogeneous curvature, there is a one-to-one relation between the curvature and the transverse displacement under compressive loading, which leads to the design of curved Miura with inhomogeneous curvatures.

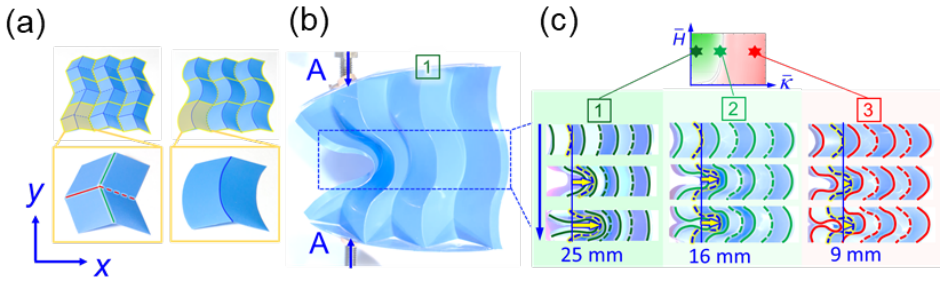

Figure 35. Design and mechanical performance of the curved Miura pattern.

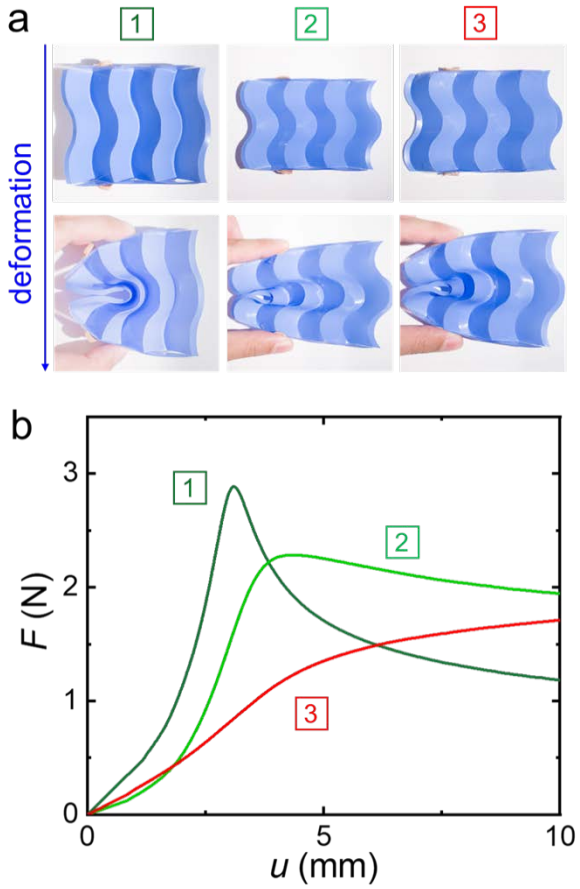

Figure 36. Photographs and Force-displacement relationship of curved origami patterns upon compressive load on *A*-*A* direction.

Curved Miura with inhomogeneous curvature can be modularly designed to achieve in situ switching and multistage stiffness manipulation. Figure 37 (a) illustrates a 4 × 3 curved Miura with in situ switchable creases along the *A*-*A* and *B*-*B* paths. Along each path, the three creases ①, ②, and ③ that were studied in Fig. 35 (c) can be turned ON or OFF to control the transmissibility of the transverse buckling deformation. As shown in Fig. 35 (c), transverse buckling always initiates at the concave site of a curved Miura and then propagates inward; thus, this 4 × 3 curved Miura has two transverse buckling paths along Γ and Ξ, and each path has three candidate curvatures ①, ②, and ③. Thus, this 4 × 3

curved Miura can achieve 6 in situ switchable and accessible states, representing the stiffness response. Considering symmetry, these states can be expressed by a 3 × 3 symmetric matrix shown in Fig. 37 (b). Figure 39 shows the configurations of these 6 states and their force/displacement responses under a uniform compressive load. Multistage stiffness manipulation is accomplished by a uniform load depending on the ON/OFF combination of different creases. The diagonal components for the matrix in Fig. 37 (b) represent the stiffness response when two identical creases are activated on both paths. When two creases □ are activated on both paths Γ and Ξ (□-□ combination), the reaction force of this curved Miura will undergo a single peak and then drop because of concurrent transverse buckling at both paths, which is denoted by a ↑↓ stiffness response (with ↑ for peak and ↓ for drop), and a similar situation occurs for a □-□ combination. When crease □ is turned ON for both paths, positive stiffness provides a monotonic increase in the force response, which is denoted by ↑. The off-diagonal components in Fig. 37 (b) are for those with nonidentical creases activated. When crease □ is activated on path Γ and □ on path Ξ (i.e., a □-□ combination), the reaction force will experience a peak-valley-peak-valley change, i.e., a ↑↓↑↓ multistage stiffness response achieved by a uniform load. The □-□ combination exhibits a peak-valley-peak pattern, i.e., ↑↓↑. The □-□ combination exhibits a peak-flat pattern, i.e., ↑→. For a curved Miura with more unit cells (e.g., a 6 × 3 pattern), the leftmost and rightmost creases have more choices in terms of curvature (e.g., 4), so a much more complicated stiffness response can be generated, which can be represented by multidimensional tensors. Inhomogeneous curved Miura with in-situ

switchable curvatures produces complicated multistage stiffness responses under uniform loading. Thus, a controllable and in situ switchable nonlinear mechanism can find many applications, such as in robotics.

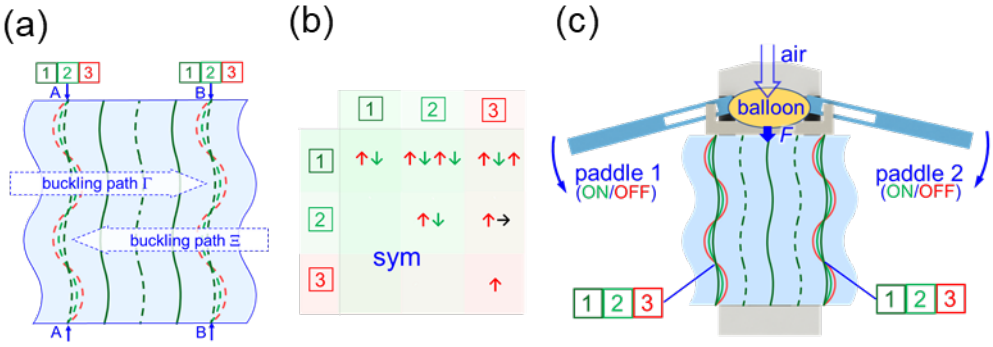

Figure 37. Design of a swimming robot based on curved Miura origami.

One of the challenges in robotics is to accomplish different moving patterns with less actuators, in order to improve the reliability and reduce the cost [226]. To solve this problem, I built a curved Miura-based swimming robot with a single pneumatic actuator, which can be switched in situ among different actuation modes (Fig. 39). When air fills the balloon, the inflation compresses the frame in grey that is glued to the curved Miura, and two paddles are attached to the frame via a sliding trench. When the frame moves downwards, the paddle rotates, and the rotation increases as the displacement of the frame increases. Based on the matrix in Fig. 37 (b), the stiffness response with a ↓ mode will lead to a sudden displacement of the frames and thus a larger rotation of the paddle. Consequently, by altering the combinations (e.g., 1-1, 1-3), six types of complex motions can be realized in situ through simple air flow. Figure 39 shows the motion of the robot on water by inflating the balloon using 50 ml of air with a constant flow within 1 s. The activated paddle during motion is highlighted by a green arrow, and the inactivated

paddle is indicated by a red cross. The displacement and rotation resulting from the inflation are also presented in Fig. 39. Modes ①-①, ②-②, and ③-③ have linear displacement without rotation because of the symmetrical buckling in paths Γ and Ξ, with mode ①-① providing the largest displacement of 63 mm in 1 s because of the largest negative stiffness snap-through, mode ②-② having a 36 mm displacement because of the snap-through, and mode ③-③ generating the least displacement of 16 mm because of positive stiffness. Modes ①-②, ①-③, and ②-③ provide both linear displacement and rotation because of the asymmetrical deformation of the two paths. The other three modes (i.e., ②-①, ③-①, and ③-②) in Fig. 37 (b) also have asymmetrical motion but clockwise rotation. In summary, the curved Miura-based swimming robot enables different moving modes including fast, slow, linear, and rotational moving with a single pneumatic actuator. This demonstration only presents one of the possible applications to employ the in situ multistage stiffness response rooted from curved origami.

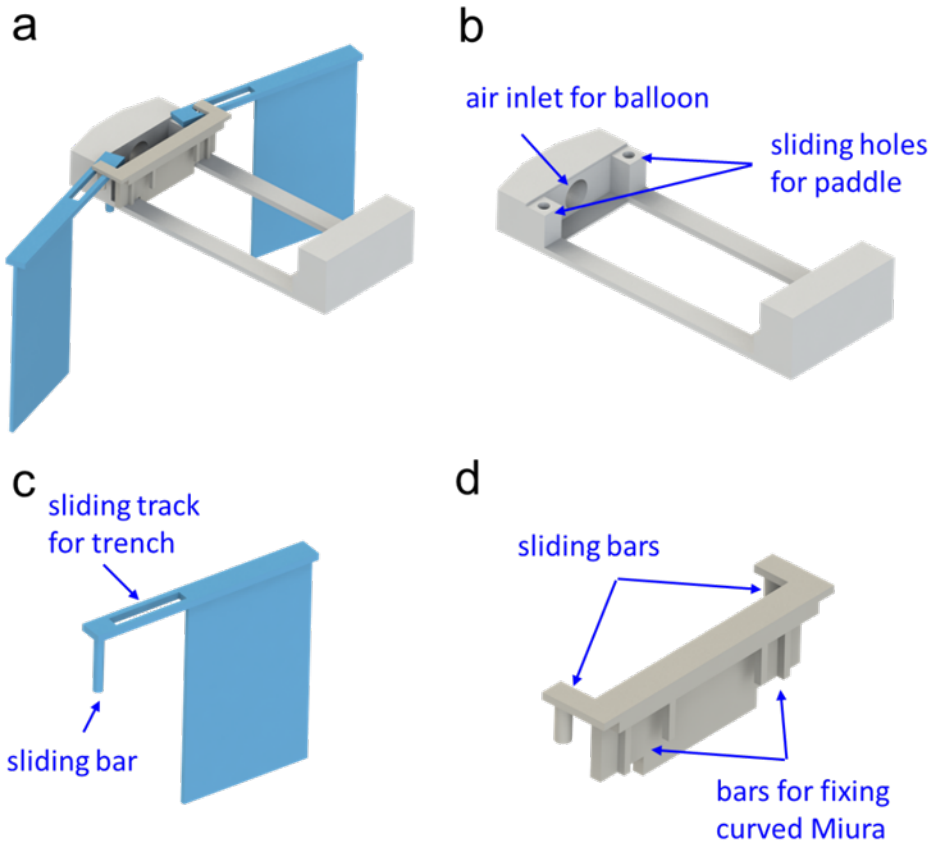

Figure 38. Design of a curved origami-based swimming robot.

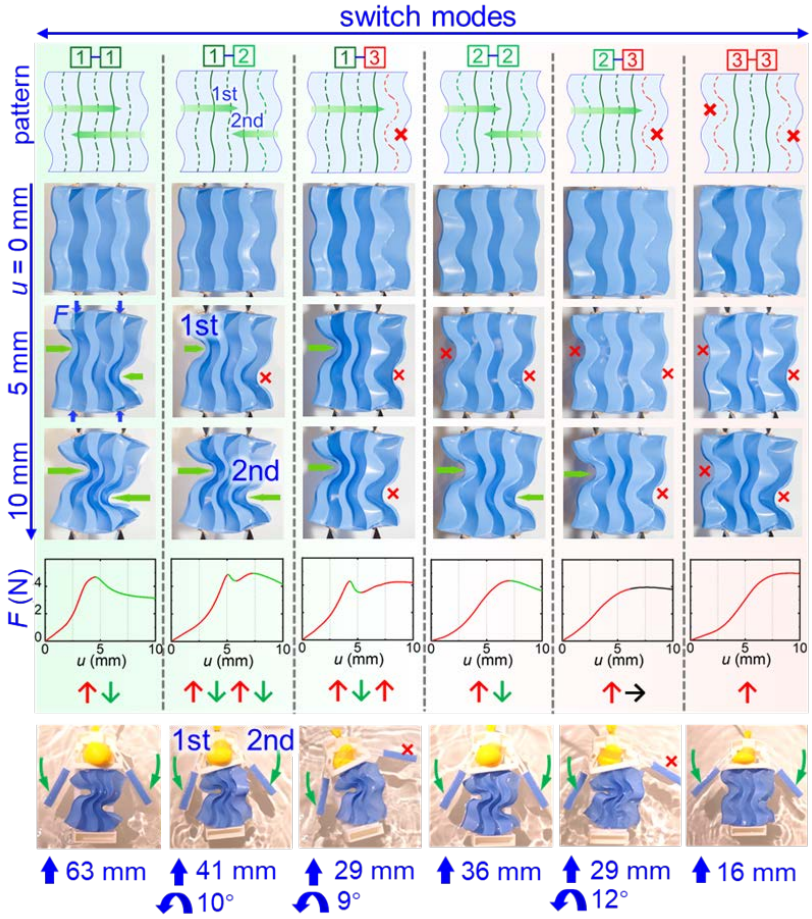

Figure 39. Configurations, force-displacement relationship, and swimming robot performances of the six different states.

3.3 Discussions

In summary, curved origami was introduced in this paper to accomplish in situ stiffness manipulation by changing the curvature of the creases. The variation in stiffness among positive, zero, and negative stiffness results from the competition of the crease folding and the panel bending, with the former providing negative stiffness and the latter providing positive stiffness. The in situ stiffness manipulation is achieved by activating different curved creases on curved origami containing multiple creases. A universal stiffness design diagram was discovered and can be used to design curved creases for

specific applications. Three demonstrations were presented to highlight the versatility of the curved origami, including a universal and lightweight gripper, a cube with tunable stiffness for controllable force transmissibility, and curved Miura patterns for in situ multistage stiffness response. This work presents an essential and elegant resolution to utilize curved origami for complicated, in situ stiffness manipulation, which opens an unexplored direction to design mechanical metamaterials.

Like many other mechanical metamaterials, the presented curved origami needs to be mechanically and manually tuned. A remote-control method will provide better applicability, which can be realized by utilizing temperature-activated [227], photoactivated [228], electronic [229], and magnetic materials [123] on the creases. Moreover, the principle of designing curved origami can be extended from the present one-dimensional (e.g., gripper and isolator applications) and two-dimensional (e.g., curved Miura patterns and their application in robots) patterns to three-dimensional and tessellated curved origami scenarios by combining curved origami patterns and other existing designs in origami, e.g., Miura tube design [40], multilayered Miura design [54], and origami-inspired structural designs [7].

CHAPTER 4

CONCLUSIONS

In the first part, this work explores the on-demand deployability and collapsibility and achieve these characteristics manually. Various type of automatic actuations, including pneumatic force[186, 230], heat[231-234], light[235-238], swelling[235, 239], and magnetic forces[240, 241], can be considered in the future to develop responsive, self-deploy/collapse, and stiff metamaterials. Although the structure is at the centimeter scale, the principle discovered can be applied to make miniaturized structure. Moreover, by connecting the metamaterials in series with each metamaterial with different stiffness at the deployed state, one can make a mechanical metamaterial with continuously tunable stiffness.

In the second part, the work represents a new and innovative approach to create a mechanical metamaterial with on-demand and selective deployability and collapsibility and great stiffness and load bearing capability. The principle in this work can be utilized to design and create versatile origami-inspired mechanical metamaterials that can find many applications, ranging from deployable structures for aerospace, civil applications, implantable medical devices, daily essentials, toys, bistable states for vibration isolations, to continuous tunable stiffness for wearable robotics.

I believe that the presented work will establish an essential principle to use various curved origami patterns for designing mechanical metamaterials with unprecedented functions, including stiffness manipulation and deformation reprogramming, which can be readily coupled with other physical fields, such as electromagnetics. Materials and structures created through this principle can be applied in many fields, including daily

essentials, protections, robotics, automobiles, aerospace components, and biomedical devices.

CHAPTER 5

FUTURE WORK

There are several directions and challenges for future research work.

First, for novel mechanical properties, new origami and kirigami designs are highly desired, but most origami and kirigami patterns have been well studied, and discovering new patterns requires tremendous work both mathematically and mechanically. The existing library of origami and kirigami provides useful information for designing metamaterials with different applications. Rigid kirigami and origami are relatively straightforward to design, though with plain mechanical responses. Deformable kirigami and origami has complex mechanical responses such as multi-stability and tunable stiffness, however the patterns are limited. An alternative solution is to combine existing patterns and knowledge from either origami or kirigami to create new hybrid patterns. There are several methods for discovering mechanical properties without discovering new patterns, such as curved origami design, hybrid origami–kirigami design, modular design, and hierarchical design.

Second, the selection of materials for origami- and kirigami-based mechanical metamaterials has been overlooked. Most origami and kirigami metamaterials are prototyped with paper, and their mechanical properties are influenced and limited by the plasticity and fragility of paper. To design origami and kirigami for real-world applications, materials with different properties should be considered, such as thin or thick, soft or hard, elastic or plastic. The creases of origami and the linkages of kirigami, where stress concentrates, should be designed specifically to prevent fatigue and improve flexibility. A

possible solution is hybrid origami–kirigami design, in which origami and kirigami can be used to relieve the stress for each other. Another solution involves designs inspired by origami and kirigami, such as truss-based designs,[7, 96, 155] where origami and kirigami structures are redesigned and replaced by mechanical components including trusses and springs, thereby preventing unnecessary issues.

Third, energy landscape and energy distribution are two powerful tools to analyze mechanical performances of origami and kirigami and should be leveraged in future investigations. Energy landscape is an effective way to visualize and evaluate the mechanical behavior of metamaterials at different deformation configurations. For example, the valleys on energy landscape indicate the stable states, high energy barrier indicates high load-bearing ability, and the slope and curvature of energy indicates the force and stiffness responses, respectively. On the other hand, the energy distribution of the origami and kirigami deformation modes essentially determines the mechanical performances and provides important guidelines to design mechanical metamaterials with different properties. For example, the contributions of crease folding energy and panel bending energy affect the mechanical stiffness and stability in curved origami. However, the deformation modes (i.e., folding, bending, and stretching) have different contributions and functions depending on the origami and kirigami patterns. For example, folding provides negative stiffness in curved origami while contributes positive stiffness in square-twist origami. Therefore, there is no universal guideline to design the deformation modes of origami and kirigami yet. In future works, there are still a lot to discover from the

perspective of energy, e.g., programmable energy landscape, multi-path energy landscape, controllable energy distribution, etc.

Lastly, to use origami and kirigami in applications such as robotics, medical devices, and deployable structures, the actuation method must be designed carefully. Currently, origami and kirigami structures are actuated by cable-driven, pneumatic, magnetic, photonic, thermal, and chemical methods, but these are not yet perfect and have their own limitations (e.g., low speed, high cost, sensitive to environment, hard to control) and may only work for specific patterns in specific environments. A universal actuation method remains highly desired to actuate different patterns efficiently and robustly.

REFERENCES

1. Zadpoor, A. A., Mechanical meta-materials. *Materials Horizons* **2016,** *3* (5), 371-381.

2. Yu, X.; Zhou, J.; Liang, H.; Jiang, Z.; Wu, L., Mechanical metamaterials associated with stiffness, rigidity and compressibility: A brief review. *Progress in Materials Science* **2018,** *94*, 114-173.

3. Bertoldi, K.; Vitelli, V.; Christensen, J.; Van Hecke, M., Flexible mechanical metamaterials. *Nature Reviews Materials* **2017,** *2* (11), 1-11.

4. Lv, C.; Krishnaraju, D.; Konjevod, G.; Yu, H.; Jiang, H., Origami based mechanical metamaterials. *Scientific reports* **2014,** *4*, 5979.

5. Dudte, L. H.; Vouga, E.; Tachi, T.; Mahadevan, L., Programming curvature using origami tessellations. *Nature materials* **2016,** *15* (5), 583-588.

6. Zhai, Z.; Wang, Y.; Lin, K.; Wu, L.; Jiang, H., In situ stiffness manipulation using elegant curved origami. *Science advances* **2020,** *6* (47), eabe2000.

7. Zhai, Z.; Wang, Y.; Jiang, H., Origami-inspired, on-demand deployable and collapsible mechanical metamaterials with tunable stiffness. *Proceedings of the National Academy of Sciences* **2018,** *115* (9), 2032-2037.

8. Harris, J.; McShane, G., Impact response of metallic stacked origami cellular materials. *International Journal of Impact Engineering* **2020,** *147*, 103730.

9. Liu, J.; Ou, H.; Zeng, R.; Zhou, J.; Long, K.; Wen, G.; Xie, Y. M., Fabrication, dynamic properties and multi-objective optimization of a metal origami tube with Miura sheets. *Thin-Walled Structures* **2019,** *144*, 106352.

10. Liu, Z.; Du, H.; Li, J.; Lu, L.; Li, Z.-Y.; Fang, N. X., Nano-kirigami with giant optical chirality. *Science advances* **2018,** *4* (7), eaat4436.

11. Guo, X.; Ni, X.; Li, J.; Zhang, H.; Zhang, F.; Yu, H.; Wu, J.; Bai, Y.; Lei, H.; Huang, Y., Designing Mechanical Metamaterials with Kirigami-Inspired, Hierarchical Constructions for Giant Positive and Negative Thermal Expansion. *Advanced Materials* **2020**, 2004919.

12. Silverberg, J. L.; Na, J.-H.; Evans, A. A.; Liu, B.; Hull, T. C.; Santangelo, C. D.; Lang, R. J.; Hayward, R. C.; Cohen, I., Origami structures with a critical transition to bistability arising from hidden degrees of freedom. *Nature materials* **2015,** *14* (4), 389-393.

13. Kang, J. H.; Kim, H.; Santangelo, C. D.; Hayward, R. C., Enabling Robust Self-Folding Origami by Pre-Biasing Vertex Buckling Direction. *Advanced Materials* **2019,** *31* (39), 0193006.

14. Blees, M. K.; Barnard, A. W.; Rose, P. A.; Roberts, S. P.; McGill, K. L.; Huang, P. Y.; Ruyack, A. R.; Kevek, J. W.; Kobrin, B.; Muller, D. A., Graphene kirigami. *Nature* **2015,** *524* (7564), 204-207.

15. Lin, Z.; Novelino, L. S.; Wei, H.; Alderete, N. A.; Paulino, G. H.; Espinosa, H. D.; Krishnaswamy, S., Folding at the Microscale: Enabling Multifunctional 3D Origami-Architected Metamaterials. *Small* **2020,** *16* (35), 2002229.

16. Song, Z.; Ma, T.; Tang, R.; Cheng, Q.; Wang, X.; Krishnaraju, D.; Panat, R.; Chan, C. K.; Yu, H.; Jiang, H., Origami lithium-ion batteries. *Nature communications* **2014,** *5* (1), 1-6.

17. Song, Z.; Wang, X.; Lv, C.; An, Y.; Liang, M.; Ma, T.; He, D.; Zheng, Y.-J.; Huang, S.-Q.; Yu, H., Kirigami-based stretchable lithium-ion batteries. *Scientific reports* **2015,** *5* (1), 1-9.

18. Zhang, K.; Jung, Y. H.; Mikael, S.; Seo, J.-H.; Kim, M.; Mi, H.; Zhou, H.; Xia, Z.; Zhou, W.; Gong, S., Origami silicon optoelectronics for hemispherical electronic eye systems. *Nature communications* **2017,** *8* (1), 1-8.

19. Gao, B.; Elbaz, A.; He, Z.; Xie, Z.; Xu, H.; Liu, S.; Su, E.; Liu, H.; Gu, Z., Bioinspired Kirigami Fish-Based Highly Stretched Wearable Biosensor for Human Biochemical–Physiological Hybrid Monitoring. *Advanced Materials Technologies* **2018,** *3* (4), 1700308.

20. Bukauskas, A.; Koronaki, A.; Lee, T.-U.; Ott, D.; Al Asali, M. W.; Jalia, A.; Bashford, T.; Gatóo, A.; Newman, J.; Gattas, J. M.; Shah, D. U.; Ramage, M., Curved-crease origami face shields for infection control. *PLOS ONE* **2021,** *16* (2), e0245737.

21. Mintchev, S.; Shintake, J.; Floreano, D., Bioinspired dual-stiffness origami. *Science Robotics* **2018,** *3* (20).

22. Li, S.; Vogt, D. M.; Rus, D.; Wood, R. J., Fluid-driven origami-inspired artificial muscles. *Proceedings of the National academy of Sciences* **2017,** *114* (50), 13132-13137.

23. Sareh, P.; Chermprayong, P.; Emmanuelli, M.; Nadeem, H.; Kovac, M., Rotorigami: A rotary origami protective system for robotic rotorcraft. *Science Robotics* **2018,** *3* (22).

24. Baek, S.-M.; Yim, S.; Chae, S.-H.; Lee, D.-Y.; Cho, K.-J., Ladybird beetle–inspired compliant origami. *Science Robotics* **2020,** *5* (41).

25. Rafsanjani, A.; Zhang, Y.; Liu, B.; Rubinstein, S. M.; Bertoldi, K., Kirigami skins make a simple soft actuator crawl. *Science Robotics* **2018,** *3* (15).

26. Dieleman, P.; Vasmel, N.; Waitukaitis, S.; van Hecke, M., Jigsaw puzzle design of pluripotent origami. *Nature Physics* **2020,** *16* (1), 63-68.

27. Yellowhorse, A.; Lang, R. J.; Tolman, K.; Howell, L. L., Creating linkage permutations to prevent self-intersection and enable deployable networks of thick-origami. *Scientific reports* **2018,** *8* (1), 1-9.

28. Zhang, J.; Karagiozova, D.; You, Z.; Chen, Y.; Lu, G., Quasi-static large deformation compressive behaviour of origami-based metamaterials. *International Journal of Mechanical Sciences* **2019,** *153*, 194-207.

29. Fuchi, K.; Buskohl, P. R.; Bazzan, G.; Durstock, M. F.; Reich, G. W.; Vaia, R. A.; Joo, J. J., Origami actuator design and networking through crease topology optimization. *Journal of Mechanical Design* **2015,** *137* (9).

30. Filipov, E. T.; Paulino, G.; Tachi, T., Origami tubes with reconfigurable polygonal cross-sections. *Proceedings of the Royal Society A: Mathematical, Physical and Engineering Sciences* **2016,** *472* (2185), 20150607.

31. Biswas, A.; Zekios, C. L.; Georgakopoulos, S. V., Transforming single-band static FSS to dual-band dynamic FSS using origami. *Scientific Reports* **2020,** *10* (1), 1-12.

32. Kshad, M. A. E.; Popinigis, C.; Naguib, H. E., 3D printing of Ron-Resch-like origami cores for compression and impact load damping. *Smart Materials and Structures* **2018,** *28* (1), 015027.

33. Kamrava, S.; Mousanezhad, D.; Ebrahimi, H.; Ghosh, R.; Vaziri, A., Origami-based cellular metamaterial with auxetic, bistable, and self-locking properties. *Scientific reports* **2017,** *7* (1), 1-9.

34. Fang, H.; Zhang, Y.; Wang, K., Origami-based earthworm-like locomotion robots. *Bioinspiration & biomimetics* **2017,** *12* (6), 065003.

35. Wang, Z.; Jing, L.; Yao, K.; Yang, Y.; Zheng, B.; Soukoulis, C. M.; Chen, H.; Liu, Y., Origami-based reconfigurable metamaterials for tunable chirality. *Advanced materials* **2017,** *29* (27), 1700412.

36. Wang, F.; Gong, H.; Chen, X.; Chen, C., Folding to curved surfaces: A generalized design method and mechanics of origami-based cylindrical structures. *Scientific reports* **2016,** *6*, 33312.

37. Brunck, V.; Lechenault, F.; Reid, A.; Adda-Bedia, M., Elastic theory of origami-based metamaterials. *Physical Review E* **2016,** *93* (3), 033005.

38. Lee, D.-Y.; Kim, J.-S.; Kim, S.-R.; Koh, J.-S.; Cho, K.-J. In *The deformable wheel robot using magic-ball origami structure*, ASME 2013 international design engineering technical conferences and computers and information in engineering conference, American Society of Mechanical Engineers Digital Collection: 2013.

39. Zhu, Y.; Filipov, E. T., An efficient numerical approach for simulating contact in origami assemblages. *Proceedings of the Royal Society A* **2019,** *475* (2230), 20190366.

40. Filipov, E. T.; Tachi, T.; Paulino, G. H., Origami tubes assembled into stiff, yet reconfigurable structures and metamaterials. *Proceedings of the National Academy of Sciences* **2015,** *112* (40), 12321-12326.

41. Fang, H.; Chang, T.-S.; Wang, K., Magneto-origami structures: Engineering multi-stability and dynamics via magnetic-elastic coupling. *Smart Materials and Structures* **2019,** *29* (1), 015026.

42. Cheung, K. C.; Tachi, T.; Calisch, S.; Miura, K., Origami interleaved tube cellular materials. *Smart Materials and Structures* **2014,** *23* (9), 094012.

43. Yasuda, H.; Yang, J., Reentrant origami-based metamaterials with negative Poisson's ratio and bistability. *Physical review letters* **2015,** *114* (18), 185502.

44. Yasuda, H.; Lee, M.; Yang, J. In *Tunable wave dynamics in origami-based mechanical metamaterials*, International Design Engineering Technical Conferences and Computers and Information in Engineering Conference, American Society of Mechanical Engineers: 2016; p V05BT07A012.

45. Jiang, W.; Ma, H.; Feng, M.; Yan, L.; Wang, J.; Wang, J.; Qu, S., Origami-inspired building block and parametric design for mechanical metamaterials. *Journal of Physics D: Applied Physics* **2016,** *49* (31), 315302.

46. Zhao, Z.; Kuang, X.; Wu, J.; Zhang, Q.; Paulino, G. H.; Qi, H. J.; Fang, D., 3D printing of complex origami assemblages for reconfigurable structures. *Soft matter* **2018,** *14* (39), 8051-8059.

47. Wickeler, A. L.; Naguib, H. E., Novel origami-inspired metamaterials: Design, mechanical testing and finite element modelling. *Materials & Design* **2020,** *186*, 108242.

48. Mukhopadhyay, T.; Ma, J.; Feng, H.; Hou, D.; Gattas, J. M.; Chen, Y.; You, Z., Programmable stiffness and shape modulation in origami materials: emergence of a distant actuation feature. *Applied Materials Today* **2020,** *19*, 100537.

49. Wei, Z. Y.; Guo, Z. V.; Dudte, L.; Liang, H. Y.; Mahadevan, L., Geometric mechanics of periodic pleated origami. *Physical review letters* **2013,** *110* (21), 215501.
50. Feng, H.; Ma, J.; Chen, Y.; You, Z., Twist of tubular mechanical metamaterials based on waterbomb origami. *Scientific reports* **2018,** *8* (1), 1-13.

51. Gillman, A.; Fuchi, K.; Buskohl, P., Truss-based nonlinear mechanical analysis for origami structures exhibiting bifurcation and limit point instabilities. *International Journal of Solids and Structures* **2018,** *147*, 80-93.

52. Treml, B.; Gillman, A.; Buskohl, P.; Vaia, R., Origami mechanologic. *Proceedings of the National Academy of Sciences* **2018,** *115* (27), 6916-6921.

53. Ma, J.; Song, J.; Chen, Y., An origami-inspired structure with graded stiffness. *International Journal of Mechanical Sciences* **2018,** *136*, 134-142.

54. Fang, H.; Chu, S. C. A.; Xia, Y.; Wang, K. W., Programmable Self-Locking Origami Mechanical Metamaterials. *Advanced Materials* **2018,** *30* (15), 1706311.

55. Zhou, X.; Zang, S.; You, Z., Origami mechanical metamaterials based on the Miura-derivative fold patterns. *Proceedings of the Royal Society A: Mathematical, Physical and Engineering Sciences* **2016,** *472* (2191), 20160361.

56. Sengupta, S.; Li, S., Harnessing the anisotropic multistability of stacked-origami mechanical metamaterials for effective modulus programming. *Journal of Intelligent Material Systems and Structures* **2018,** *29* (14), 2933-2945.

57. Fang, H.; Wang, K.; Li, S., Asymmetric energy barrier and mechanical diode effect from folding multi-stable stacked-origami. *Extreme Mechanics Letters* **2017,** *17*, 7-15.

58. Li, M.; Shen, L.; Jing, L.; Xu, S.; Zheng, B.; Lin, X.; Yang, Y.; Wang, Z.; Chen, H., Origami Metawall: Mechanically Controlled Absorption and Deflection of Light. *Advanced Science* **2019,** *6* (23), 1901434.

59. Du, Y.; Keller, T.; Song, C.; Xiao, Z.; Wu, L.; Xiong, J., Design and foldability of Miura-based cylindrical origami structures. *Thin-Walled Structures* **2020**, 107311.

60. Wu, H.; Fang, H.; Chen, L.; Xu, J., Transient Dynamics of a Miura-Origami Tube during Free Deployment. *arXiv preprint arXiv:2005.07340* **2020**.

61. Li, Z.; Yang, Q.; Fang, R.; Chen, W.; Hao, H., Origami metamaterial with two-stage programmable compressive strength under quasi-static loading. *International Journal of Mechanical Sciences* **2020,** *189*, 105987.

62. 0Han, H.; Tang, L.; Cao, D.; Liu, L., Modeling and analysis of dynamic characteristics of multi-stable waterbomb origami base. *Nonlinear Dynamics* **2020**, 1-24.

63. Hu, Y.; Liang, H.; Duan, H., Design of cylindrical and axisymmetric origami structures based on generalized Miura-ori cell. *Journal of Mechanisms and Robotics* **2019,** *11* (5).

64. Li, S.; Fang, H.; Wang, K., Recoverable and programmable collapse from folding pressurized origami cellular solids. *Physical review letters* **2016,** *117* (11), 114301.

65. Boatti, E.; Vasios, N.; Bertoldi, K., Origami metamaterials for tunable thermal expansion. *Advanced Materials* **2017,** *29* (26), 1700360.

66. Yasuda, H.; Chong, C.; Charalampidis, E. G.; Kevrekidis, P. G.; Yang, J., Formation of rarefaction waves in origami-based metamaterials. *Physical review E* **2016,** *93* (4), 043004.

67. Yuan, L.; Dai, H.; Song, J.; Ma, J.; Chen, Y., The behavior of a functionally graded origami structure subjected to quasi-static compression. *Materials & Design* **2020,** *189*, 108494.

68. Zhang, P.; Li, X.; Wang, Z.; Zhao, L.; Yan, X., Dynamic blast loading response of sandwich beam with origami-inspired core. *Results in Physics* **2018,** *10*, 946-955.

69. Zhang, Q.; Fang, H.; Xu, J., Programmable stopbands and supratransmission effects in a stacked Miura-origami metastructure. *Physical Review E* **2020,** *101* (4), 042206.

70. Fuchi, K.; Buskohl, P. R.; Joo, J. J.; Reich, G. W.; Vaia, R. A. In *Resonance tuning of RF devices through origami folding*, Proc. 20th Int. Conf. on Composite Materials (Copenhagen, Denmark), 2015; pp 1-10.

71. Zhang, J.; Liu, S.; Zhang, L.; Wang, C., Origami-Based Metasurfaces: Design and Radar Cross Section Reduction. *AIAA Journal* **2020,** *58* (12), 5478-5482.

72. Schenk, M.; Guest, S. D., Geometry of Miura-folded metamaterials. *Proceedings of the National Academy of Sciences* **2013,** *110* (9), 3276-3281.

73. Chen, Y.; Feng, H.; Ma, J.; Peng, R.; You, Z., Symmetric waterbomb origami. *Proceedings of the Royal Society A: Mathematical, Physical and Engineering Sciences* **2016,** *472* (2190), 20150846.

74. Miura, K., *Zeta-Core Sandwich- Its Concept and Realization*. Institute of Space and Aeronautical Science, University of Tokyo: 1972.

75. Chen, Y.; Peng, R.; You, Z., Origami of thick panels. *Science* **2015,** *349* (6246), 396-400.

76. Yasuda, H.; Yein, T.; Tachi, T.; Miura, K.; Taya, M., Folding behaviour of Tachi–Miura polyhedron bellows. *Proceedings of the Royal Society A: Mathematical, Physical and Engineering Sciences* **2013,** *469* (2159), 20130351.

77. Yasuda, H.; Gopalarethinam, B.; Kunimine, T.; Tachi, T.; Yang, J., Origami-Based Cellular Structures with In Situ Transition between Collapsible and Load-Bearing Configurations. *Advanced Engineering Materials* **2019,** *21* (12), 1900562.

78. McInerney, J.; Chen, B. G.-g.; Theran, L.; Santangelo, C. D.; Rocklin, D. Z., Hidden symmetries generate rigid folding mechanisms in periodic origami. *Proceedings of the National Academy of Sciences* **2020,** *117* (48), 30252-30259.

79. Masana, R.; Khazaaleh, S.; Alhussein, H.; Crespo, R.; Daqaq, M., An origami-inspired dynamically actuated binary switch. *Applied Physics Letters* **2020,** *117* (8), 081901.

80. Yasuda, H.; Miyazawa, Y.; Charalampidis, E. G.; Chong, C.; Kevrekidis, P. G.; Yang, J., Origami-based impact mitigation via rarefaction solitary wave creation. *Science advances* **2019,** *5* (5), eaau2835.

81. Novelino, L. S.; Ze, Q.; Wu, S.; Paulino, G. H.; Zhao, R., Untethered control of functional origami microrobots with distributed actuation. *Proceedings of the National Academy of Sciences* **2020,** *117* (39), 24096-24101.

82. Liu, K.; Tachi, T.; Paulino, G. H., Invariant and smooth limit of discrete geometry folded from bistable origami leading to multistable metasurfaces. *Nature communications* **2019,** *10* (1), 1-10.

83. Schenk, M.; Guest, S. D., Origami folding: A structural engineering approach. *Origami* **2011,** *5*, 291-304.

84. Chen, Y.; Sareh, P.; Yan, J.; Fallah, A. S.; Feng, J., An integrated geometric-graph-theoretic approach to representing origami structures and their corresponding truss frameworks. *Journal of Mechanical Design* **2019,** *141* (9).

85. Liu, B.; Silverberg, J. L.; Evans, A. A.; Santangelo, C. D.; Lang, R. J.; Hull, T. C.; Cohen, I., Topological kinematics of origami metamaterials. *Nature Physics* **2018,** *14* (8), 811-815.

86. Yasuda, H.; Yang, J., Tunable frequency band structure of origami-based mechanical metamaterials. *Journal of the International Association for Shell and Spatial Structures* **2017,** *58* (4), 287-294.

87. Liu, K.; Novelino, L. S.; Gardoni, P.; Paulino, G. H., Big influence of small random imperfections in origami-based metamaterials. *Proceedings of the Royal Society A* **2020,** *476* (2241), 20200236.

88. Kidambi, N.; Wang, K., Dynamics of Kresling origami deployment. *Physical Review E* **2020,** *101* (6), 063003.

89. Evans, A. A.; Silverberg, J. L.; Santangelo, C. D., Lattice mechanics of origami tessellations. *Physical Review E* **2015,** *92* (1), 013205.

90. Liu, K.; Paulino, G., Nonlinear mechanics of non-rigid origami: an efficient computational approach. *Proceedings of the Royal Society A: Mathematical, Physical and Engineering Sciences* **2017,** *473* (2206), 20170348.

91. Cai, J.; Deng, X.; Feng, J.; Zhou, Y., Geometric design and mechanical behavior of a deployable cylinder with Miura origami. *Smart Materials and Structures* **2015,** *24* (12), 125031.

92. Chen, B. G.-g.; Liu, B.; Evans, A. A.; Paulose, J.; Cohen, I.; Vitelli, V.; Santangelo, C., Topological mechanics of origami and kirigami. *Physical review letters* **2016,** *116* (13), 135501.

93. Filipov, E.; Redoutey, M., Mechanical characteristics of the bistable origami hypar. *Extreme Mechanics Letters* **2018,** *25*, 16-26.

94. Du, Y.; Song, C.; Xiong, J.; Wu, L., Fabrication and mechanical behaviors of carbon fiber reinforced composite foldcore based on curved-crease origami. *Composites Science and Technology* **2019,** *174*, 94-105.

95. Silverberg, J. L.; Evans, A. A.; McLeod, L.; Hayward, R. C.; Hull, T.; Santangelo, C. D.; Cohen, I., Using origami design principles to fold reprogrammable mechanical metamaterials. *science* **2014,** *345* (6197), 647-650.

96. Yasuda, H.; Tachi, T.; Lee, M.; Yang, J., Origami-based tunable truss structures for non-volatile mechanical memory operation. *Nature communications* **2017,** *8* (1), 1-7.

97. Masana, R.; Daqaq, M. F., Equilibria and bifurcations of a foldable paper-based spring inspired by Kresling-pattern origami. *Physical Review E* **2019,** *100* (6), 063001.

98. Kim, S.-R.; Lee, D.-Y.; Ahn, S.-J.; Koh, J.-S.; Cho, K.-J., Morphing Origami Block for Lightweight Reconfigurable System. *IEEE Transactions on Robotics* **2020**.

99. Li, Z.; Kidambi, N.; Wang, L.; Wang, K.-W., Uncovering rotational multifunctionalities of coupled Kresling modular structures. *Extreme Mechanics Letters* **2020**, 100795.

100. Wang, L. C.; Song, W. L.; Zhang, Y. J.; Qu, M. J.; Zhao, Z.; Chen, M.; Yang, Y.; Chen, H.; Fang, D., Active Reconfigurable Tristable Square-Twist Origami. *Advanced Functional Materials* **2020,** *30* (13), 1909087.

101. Gustafson, K.; Angatkina, O.; Wissa, A., Model-based design of a multistable origami-enabled crawling robot. *Smart Materials and Structures* **2019,** *29* (1), 015013.

102. Tahouni, Y.; Cheng, T.; Wood, D.; Sachse, R.; Thierer, R.; Bischoff, M.; Menges, A. In *Self-shaping Curved Folding: A 4D-printing method for fabrication of self-folding curved crease structures*, Symposium on Computational Fabrication, 2020; pp 1-11.

103. Pratapa, P. P.; Suryanarayana, P.; Paulino, G. H., Bloch wave framework for structures with nonlocal interactions: Application to the design of origami acoustic metamaterials. *Journal of the Mechanics and Physics of Solids* **2018,** *118*, 115-132.

104. Xiang, X.; Lu, G.; You, Z., Energy absorption of origami inspired structures and materials. *Thin-Walled Structures* **2020,** *157*, 107130.

105. Grey, S. W.; Scarpa, F.; Schenk, M., Strain reversal in actuated origami structures. *Physical review letters* **2019,** *123* (2), 025501.

106. Filipov, E.; Liu, K.; Tachi, T.; Schenk, M.; Paulino, G., Bar and hinge models for scalable analysis of origami. *International Journal of Solids and Structures* **2017,** *124*, 26-45.

107. Chen, T.; Bilal, O. R.; Lang, R.; Daraio, C.; Shea, K., Autonomous deployment of a solar panel using elastic origami and distributed shape-memory-polymer actuators. *Physical Review Applied* **2019,** *11* (6), 064069.

108. Chang, Z.; Ta, T. D.; Narumi, K.; Kim, H.; Okuya, F.; Li, D.; Kato, K.; Qi, J.; Miyamoto, Y.; Saito, K. In *Kirigami Haptic Swatches: Design Methods for Cut-and-Fold Haptic Feedback Mechanisms*, Proceedings of the 2020 CHI Conference on Human Factors in Computing Systems, 2020; pp 1-12.

109. Dias, M. A.; Dudte, L. H.; Mahadevan, L.; Santangelo, C. D., Geometric mechanics of curved crease origami. *Physical review letters* **2012,** *109* (11), 114301.

110. Grey, S. W.; Scarpa, F.; Schenk, M., Embedded Actuation for Shape-Adaptive Origami. *Journal of Mechanical Design* **2021**, 1-11.

111. Lee, T.-U.; You, Z.; Gattas, J. M., Elastica surface generation of curved-crease origami. *International Journal of Solids and Structures* **2018,** *136*, 13-27.

112. Lee, T.-U.; Yang, X.; Ma, J.; Chen, Y.; Gattas, J. M., Elastic buckling shape control of thin-walled cylinder using pre-embedded curved-crease origami patterns. *International Journal of Mechanical Sciences* **2019,** *151*, 322-330.

113. Woodruff, S. R.; Filipov, E. T., A bar and hinge model formulation for structural analysis of curved-crease origami. *International Journal of Solids and Structures* **2020,** *204*, 114-127.

114. Bhovad, P.; Kaufmann, J.; Li, S., Peristaltic locomotion without digital controllers: Exploiting multi-stability in origami to coordinate robotic motion. *Extreme Mechanics Letters* **2019,** *32*, 100552.

115. Woodruff, S. R.; Filipov, E. T., Curved creases redistribute global bending stiffness in corrugations: theory and experimentation. *Meccanica* **2020**.

116. Choi, G. P.; Dudte, L. H.; Mahadevan, L., Programming shape using kirigami tessellations. *Nature materials* **2019,** *18* (9), 999-1004.

117. Jin, L.; Forte, A. E.; Deng, B.; Rafsanjani, A.; Bertoldi, K., Kirigami-Inspired Inflatables with Programmable Shapes. *Advanced Materials* **2020,** *32* (33), 2001863.

118. An, N.; Domel, A. G.; Zhou, J.; Rafsanjani, A.; Bertoldi, K., Programmable hierarchical kirigami. *Advanced Functional Materials* **2020,** *30* (6), 1906711.

119. Rafsanjani, A.; Bertoldi, K., Buckling-induced kirigami. *Physical review letters* **2017,** *118* (8), 084301.

120. Jiralerspong, T.; Bae, G.; Lee, J.-H.; Kim, S.-K., Wireless Control of Two-and Three-Dimensional Actuations of Kirigami Patterns Composed of Magnetic-Particles–Polymer Composites. *ACS nano* **2020**.

121. Shang, X.; Liu, L.; Rafsanjani, A.; Pasini, D., Durable bistable auxetics made of rigid solids. *Journal of Materials Research* **2018,** *33* (3), 300-308.

122. Hwang, D.-G.; Trent, K.; Bartlett, M. D., Kirigami-inspired structures for smart adhesion. *ACS applied materials & interfaces* **2018,** *10* (7), 6747-6754.

123. Kim, Y.; Yuk, H.; Zhao, R.; Chester, S. A.; Zhao, X., Printing ferromagnetic domains for untethered fast-transforming soft materials. *Nature* **2018,** *558* (7709), 274-279.

124. Xu, L.; Wang, X.; Kim, Y.; Shyu, T. C.; Lyu, J.; Kotov, N. A., Kirigami nanocomposites as wide-angle diffraction gratings. *ACS nano* **2016,** *10* (6), 6156-6162.

125. Xu, S.; Yan, Z.; Jang, K.-I.; Huang, W.; Fu, H.; Kim, J.; Wei, Z.; Flavin, M.; McCracken, J.; Wang, R., Assembly of micro/nanomaterials into complex, three-dimensional architectures by compressive buckling. *Science* **2015,** *347* (6218), 154-159.

126. Yan, Z.; Zhang, F.; Liu, F.; Han, M.; Ou, D.; Liu, Y.; Lin, Q.; Guo, X.; Fu, H.; Xie, Z., Mechanical assembly of complex, 3D mesostructures from releasable multilayers of advanced materials. *Science advances* **2016,** *2* (9), e1601014.

127. Zhang, H.; Wu, J.; Fang, D.; Zhang, Y., Hierarchical mechanical metamaterials built with scalable tristable elements for ternary logic operation and amplitude modulation. *Science Advances* **2021,** *7* (9), eabf1966.

128. Zhang, X.; Medina, L.; Cai, H.; Aksyuk, V.; Espinosa, H. D.; Lopez, D., Kirigami Engineering—Nanoscale Structures Exhibiting a Range of Controllable 3D Configurations. *Advanced Materials* **2020**, 2005275.

129. Zhao, R.; Lin, S.; Yuk, H.; Zhao, X., Kirigami enhances film adhesion. *Soft Matter* **2018,** *14* (13), 2515-2525.

130. Xue, R.; Li, R.; Du, Z.; Zhang, W.; Zhu, Y.; Sun, Z.; Guo, X., Kirigami pattern design of mechanically driven formation of complex 3D structures through topology optimization. *Extreme Mechanics Letters* **2017,** *15*, 139-144.

131. Isobe, M.; Okumura, K., Initial rigid response and softening transition of highly stretchable kirigami sheet materials. *Scientific reports* **2016,** *6*, 24758.

132. Choi, W. J.; Cheng, G.; Huang, Z.; Zhang, S.; Norris, T. B.; Kotov, N. A., Terahertz circular dichroism spectroscopy of biomaterials enabled by kirigami polarization modulators. *Nature materials* **2019,** *18* (8), 820.

133. Zhang, Y.; Yan, Z.; Nan, K.; Xiao, D.; Liu, Y.; Luan, H.; Fu, H.; Wang, X.; Yang, Q.; Wang, J., A mechanically driven form of Kirigami as a route to 3D mesostructures in micro/nanomembranes. *Proceedings of the National Academy of Sciences* **2015,** *112* (38), 11757-11764.

134. Tang, Y.; Lin, G.; Yang, S.; Yi, Y. K.; Kamien, R. D.; Yin, J., Programmable Kiri-Kirigami Metamaterials. *Advanced Materials* **2017,** *29* (10), 1604262.

135. Moshe, M.; Esposito, E.; Shankar, S.; Bircan, B.; Cohen, I.; Nelson, D. R.; Bowick, M. J., Kirigami mechanics as stress relief by elastic charges. *Physical review letters* **2019,** *122* (4), 048001.

136. Shyu, T. C.; Damasceno, P. F.; Dodd, P. M.; Lamoureux, A.; Xu, L.; Shlian, M.; Shtein, M.; Glotzer, S. C.; Kotov, N. A., A kirigami approach to engineering elasticity in nanocomposites through patterned defects. *Nature materials* **2015,** *14* (8), 785-789.

137. Andrews, D. W.; Avila, A.; Butler, J.; Magleby, S. P.; Howell, L. L. In *Kirigami-Based Deployable Transcrease Hard Stop Models Usable in Origami Patterns*, ASME 2019 International Design Engineering Technical Conferences and Computers and Information in Engineering Conference, American Society of Mechanical Engineers Digital Collection: 2019.

138. Fang, H.; Yu, X.; Cheng, L., Reconfigurable origami silencers for tunable and programmable sound attenuation. *Smart Materials and Structures* **2018,** *27* (9), 095007.

139. Hou, Y.; Neville, R.; Scarpa, F.; Remillat, C.; Gu, B.; Ruzzene, M., Graded conventional-auxetic Kirigami sandwich structures: Flatwise compression and edgewise loading. *Composites Part B: Engineering* **2014,** *59*, 33-42.

140. Jiang, C.; Rist, F.; Pottmann, H.; Wallner, J., Freeform quad-based kirigami. *ACM Transactions on Graphics (TOG)* **2020,** *39* (6), 1-11.

141. Jing, L.; Wang, Z.; Zheng, B.; Wang, H.; Yang, Y.; Shen, L.; Yin, W.; Li, E.; Chen, H., Kirigami metamaterials for reconfigurable toroidal circular dichroism. *NPG Asia Materials* **2018,** *10* (9), 888-898.

142. Le, D. H.; Xu, Y.; Tentzeris, M. M.; Lim, S., Transformation from 2D meta-pixel to 3D meta-pixel using auxetic kirigami for programmable multifunctional electromagnetic response. *Extreme Mechanics Letters* **2020**, 100670.

143. Li, Z.; Chen, W.; Hao, H. In *Blast resistant performance of multi-layer square dome shape kirigami folded structure*, 6th international conference on design and analysis of protective structures, 2017.

144. Melo, H.; Dias, C.; Araújo, N., Optimal number of faces for fast self-folding kirigami. *Communications Physics* **2020,** *3* (1), 1-5.

145. Miranda, R.; Babilio, E.; Singh, N.; Santos, F.; Fraternali, F., Mechanics of smart origami sunscreens with energy harvesting ability. *Mechanics Research Communications* **2020,** *105*, 103503.

146. Neville, R.; Scarpa, F.; Leng, J. In *Smart Kirigami open honeycombs in shape changing actuation and dynamics*, Health Monitoring of Structural and Biological Systems 2017, International Society for Optics and Photonics: 2017; p 101701L.

147. Neville, R. M.; Chen, J.; Guo, X.; Zhang, F.; Wang, W.; Dobah, Y.; Scarpa, F.; Leng, J.; Peng, H.-X., A Kirigami shape memory polymer honeycomb concept for deployment. *Smart Materials and Structures* **2017,** *26* (5), 05LT03.

148. Ouisse, M.; Collet, M.; Scarpa, F., A piezo-shunted kirigami auxetic lattice for adaptive elastic wave filtering. *Smart Materials and Structures* **2016,** *25* (11), 115016.

149. Overvelde, J. T.; De Jong, T. A.; Shevchenko, Y.; Becerra, S. A.; Whitesides, G. M.; Weaver, J. C.; Hoberman, C.; Bertoldi, K., A three-dimensional actuated origami-inspired transformable metamaterial with multiple degrees of freedom. *Nature communications* **2016,** *7* (1), 1-8.

150. Castle, T.; Sussman, D. M.; Tanis, M.; Kamien, R. D., Additive lattice kirigami. *Science advances* **2016,** *2* (9), e1601258.

151. Yang, N.; Zhang, M.; Zhu, R., 3D kirigami metamaterials with coded thermal expansion properties. *Extreme Mechanics Letters* **2020,** *40*, 100912.

152. Yang, N.; Deng, Y.; Mao, Z.; Chen, Y.; Wu, N.; Niu, X., New network architectures with tunable mechanical properties inspired by origami. *Materials Today Advances* **2019,** *4*, 100028.

153. 0Wang, W.; Li, C.; Rodrigue, H.; Yuan, F.; Han, M. W.; Cho, M.; Ahn, S. H., Kirigami/Origami-Based Soft Deployable Reflector for Optical Beam Steering. *Advanced Functional Materials* **2017,** *27* (7), 1604214.

154. An, N.; Li, M.; Zhou, J., Modeling SMA-enabled Soft Deployable Structures for Kirigami/Origami Reflectors. *International Journal of Mechanical Sciences* **2020**, 105753.

155. Bobbert, F.; Janbaz, S.; van Manen, T.; Li, Y.; Zadpoor, A., Russian doll deployable meta-implants: Fusion of kirigami, origami, and multi-stability. *Materials & Design* **2020**, 108624.

156. Eidini, M., Zigzag-base folded sheet cellular mechanical metamaterials. *Extreme Mechanics Letters* **2016,** *6*, 96-102.

157. Kamrava, S.; Ghosh, R.; Wang, Z.; Vaziri, A., Origami-Inspired Cellular Metamaterial With Anisotropic Multi-Stability. *Advanced Engineering Materials* **2019,** *21* (2), 1800895.

158. Li, Z.; Chen, W.; Hao, H.; Yang, Q.; Fang, R., Energy absorption of kirigami modified corrugated structure. *Thin-Walled Structures* **2020,** *154*, 106829.

159. Liu, S.; Zhu, Y.; Zhang, Z.; Fang, Z.; Tan, J.; Peng, J.; Song, C.; Asada, H.; Wang, Z., Otariidae-inspired Soft-robotic Supernumerary Flippers by Fabric Kirigami and Origami. *IEEE/ASME Transactions on Mechatronics* **2020**.

160. Ma, W.; Zhang, Z.; Zhang, H.; Li, Y.; Wu, H.; Jiang, S.; Chai, G., An origami-inspired cube pipe structure with bistable anti-symmetric CFRP shells driven by magnetic field. *Smart Materials and Structures* **2019,** *28* (2), 025028.

161. Ming, S.; Zhou, C.; Li, T.; Song, Z.; Wang, B., Energy absorption of thin-walled square tubes designed by kirigami approach. *International Journal of Mechanical Sciences* **2019,** *157*, 150-164.

162. van Manen, T.; Janbaz, S.; Ganjian, M.; Zadpoor, A. A., Kirigami-enabled self-folding origami. *Materials Today* **2020,** *32*, 59-67.

163. Zhang, M.; Yang, J.; Zhu, R. In *Flexural wave control via origami-based elastic metamaterials*, Health Monitoring of Structural and Biological Systems XIII, International Society for Optics and Photonics: 2019; p 109720Q.

164. Zhou, C.; Xia, C.; Ming, S.; Bi, X.; Li, T., Low-velocity impact response of discontinuous kirigami cruciform sandwich panel. *International Journal of Applied Mechanics* **2019,** *11* (05), 1950046.

165. Eidini, M.; Paulino, G. H., Unraveling metamaterial properties in zigzag-base folded sheets. *Science advances* **2015,** *1* (8), e1500224.

166. Tachi, T., Simulation of rigid origami. *Origami* **2009,** *4* (08), 175-187.

167. Tang, R.; Huang, H.; Tu, H.; Liang, H.; Liang, M.; Song, Z.; Xu, Y.; Jiang, H.; Yu, H., Origami-enabled deformable silicon solar cells. *Applied Physics Letters* **2014,** *104* (8), 083501.

168. Liu, C.; Felton, S. M., Transformation dynamics in origami. *Physical review letters* **2018,** *121* (25), 254101.

169. Zhao, Z.; Wu, J.; Mu, X.; Chen, H.; Qi, H. J.; Fang, D., Origami by frontal photopolymerization. *Science advances* **2017,** *3* (4), e1602326.

170. Chen, Y.; Yan, J.; Feng, J.; Sareh, P., Particle Swarm Optimization-Based Metaheuristic Design Generation of Non-Trivial Flat-Foldable Origami Tessellations With Degree-4 Vertices. *Journal of Mechanical Design* **2020**, 1-25.

171. Kamrava, S.; Mousanezhad, D.; Felton, S. M.; Vaziri, A., Programmable origami strings. *Advanced Materials Technologies* **2018,** *3* (3), 1700276.

172. Nauroze, S. A.; Novelino, L. S.; Tentzeris, M. M.; Paulino, G. H., Continuous-range tunable multilayer frequency-selective surfaces using origami and inkjet printing. *Proceedings of the National Academy of Sciences* **2018,** *115* (52), 13210-13215.

173. Li, S.; Wang, K., Fluidic origami with embedded pressure dependent multi-stability: a plant inspired innovation. *Journal of The Royal Society Interface* **2015,** *12* (111), 20150639.

174. Li, S.; Wang, K., Fluidic origami: a plant-inspired adaptive structure with shape morphing and stiffness tuning. *Smart Materials and Structures* **2015,** *24* (10), 105031.

175. Sadeghi, S.; Li, S. In *Harnessing the quasi-zero stiffness from fluidic origami for low frequency vibration isolation*, Smart Materials, Adaptive Structures and Intelligent Systems, American Society of Mechanical Engineers: 2017; p V002T03A008.

176. Sadeghi, S.; Li, S., Fluidic origami cellular structure with asymmetric quasi-zero stiffness for low-frequency vibration isolation. *Smart Materials and Structures* **2019,** *28* (6), 065006.

177. Mousanezhad, D.; Kamrava, S.; Vaziri, A., Origami-based building blocks for modular construction of foldable structures. *Scientific reports* **2017,** *7* (1), 1-8.

178. Chen, Z.; Wu, T.; Nian, G.; Shan, Y.; Liang, X.; Jiang, H.; Qu, S., Ron Resch origami pattern inspired energy absorption structures. *Journal of Applied Mechanics* **2019,** *86* (1).

179. Jianguo, C.; Xiaowei, D.; Ya, Z.; Jian, F.; Yongming, T., Bistable behavior of the cylindrical origami structure with Kresling pattern. *Journal of Mechanical Design* **2015,** *137* (6).

180. Kuribayashi, K.; Tsuchiya, K.; You, Z.; Tomus, D.; Umemoto, M.; Ito, T.; Sasaki, M., Self-deployable origami stent grafts as a biomedical application of Ni-rich TiNi shape memory alloy foil. *Materials Science and Engineering a-Structural Materials Properties Microstructure and Processing* **2006,** *419* (1-2), 131-137.

181. Miura, K. *Method of packaging and deployment of large membranes in space*; Institute of Space and Astronomical Sciences: 1985.

182. Xu, S.; Yan, Z.; Jang, K. I.; Huang, W.; Fu, H. R.; Kim, J.; Wei, Z.; Flavin, M.; McCracken, J.; Wang, R.; Badea, A.; Liu, Y.; Xiao, D. Q.; Zhou, G. Y.; Lee, J.; Chung,

H. U.; Cheng, H. Y.; Ren, W.; Banks, A.; Li, X. L.; Paik, U.; Nuzzo, R. G.; Huang, Y. G.; Zhang, Y. H.; Rogers, J. A., Assembly of micro/nanomaterials into complex, three-dimensional architectures by compressive buckling. *Science* **2015,** *347* (6218), 154-159.

183. Song, Z.; Lv, C.; Liang, M. B.; Sanphuang, V.; Wu, K.; Chen, B.; Zhao, Z.; Bai, J.; Wang, X.; Volakis, J. L.; Wang, L. P.; He, X. M.; Yao, Y.; Tongay, S.; Jiang, H. Q., Microscale Silicon Origami. *Small* **2016,** *12* (39), 5401-5406.

184. Thrall, A. P.; Quaglia, C. P., Accordion shelters: A historical review of origami-like deployable shelters developed by the US military. *Engineering Structures* **2014,** *59* (Supplement C), 686-692.

185. Filipov, E. T.; Tachi, T.; Paulino, G. H., Origami tubes assembled into stiff, yet reconfigurable structures and metamaterials. *Proceedings of the National Academy of Sciences of the United States of America* **2015,** *112* (40), 12321-12326.

186. Overvelde, J. T. B.; de Jong, T. A.; Shevchenko, Y.; Becerra, S. A.; Whitesides, G. M.; Weaver, J. C.; Hoberman, C.; Bertoldi, K., A three-dimensional actuated origami-inspired transformable metamaterial with multiple degrees of freedom. *Nature Communications* **2016,** *7*.

187. Lin, C.-H.; Tsai, D.-S.; Wei, T.-C.; Lien, D.-H.; Ke, J.-J.; Su, C.-H.; Sun, J.-Y.; Liao, Y.-C.; He, J.-H., Highly Deformable Origami Paper Photodetector Arrays. *ACS Nano* **2017**.

188. Wang, Z.; Jing, L.; Yao, K.; Yang, Y.; Zheng, B.; Soukoulis, C. M.; Chen, H.; Liu, Y., Origami-Based Reconfigurable Metamaterials for Tunable Chirality. *Advanced Materials* **2017,** *29* (27), 1700412.

189. Dudte, L. H.; Vouga, E.; Tachi, T.; Mahadevan, L., Programming curvature using origami tessellations. *Nature Materials* **2016,** *15* (5), 583-+.

190. Lv, C.; Krishnaraju, D.; Konjevod, G.; Yu, H.; Jiang, H., Origami based Mechanical Metamaterials. *Scientific Reports* **2014,** *4:5979.*

191. Yasuda, H.; Yein, T.; Tachi, T.; Miura, K.; Taya, M., Folding behaviour of Tachi-Miura polyhedron bellows. *Proceedings of the Royal Society a-Mathematical Physical and Engineering Sciences* **2013,** *469* (2159).

192. Silverberg, J. L.; Na, J. H.; Evans, A. A.; Liu, B.; Hull, T. C.; Santangelo, C. D.; Lang, R. J.; Hayward, R. C.; Cohen, I., Origami structures with a critical transition to bistability arising from hidden degrees of freedom. *Nature Materials* **2015,** *14* (4), 389-393.

193. Hunt, G. W.; Ario, I., Twist buckling and the foldable cylinder: an exercise in origami. *International Journal of Non-Linear Mechanics* **2005,** *40* (6), 833-843.

194. Guest, S. D.; Pellegrino, S., THE FOLDING OF TRIANGULATED CYLINDERS .1. GEOMETRIC CONSIDERATIONS. *Journal of Applied Mechanics-Transactions of the Asme* **1994,** *61* (4), 773-777.

195. Borodulina, S.; Kulachenko, A.; Galland, S.; Nygårds, M., Stress-strain curve of paper revisited. *Nordic Pulp and Paper Research Journal* **2012,** *27* (2), 318.

196. Yokoyama, T.; Nakai, K.; Odamura, T., Tensile Stress-strain Properties of Paper and Paperboard and Their Constitutive Equations. *Journal of the Japanese Society for Experimental Mechanics* **2007,** *7* (Special_Issue), s68-s73.

197. Poston, T.; Stewart, I., *Catastrophe Theory and its Applications.* Dover Publications: 2012.

198. Beer, F. P.; Johnston, E. R.; DeWolf, J. T., *Mechanics of Materials*. McGraw-Hill Higher Education: 2006.

199. Carrella, A.; Brennan, M.; Waters, T., Static analysis of a passive vibration isolator with quasi-zero-stiffness characteristic. *Journal of sound and vibration* **2007,** *301* (3-5), 678-689.

200. Haghpanah, B.; Salari-Sharif, L.; Pourrajab, P.; Hopkins, J.; Valdevit, L., Multistable shape-reconfigurable architected materials. *Advanced Materials* **2016,** *28* (36), 7915-7920.

201. Chen, T.; Bilal, O. R.; Shea, K.; Daraio, C., Harnessing bistability for directional propulsion of soft, untethered robots. *Proceedings of the National Academy of Sciences* **2018,** *115* (22), 5698-5702.

202. Overvelde, J. T. B.; Kloek, T.; D'haen, J. J. A.; Bertoldi, K., Amplifying the response of soft actuators by harnessing snap-through instabilities. *Proceedings of the National Academy of Sciences* **2015,** *112* (35), 10863-10868.

203. Churchill, C. B.; Shahan, D. W.; Smith, S. P.; Keefe, A. C.; McKnight, G. P., Dynamically variable negative stiffness structures. *Science advances* **2016,** *2* (2), e1500778.

204. Jin, L.; Khajehtourian, R.; Mueller, J.; Rafsanjani, A.; Tournat, V.; Bertoldi, K.; Kochmann, D. M., Guided transition waves in multistable mechanical metamaterials. *Proceedings of the National Academy of Sciences* **2020,** *117* (5), 2319-2325.

205. Ferris, D. P.; Liang, K.; Farley, C. T., Runners adjust leg stiffness for their first step on a new running surface. *Journal of biomechanics* **1999,** *32* (8), 787-794.

206. Dickinson, M. H.; Farley, C. T.; Full, R. J.; Koehl, M. A. R.; Kram, R.; Lehman, S., How Animals Move: An Integrative View. *Science* **2000,** *288* (5463), 100-106.

207. Sharp, R.; Hassan, S., An evaluation of passive automotive suspension systems with variable stiffness and damping parameters. *Vehicle System Dynamics* **1986,** *15* (6), 335-350.

208. Wei, Y.; Chen, Y.; Ren, T.; Chen, Q.; Yan, C.; Yang, Y.; Li, Y., A novel, variable stiffness robotic gripper based on integrated soft actuating and particle jamming. *Soft Robotics* **2016,** *3* (3), 134-143.

209. Kuder, I. K.; Arrieta, A. F.; Raither, W. E.; Ermanni, P., Variable stiffness material and structural concepts for morphing applications. *Progress in Aerospace Sciences* **2013,** *63*, 33-55.

210. Pu, H.; Yuan, S.; Peng, Y.; Meng, K.; Zhao, J.; Xie, R.; Huang, Y.; Sun, Y.; Yang, Y.; Xie, S., Multi-layer electromagnetic spring with tunable negative stiffness for semi-active vibration isolation. *Mechanical Systems and Signal Processing* **2019,** *121*, 942-960.

211. Nelson, B. J.; Kaliakatsos, I. K.; Abbott, J. J., Microrobots for minimally invasive medicine. *Annual review of biomedical engineering* **2010,** *12*, 55-85.

212. Kim, S.; Laschi, C.; Trimmer, B., Soft robotics: a bioinspired evolution in robotics. *Trends in biotechnology* **2013,** *31* (5), 287-294.

213. Collins, S.; Ruina, A.; Tedrake, R.; Wisse, M., Efficient bipedal robots based on passive-dynamic walkers. *Science* **2005,** *307* (5712), 1082-1085.

214. Berger, J.; Wadley, H.; McMeeking, R., Mechanical metamaterials at the theoretical limit of isotropic elastic stiffness. *Nature* **2017,** *543* (7646), 533-537.

215. Janbaz, S.; Bobbert, F.; Mirzaali, M.; Zadpoor, A., Ultra-programmable buckling-driven soft cellular mechanisms. *Materials Horizons* **2019,** *6* (6), 1138-1147.

216. Yan, Z.; Zhang, F.; Wang, J.; Liu, F.; Guo, X.; Nan, K.; Lin, Q.; Gao, M.; Xiao, D.; Shi, Y.; Qiu, Y.; Luan, H.; Kim, J. H.; Wang, Y.; Luo, H.; Han, M.; Huang, Y.; Zhang, Y.; Rogers, J. A., Controlled Mechanical Buckling for Origami-Inspired Construction of 3D Microstructures in Advanced Materials. *Advanced Functional Materials* **2016,** *26* (16), 2629-2639.

217. Zhang, Y.; Zhang, F.; Yan, Z.; Ma, Q.; Li, X.; Huang, Y.; Rogers, J. A., Printing, folding and assembly methods for forming 3D mesostructures in advanced materials. *Nature Reviews Materials* **2017,** *2* (4), 1-17.

218. Huang, T.-Y.; Huang, H.-W.; Jin, D.; Chen, Q.; Huang, J.; Zhang, L.; Duan, H., Four-dimensional micro-building blocks. *Science Advances* **2020,** *6* (3), eaav8219.

219. Liu, K.; Tachi, T.; Paulino, G. H., Invariant and smooth limit of discrete geometry folded from bistable origami leading to multistable metasurfaces. *Nature Communications* **2019,** *10* (1), 4238.

220. Faber, J. A.; Arrieta, A. F.; Studart, A. R., Bioinspired spring origami. *Science* **2018,** *359* (6382), 1386-1391.

221. Lee, T. U., Chen, Y. and Gattas, J.M. In *Curved-Crease Origami with Multiple States*, Origami 7: Seventh International Meeting of Origami Science, Mathematics, and Education, 2018; pp 849-864.

222. Noel, A. C.; Guo, H.-Y.; Mandica, M.; Hu, D. L., Frogs use a viscoelastic tongue and non-Newtonian saliva to catch prey. *Journal of the Royal Society Interface* **2017,** *14* (127), 20160764.

223. Maloiy, G.; Heglund, N. C.; Prager, L.; Cavagna, G. A.; Taylor, C. R., Energetic cost of carrying loads: have African women discovered an economic way? *Nature* **1986,** *319* (6055), 668-669.

224. Alexander, R. M., *Elastic mechanisms in animal movement*. Cambridge University Press Cambridge: 1988; p 141.

225. Den Hartog, J. P., *Mechanical vibrations*. Courier Corporation: 1985.

226. Trivedi, D.; Rahn, C. D.; Kier, W. M.; Walker, I. D., Soft robotics: Biological inspiration, state of the art, and future research. *Applied bionics and biomechanics* **2008,** *5* (3), 99-117.

227. Tolley, M. T.; Felton, S. M.; Miyashita, S.; Aukes, D.; Rus, D.; Wood, R. J., Self-folding origami: shape memory composites activated by uniform heating. *Smart Materials and Structures* **2014,** *23* (9), 094006.

228. Liu, Y.; Shaw, B.; Dickey, M. D.; Genzer, J., Sequential self-folding of polymer sheets. *Science Advances* **2017,** *3* (3), e1602417.

229. Hawkes, E.; An, B.; Benbernou, N. M.; Tanaka, H.; Kim, S.; Demaine, E. D.; Rus, D.; Wood, R. J., Programmable matter by folding. *Proceedings of the National Academy of Sciences* **2010,** *107* (28), 12441-12445.

230. Martinez, R. V.; Fish, C. R.; Chen, X.; Whitesides, G. M., Elastomeric Origami: Programmable Paper-Elastomer Composites as Pneumatic Actuators. *Advanced Functional Materials* **2012,** *22* (7), 1376-1384.

231. Hawkes, E.; An, B.; Benbernou, N. M.; Tanaka, H.; Kim, S.; Demaine, E. D.; Rus, D.; Wood, R. J., Programmable matter by folding. *Proceedings of the National Academy of Sciences of the United States of America* **2010,** *107* (28), 12441-12445.

232. Leong, T. G.; Randall, C. L.; Benson, B. R.; Bassik, N.; Stern, G. M.; Gracias, D. H., Tetherless thermobiochemically actuated microgrippers. *Proceedings of the National Academy of Sciences of the United States of America* **2009,** *106* (3), 703-708.

233. Liu, Y.; Boyles, J. K.; Genzer, J.; Dickey, M. D., Self-folding of polymer sheets using local light absorption. *Soft Matter* **2012,** *8* (6), 1764-1769.

234. Kim, J.; Hanna, J. A.; Hayward, R. C.; Santangelo, C. D., Thermally responsive rolling of thin gel strips with discrete variations in swelling. *Soft Matter* **2012,** *8* (8), 2375-2381.

235. Na, J.-H.; Evans, A. A.; Bae, J.; Chiappelli, M. C.; Santangelo, C. D.; Lang, R. J.; Hull, T. C.; Hayward, R. C., Programming Reversibly Self-Folding Origami with Micropatterned Photo-Crosslinkable Polymer Trilayers. *Advanced Materials* **2015,** *27* (1), 79-85.

236. Ryu, J.; D'Amato, M.; Cui, X. D.; Long, K. N.; Qi, H. J.; Dunn, M. L., Photo-origami-Bending and folding polymers with light. *Applied Physics Letters* **2012,** *100* (16).

237. Mu, X. M.; Sowan, N.; Tumbic, J. A.; Bowman, C. N.; Mather, P. T.; Qi, H. J., Photo-induced bending in a light-activated polymer laminated composite. *Soft Matter* **2015,** *11* (13), 2673-2682.

238. Ge, Q.; Dunn, C. K.; Qi, H. J.; Dunn, M. L., Active origami by 4D printing. *Smart Materials and Structures* **2014,** *23* (9).

239. Kim, J.; Hanna, J. A.; Byun, M.; Santangelo, C. D.; Hayward, R. C., Designing Responsive Buckled Surfaces by Halftone Gel Lithography. *Science* **2012,** *335* (6073), 1201-1205.

240. Judy, J. W.; Muller, R. S., Magnetically actuated, addressable microstructures. *Journal of Microelectromechanical Systems* **1997,** *6* (3), 249-256.

241. Yi, Y. W.; Liu, C., Magnetic actuation of hinged microstructures. *Journal of Microelectromechanical Systems* **1999,** *8* (1), 10-17.

242. Pitre, J. J.; Bull, J. L., Imaging the Mechanical Properties of Porous Biological Tissue. In *Handbook of Thermal Science and Engineering*, Kulacki, F. A., Ed. Springer International Publishing: Cham, 2017; pp 1-27.

APPENDIX A

DETAILS IN KRESLING ORIGAMI MODELING

Geometry of triangulated cylinder patterns

Figure 40 shows a unit cell of a triangulated cylinder pattern from the crease pattern (**Fig 1a**). At the planar state,

$$L_{AB} = a\,, \tag{1}$$

and the law of sines gives

$$\frac{L_{AB}}{\sin\beta} = \frac{L_{AC}}{\sin\angle ABC} = \frac{L_{BC}}{\sin\alpha}\,, \tag{2}$$

Thus,

$$L_{BC} = a\frac{\sin\alpha}{\sin\beta} \tag{3}$$

$$L_{AC} = a\frac{\sin(\alpha+\beta)}{\sin\beta} \tag{4}$$

At the folded state, height *h*, twist angle ϕ, and radius *r* are used to characterize the geometry (Fig. 40). The coordinates of the points *O*, *O'*, *A*, *B*, and *C* are given by,

$$\begin{aligned} &O\,(0,0,0), \qquad O'(0,0,h), \qquad A(r,0,0) \\ &B\left(r\cos\frac{2\pi}{n}, -r\sin\frac{2\pi}{n}, 0\right), \qquad C\left(r\cos\left(\frac{2\pi}{n}+\phi\right), -r\sin\left(\frac{2\pi}{n}+\phi\right), h\right). \end{aligned} \tag{5}$$

Then the length of the three folding lines, *AB*, *BC*, and *AC* at the folded state become

$$l_{AB} = 2r\sin\frac{\pi}{n} \tag{6}$$

$$l_{BC} = \sqrt{h^2 - 2r^2\cos\phi + 2r^2} \tag{7}$$

$$l_{AC} = \sqrt{h^2 - 2r^2\cos\left(\frac{2\pi}{n}+\phi\right) + 2r^2} \tag{8}$$

The strains in these three folding lines are

$$\varepsilon_{AB} = \frac{l_{AB} - L_{AB}}{L_{AB}} = 2\bar{r}\sin\frac{\pi}{n} - 1 \tag{9}$$

$$\varepsilon_{BC} = \frac{l_{BC} - L_{BC}}{L_{BC}} = \frac{\sin\beta}{\sin\alpha}\sqrt{\bar{h}^2 - 2\bar{r}^2\cos\phi + 2\bar{r}^2} - 1 \tag{10}$$

$$\varepsilon_{AC} = \frac{l_{AC} - L_{AC}}{L_{AC}} = \frac{\sin\beta}{\sin(\alpha+\beta)}\sqrt{\bar{h}^2 - 2\bar{r}^2\cos\left(\phi + \frac{2\pi}{n}\right) + 2\bar{r}^2} - 1 \tag{11}$$

Here $\bar{h} = \frac{h}{a}$, and $\bar{r} = \frac{r}{a}$ are normalized height *h*, and radius *r*, respectively.

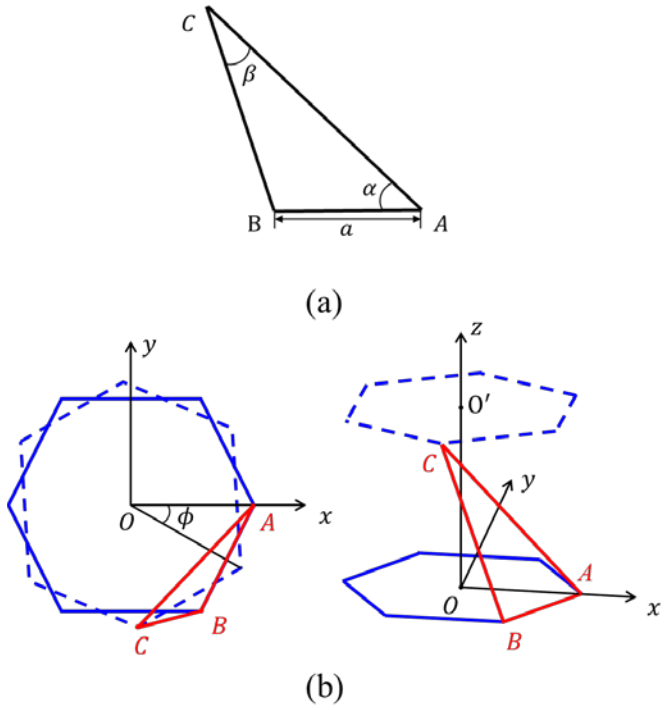

Figure 40. Illustrations of the triangulated cylinder origami.

Deformation energy analysis

For a stripe (highlighted in Fig. 3), the deformation energy is given by

$$U = \frac{nEA}{2}(L_{AB}\varepsilon_{AB}^2 + L_{BC}\varepsilon_{BC}^2 + L_{AC}\varepsilon_{AC}^2) \tag{12}$$

As shown in Eqs. (9) to (11), the deformation energy U depends on three variables, namely height h, twist angle f, and radius r. Using the principle of stationary potential energy, optimization with respect to these variables determines the folded states. Specifically, when only height h is prescribed, the folded state can be obtained by solving the following nonlinear equations,

$$\left.\frac{\partial U}{\partial \phi}\right|_h = \left.\frac{\partial U}{\partial r}\right|_h = 0, \qquad \left.\frac{\partial^2 U}{\partial \phi^2}\right|_h > 0, \qquad \left.\frac{\partial^2 U}{\partial r^2}\right|_h > 0 . \tag{13}$$

When both h and ϕ are prescribed, the following equations will be solved,

$$\left.\frac{\partial U}{\partial r}\right|_h = 0, \qquad \left.\frac{\partial^2 U}{\partial r^2}\right|_h > 0 . \tag{14}$$

MATLAB was used to solve these nonlinear equations.

APPENDIX B

DETAILS IN CURVED ORIGAMI MODELING

Modelling of a Quadrilateral Rigid Origami Cell upon Compression

This model is based on the theory of rigid origami, where the strain energy is only stored in linear elastic creases. Fig. 41 (a) shows the folding pattern of a quadrilateral rigid origami unit cell. The angle between crease 1 and crease 2 is β. The summed length of the creases 2 and 4 is 2*c*. The length of crease 1 (or crease 3) is *b* and can be expresses by β and *c* as

$$b = \frac{c}{\sin(\beta)} \tag{15}$$

By compressing the origami through the top and bottom vertices, the origami will deform into a configuration as shown in Fig. 41 (b). The spatial geometry of the origami is very similar to the Miura pattern, as shown in Fig. 41 (c), and the same angle β is used. The geometry of Miura pattern during folding has been studied somewhere else[4], which will be used to study the relationship between force and displacement. The same notations[4] are adopted here in Fig. 41 (c). The projection angle between two ridges is ϕ. The dihedral angles α_1 at crease 4 and α_2 at crease 3 can be expressed as functions of ϕ as [4]

$$\alpha_1(\phi) = \cos^{-1}\left[1 - 2\frac{\sin^2\left(\frac{\phi}{2}\right)}{\sin^2(\beta)}\right] \tag{16}$$

$$\alpha_2(\phi) = \cos^{-1}\left[1 - 2\cot^2(\beta)\cdot\tan^2\left(\frac{\phi}{2}\right)\right] \tag{17}$$

l is the distance between the top and bottom vertices and can characterize the deformation with $l = 2c$ for undeformed state. Angle ϕ can be expressed as a function of *l*,

$$\phi(l) = 2\sin^{-1}\left(\frac{l}{2b}\right) \tag{18}$$

Given the crease modulus H (unit: N), the strain energy of the unit cell U can be expressed as

$$U = \frac{1}{2}2cH\left(\pi - \alpha_1\right)^2 + \frac{1}{2}2bH\left(\pi - \alpha_2\right)^2 = H\left[c\left(\pi - \alpha_1\right)^2 + b\left(\pi - \alpha_2\right)^2\right] \tag{19}$$

The reaction force F can be calculated as a derivative of U with respect to l,

$$F = \frac{\partial U}{\partial l} = 2H\left[\left(\alpha_1 - \pi\right)\frac{\partial \alpha_1}{\partial \phi}\sin\beta + \left(\alpha_2 - \pi\right)\frac{\partial \alpha_2}{\partial \phi}\right]\frac{1}{\sqrt{1-\left(\frac{l}{2b}\right)^2}}, \tag{20}$$

The force F can be normalized as

$$\overline{F}(l) = \frac{F}{H} = 2\left[\left(\alpha_1 - \pi\right)\frac{\partial \alpha_1}{\partial \phi}\sin\beta + \left(\alpha_2 - \pi\right)\frac{\partial \alpha_2}{\partial \phi}\right]\frac{1}{\sqrt{1-\left(\frac{l}{2b}\right)^2}} \tag{21}$$

The normalized reaction force due to creases 1 and 3 $\overline{F}_{1,3}$ is expressed as the second part of Eq. (21),

$$\overline{F}_{1,3}(l) = \frac{2\left(\alpha_2 - \pi\right)\frac{\partial \alpha_2}{\partial \phi}}{\sqrt{1-\left(\frac{l}{2b}\right)^2}} \tag{22}$$

The normalized reaction force due to creases 2 and 4 $\overline{F}_{2,4}$ is expressed as the first part of Eq. (21),

$$\bar{F}_{2,4}(l)=\frac{2(\alpha_1-\pi)\dfrac{\partial\alpha_1}{\partial\phi}\sin\beta}{\sqrt{1-\left(\dfrac{l}{2b}\right)^2}} \tag{23}$$

Define the collapsing ratio as $1-\frac{l}{2c}$. Figures 41 (d), (e), and (f) show the normalized forces versus the collapsing ratio.

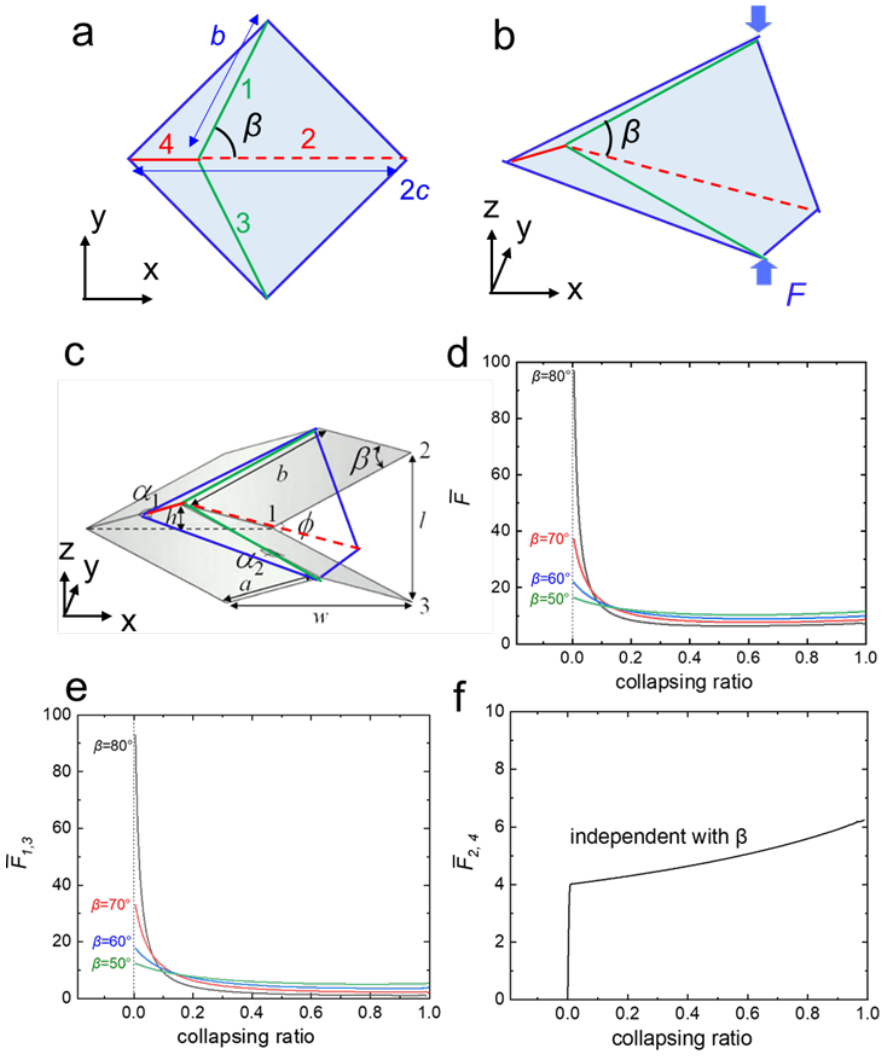

Figure 41. Mechanical behavior of a quadrilateral rigid origami cell.

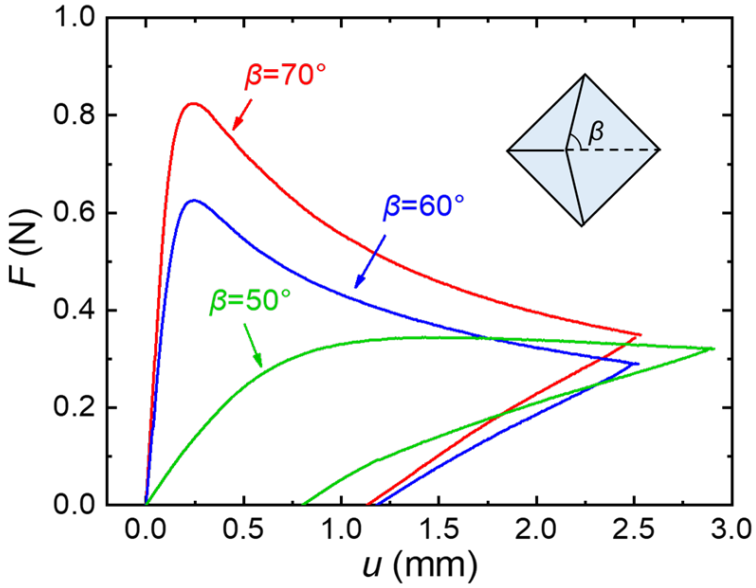

Figure 42. Force-displacement relationship of quadrilateral rigid origami cells upon compression.

Modeling of Creases in Finite Element Simulation

We model the creases as linear elastic perfectly plastic materials in finite element simulations using ABAQUS. Using this model, the reaction moment per unit crease length as a function of rotation angle is shown in Fig. 43 (a). The slope of the curve in the elastic range $\left(\text{unit: } N \cdot m / m = N\right)$ is the crease modulus *H*. The yield rotation angle is set as 1 rad, which is verified by the following experiments as shown in Fig. 43 (b), in which a square-shaped origami with a straight crease in the middle is used, with the right part of the origami is constrained and the left part is free to rotate about the straight crease. A tweezer is used to rotate the left part of origami to a specific angle (i.e., 130° in Fig. 43 (c)) and then released (i.e., 80° in Fig. 43 (d)). We then used the linear elastic and perfect plastic model to theoretically predict the relaxed angle. For example, as shown in Fig. 43 (e), for a given rotation angle 130°, the predicted relaxed angle is 73°, which agrees reasonably well with the experiments (Fig. 43 (d)). The comparison between the experiment results and the

predictions for different angles is shown in **Fig. 43 (f)**, where the experimental and the predicted results show a same trend. Therefore, a linear elastic perfect plastic model with yield angle of 1 rad is verified to be reasonable for the simulation.

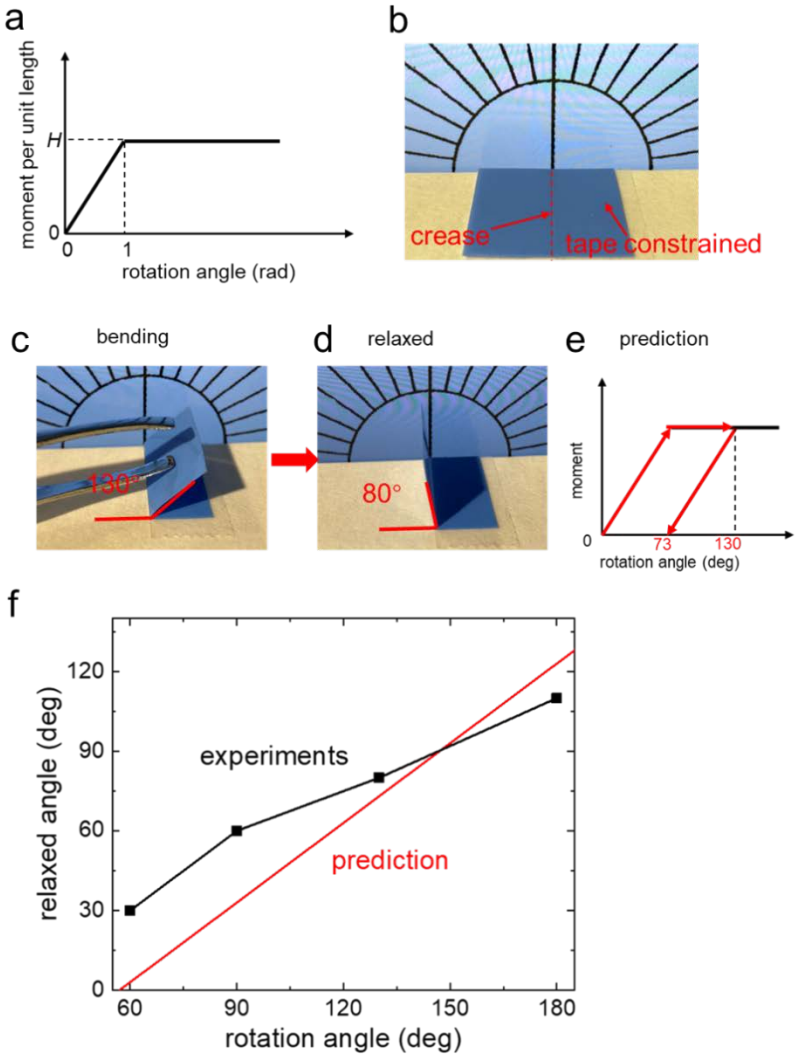

Figure 43. Rationale of the linear elastic perfectly plastic model of creases used in simulation.

Loading Steps in The Finite Element Simulations

As shown in Fig. 44, the curved origami is undeformed and has zero energy at the initial state (step 0). The curved origami is bent for 250° in step 1, and released in step 2.

In step 3, the curved origami is compressed under a displacement load u = 0.2. In step 4, the displacement load is gradually released to zero. In the following steps, the displacement load is applied and removed periodically as steps 3 and 4. The plastic dissipation energy U_p increased during the 1st and 3rd step, and keeps constant after the step 4, which means no dissipation exists during the repeated loading and unloading steps of curved origami afterwards.

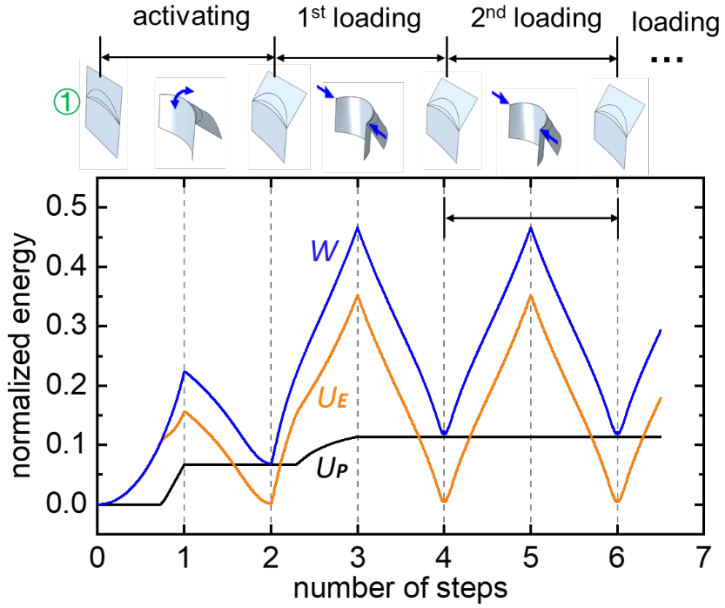

Figure 44. Loading steps in the finite element simulations.

Normalization of the Parameters

Three basic parameters, i.e., unit cell length a, thickness t, and panel modulus E, are used for normalization. The displacement is normalized as $\bar{u} = \frac{u}{a}$. Curvature is normalized as $\bar{\kappa} = \kappa a$. The energy, force, and stiffness are normalized by a bending deformation of panel. The bending energy of the panel for normalization U_{norm} has the unit

of $U_{norm} \sim EI_x \kappa_{panel}^2 a \sim Et^3 a \left(\frac{1}{a}\right)^2 a = Et^3$, where the second moment of cross-sectional area about x axis $I_x \sim t^3 a$, and curvature of panel $\kappa_{panel} \sim \frac{1}{a}$. Therefore, the energy of the curved origami unit cell can be normalized as $U = \frac{U}{Et^3}$. The reaction force due to bending has the unit of $F_{norm} \sim \frac{U_{norm}}{a} \sim \frac{Et^3}{a}$. Thus, the reaction force of the curved origami unit cell F is normalized as $\bar{F} = \frac{Fa}{Et^3}$. Since crease modulus has the same unit as force, it is also normalized as $\bar{H} = \frac{Fa}{Et^3}$. Stress has the unit of $\sigma_{norm} \sim \frac{F_{norm}}{at} = \frac{Et^2}{a^2}$, so normalized stress $\bar{\sigma}$ is expressed as $\bar{\sigma} = \frac{\sigma a^2}{Et^2}$.

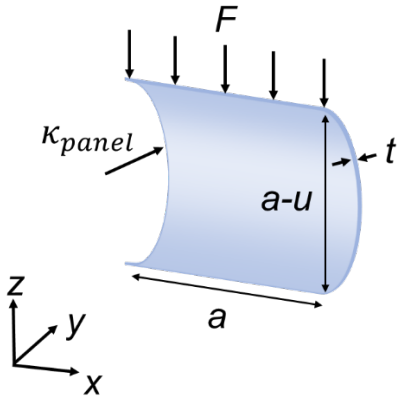

Figure 45. A square shaped panel of length a and thickness t bent by a uniform force F.

Estimation of the Crease Modulus

We performed compression test for a simple straight crease origami made of the plastic in Fig. 46. The depth of the crease is 100 μm. The experimental result is shown in

Fig. 46 (a). The same relationship between normalized reaction force $\bar{F} = \frac{F}{H}$ and compressive strain was also theoretically studied and shown in **Fig. S1f**. By fitting the experimental result with theoretical result (**Fig. S10b**), we have H = 0.01667 N. For the plastic film used in this study, the film Young's modulus E = 3.54 GPa (**Fig. S9**). For a crease of 100 μm cut depth, film thickness t = 125 μm and unit cell length a, the normalized crease stiffness can be expressed as

$$\bar{H} = \frac{Ha}{Et^3} = \frac{0.01667\text{N} \times a}{3.54 \times 10^9\,\text{N} \cdot \text{m}^{-2} \times \left(1.25 \times 10^{-4}\,\text{m}\right)^3} = (2.41\text{m}^{-1}) \cdot a\,.$$

For example, if a =30 mm (**Fig. 3a**), normalized crease stiffness is $\bar{H} = (2.41\text{m}^{-1}) \cdot (0.03m) = 0.072\,.$

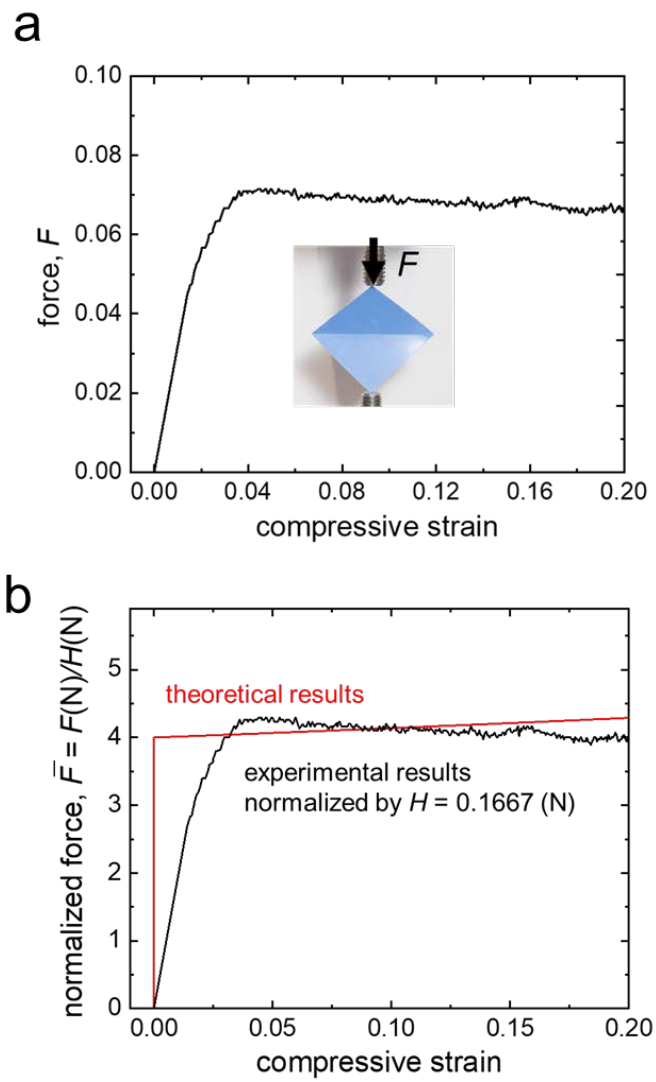

Figure 46**.** Comparison between theoretical and experimental normalized forces as functions of compressive strain.

Mechanical Characterization of Soft Tofu

We conducted a compression test to measure the mechanical properties of soft tofu. A piece of soft tofu in cylindrical shape with height h = 22 mm and diameter d = 43 mm was used. The photographs of the tofu before and after compression are shown in Fig. 47 (a) and (b), respectively. The force-displacement relationship is shown in Fig. 47 (c). The true strain is calculated as

$$\varepsilon = \ln\left(\frac{h-u}{h}\right), \tag{24}$$

where u is the vertical displacement. The true stress is calculated as

$$\sigma = \frac{4(h-u)F}{h\pi d^2} \tag{25}$$

assuming the tofu is uncompressible.[242] The true stress-true strain relationship is shown in Fig. 47 (d). The Young's modulus of soft tofu is calculated as

$$E_{tofu} = \frac{\Delta\sigma}{\Delta\varepsilon} = 8.005\text{kPa} \tag{26}$$

The strength of the soft tofu is 3.298 kPa. The toughness of soft tofu is calculated as

$$T_{tofu} = \int_o^{\varepsilon_f} \sigma \mathrm{d}\varepsilon = 875\,\text{J/m}^2 \tag{27}$$

where $\varepsilon_f = 0.4$ is the fracture strain.

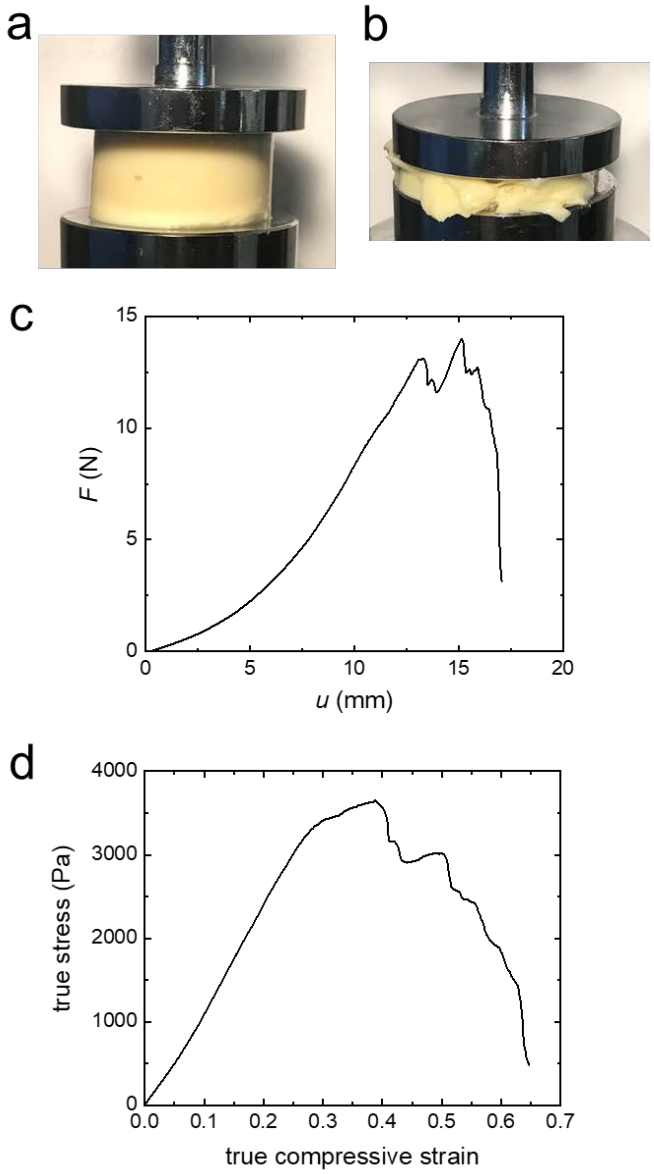

Figure 47. Mechanical characterization of soft tofu

APPENDIX C

COPYRIGHTS AND CO-AUTHOR APPROVAL

Chapter 1 contains publishable work, which is reproduce with permission from Mechanical Metamaterials Based on Origami and Kirigami. *Applied Physics Reviews*, 2021, accepted for publication. Copyright 2021 American Institute of Physics. After it is published, it will be found at https://aip.scitation.org/journal/are.

Chapter 2 contains published work, which is reproduced with permission from Zhai, Z., Wang, Y., & Jiang, H. (2018). Origami-Inspired, On-Demand Deployable and Collapsible Mechanical Metamaterials with Tunable Stiffness. *Proceedings of the National Academy of Sciences*, 115(9), 2032-2037. Copyright 2018 National Academy of Sciences.

Chapter 3 contains published work, which is reproduced with permission from Zhai, Z., Wang, Y., Lin, K., Wu, L., & Jiang, H. (2020). In Situ Stiffness Manipulation Using Elegant Curved Origami. *Science Advances*, 6(47), eabe2000. Copyright 2020 Authors, licensed under a Creative Commons Attribution (CC BY) license.

The materials used in this dissertation have approved by all the co-authors including Lingling Wu (Xi'an JiaoTong University), Yong Wang (Zhejiang University), Ken Lin (Zhejiang University), Hanqing Jiang (Westlake University).